The dormancy specific regulator, SutA, is an intrinsically-disordered protein that modulates transcription initiation in *Pseudomonas aeruginosa*

Megan Bergkessel[1], Brett M. Babin[2], David VanderVelde[2], Michael J. Sweredoski[3], Annie Moradian[3], Roxana Eggleston-Rangel[3], Sonia J. Hess[3], David A. Tirrell[2], Irina Artsimovitch[5,6], Dianne K. Newman[1,4,6]

[1]Division of Biology and Biological Engineering

[2]Division of Chemistry and Chemical Engineering

[3]Proteome Exploration Laboratory, Beckman Institute

[4]Division of Geological and Planetary Sciences

California Institute of Technology, Pasadena, California, United States

[5]Department of Microbiology, The Ohio State University, Columbus, Ohio, United States

[6]To whom correspondence should be addressed

ABSTRACT

SutA is upregulated during growth arrest in *Pseudomonas aeruginosa* and binds RNA polymerase (RNAP), causing widespread changes in gene expression. Using biochemical, structural and genetic methods, we examined how SutA interacts with RNAP and the functional consequences of these interactions. SutA consists of a central α-helix with unstructured N and C-terminal tails. It binds to the β1 domain of RNAP and competes with DNA, leading to effects that are either activating or repressing, depending on the sigma (σ) factor and promoter. Our data suggest that SutA is unlike conventional DNA-binding transcription factors, in that interactions between its α-helix and RNAP allow its acidic N-terminal tail to modulate the path of DNA within the transcription initiation complex, while its C-terminal tail stabilizes its interaction with RNAP. These activities help enhance expression of diverse genes, including essential ones such as the ribosomal RNA operons, under conditions of long-term resource limitation.

INTRODUCTION

Despite the fact that most natural environments do not allow bacteria to double every 20-30 minutes, our understanding of essential cellular processes—such as DNA replication, transcription and translation—has been shaped by studies of a few model organisms growing exponentially at these rates, or responding to a rapid shift from exponential to slow growth. An open question of general importance is how the molecular machines responsible for transcription and translation, tightly coupled processes that are necessary to maintain homeostasis even when cell division is not occurring, adapt to long periods of low and uneven substrate availability (Bergkessel et al., 2016). Perhaps the best-studied example of growth-rate responsive control of bacterial gene expression is that of the *E. coli* ribosomal RNA operon (*rrn*). Many studies have shown that complex interactions involving the specific characteristics of the *rrn* promoter, the activities of global regulators, and the physical realities of a nutrient-limited cell contribute to strong repression of *rrn* expression during slow growth or dormancy (Dennis et al., 2004). The major *rrn* promoter (P1) forms an extremely unstable open complex (OC), which helps drive high-level transcription by lowering the barrier for escape of RNAP from the promoter but also sensitizes it to perturbations during nutrient downshifts (Paul et al., 2004b). This sensitivity is exacerbated by the signaling molecule (p)ppGpp and its co-regulator DksA, which bind to RNAP and further destabilize the OC during early stationary phase, triggering RNAP dissociation, which can re-direct the available transcriptional resources toward stress responses (Ross et al., 2016). If nutrient levels stay low, NTP concentrations drop, further repressing expression from *rrn* P1, as its unstable OC also makes it highly sensitive to the concentration of the initiating nucleotides (iNTPs) (Murray et al., 2003b). Other stationary-phase changes, such as an increase in the abundance of active holoenzyme associated with the stress sigma factor ($E\sigma^S$) relative to that associated with the housekeeping sigma factor ($E\sigma^{70}$) (Ishihama, 2000), differences in the expression patterns of nucleoid-associated proteins, and a decrease in the DNA supercoiling imposed by transcription and replication activity, are also

thought to negatively impact initiation from *rrn* P1 (Meyer and Grainger, 2013). A second *rrn* promoter that drives low levels of expression and is insensitive to regulatory inputs, termed P2, has been proposed as the mechanism by which some rRNA transcription can be maintained during stationary phase (Murray et al., 2003a; Murray and Gourse, 2004); this paradigm implies that ribosome biogenesis is not actively modulated during protracted nutrient limitation.

However, regulatory mechanisms, even for highly conserved processes like ribosome biogenesis in bacteria, are diverse (Stallings et al., 2009), and mechanisms operating during prolonged growth arrest have not been studied in great detail in any organism. *P. aeruginosa* and many other members of the Pseudomonadales order are notable opportunists, capable of utilizing diverse substrates for rapid growth but also capable of persisting in dormancy for long periods of time in low-nutrient environments (Udikovic-Kolic et al., 2014), making them attractive model systems for such studies. Furthermore, a better understanding of slow-growing or dormant states in *P. aeruginosa* is of clinical importance, as these states are thought to contribute to the notorious antibiotic tolerance of this organism during chronic infections (Babin et al., 2017; Ciofu et al., 2015; Olivares et al., 2013). Accordingly, in previous work we undertook a proteomics-based screen to identify *P. aeruginosa* regulators that are preferentially expressed during hypoxia-induced growth arrest. We previously identified an RNAP-binding protein, SutA, with broad impacts on gene expression that affected the ability of *P. aeruginosa* to form biofilms and produce virulence factors. Notably, SutA appeared to increase expression of the rRNA and r-protein genes under slow-growth conditions, as well as many genes with roles in nutrient scavenging, alternative metabolic pathways, and housekeeping functions, while repressing genes involved in virulence, motility, and defense (Babin et al., 2016).

These observations led us to seek a mechanistic understanding of how SutA globally affects transcription during slow growth. Here we report biochemical, structural, and genetic studies aimed at elucidating

how SutA binds to RNAP and perturbs its function. Though our work focuses on a specific transcription factor in *P. aeruginosa*, the topic it tackles and the questions it raises are broadly relevant to understanding how bacteria survive periods of slow growth or dormancy in diverse environments.

RESULTS

SutA consists of a conserved alpha helix flanked by flexible N- and C-terminal tails

SutA is a small (105 amino acids) protein with no similarity to any known domains. We began by looking at structure predictions (using the Jpred4 algorithm for secondary structure and DISOPRED3 for intrinsic disorder) and sequence conservation (Buchan et al., 2013; Drozdetskiy et al., 2015; Jones and Cozzetto, 2015). SutA homologs are found in most organisms in the "Pseudomonadales-Oceanospirallales" clade of Gammaproteobacteria (Williams et al., 2010). Residues 56-76 are predicted to form an α-helix, followed by a 4-residue β-strand comprising residues 81-84, but the rest of the protein has no predicted secondary structural elements and residues 1-50 and 101-105 are predicted to be intrinsically disordered (Figure 1A). While the central, potentially structured region is reasonably well conserved, some homologs completely lack the last 15-18 residues, while others lack most or all of the first 40 residues (Figure 1 – figure supplement 1). This suggests that the N-and C-terminal tails (N-tail and C-tail) might function independently and could be removed without affecting folding/function of other SutA regions.

For structural characterization by NMR, we purified ^{15}N and ^{13}C labeled full-length SutA, as well as a ^{15}N and ^{13}C labeled construct that lacked most of the predicted disordered residues, SutA 46-101. We also constructed N-terminal (SutA ΔN, retaining residues 41-105) and C-terminal (SutA ΔC, retaining residues 1-87) deletion mutants (Figure 1B).

We were able to assign resonances and determine backbone chemical shifts for about 85% of the residues of the full-length protein (Table 1). Low sequence complexity and large regions of disorder caused a high degree of overlap in the spectra and made assignment difficult, but spectra from the 46-101 variant were easier to assign, and served as a starting point for making assignments for the full-length SutA. We focused on characterizing secondary structure chemical shift index values, R_2 relaxation rates, and ^{1}H-^{15}N NOE magnitude and sign to gain insight into secondary structure elements and degree of disorder for each residue that we could assign. We also embedded the protein in a stretched polyacrylamide gel to achieve weak alignment, and calculated residual dipolar couplings (RDCs) by measuring differences in in-phase-antiphase spectra between the isotropic solution sample and the anisotropic stretched gel sample (Figure 1C). The results of these analyses lend credence to the bioinformatics predictions. Residues 56-76 show the positive Cα and CO and negative Hα secondary chemical shifts associated with α-helical structure (Wishart et al., 1991), and also show fast R_2 relaxation rates and positive (^{1}H-^{15}N)NOE, signs that they are not disordered (Reddy and Rainey, 2010). Amide signals from disordered regions of the protein were almost completely absent from a ^{15}N HSQC spectrum acquired with NOE, whereas amides in the helix gave positive peaks, and the residues very close to the N and C termini gave negative peaks. RDCs for the helix region are also positive, as has been observed for α-helical regions of a partially denatured protein (Mohana-Borges et al., 2004). While the short β-strand is less strongly supported, secondary shifts for those residues are mostly of the appropriate sign for a β-strand albeit of small magnitudes. In the N-tail, a small number of residues have a positive NOE signal or secondary shifts that are not near zero, but in general, the residues of this region have the low R_2, secondary shift, and RDC values that are characteristic of disorder. The C-tail has several residues that show somewhat higher R_2 values and non-zero RDCs suggestive of some degree of structure, but classic secondary structure elements are not apparent. To rule out the possibility that the disorder we observed might be a non-native state of SutA, we tested the protein we produced for the

NMR studies in our *in vitro* activity assays and found that its activity was the same as that of the unlabeled protein we produced by standard methods (Figure1 – figure supplement 2). We also collected ^{15}N HSQC spectra for ^{15}N-labeled ΔN and ΔC mutants, and compared them to the full-length SutA (Figure 1 – figure supplement 3). Consistent with phylogenetic analysis, the deletion of either tail had little impact on the remaining residues, affecting only the 2-4 residues adjacent to the newly created N- or C-terminus, justifying using these truncation mutants to assess the functions of the N- and C-tails.

The difficulty of making unambiguous assignments for all residues and the high likelihood that much of the protein is intrinsically disordered precluded building a full NMR-based structural model of SutA. To model some of the conformations that might be adopted by SutA, we used the Robetta Server and PyRosetta to perform low-resolution Monte Carlo-based modeling, utilizing the chemical shifts and RDC values from our NMR analysis to guide fragment library construction (Bowers et al., 2000; Kim et al., 2004; Rohl and Baker, 2002). A resulting model that conforms to the observations and predictions described above is shown in Figure 1D. On the left, sequence conservation across 25 representative homologs is shown; on the right, charged residues in the *P. aeruginosa* sequence. The most highly conserved residues are found in the α-helix, and the C-tail is also highly conserved among homologs that have it. The N-tail is less conserved and varies in length, but is generally strikingly acidic. Additional models are shown in Figure 1 – figure supplement 4 (see materials and methods for modeling details).

SutA affects transcription initiation *in vitro*

We next wanted to investigate the direct effects of SutA on RNAP activity. We first asked whether SutA affects transcription by the closely related *E. coli* RNAP enzyme. We found that overexpressing SutA in *E. coli* did not lead to *rrn* upregulation *in vivo* as it did in *P. aeruginosa* (Figure 2 – figure supplement 1) necessitating using the cognate *P. aeruginosa in vitro* transcription system. We purified the core RNAP (E) natively from a Δ*sutA* strain using a protocol originally designed for purifying *E. coli* RNAP and

previously used to purify RNAP from *P. aeruginosa* (Burgess and Jendrisak, 1975; Hager et al., 1990; Kuznedelov et al., 2011). The *P. aeruginosa* homologs of σ^S, σ^{70}, and DksA, as well as SutA, were heterologously expressed in *E. coli* with cleavable N-terminal 6xHis tags and purified by metal affinity and size exclusion chromatography. We focused on initiation at three different *P. aeruginosa* promoters that we showed were upregulated by SutA *in vivo* (Babin et al., 2016) (Figure 2A). These promoters drive expression of a hypothetical bacteriocin (herein referred to as *bcn*, PA14_10380); a secreted amino peptidase (*pepB*, PA14_26020) and the ribosomal RNA operons (*rrn*). For *bcn* and *pepB*, transcription start sites have been determined by two RNA-Seq studies that are in agreement (Schulz et al., 2015; Wurtzel et al., 2012). *pepB* has been experimentally confirmed to be part of the σ^S regulon, while *bcn* is transcribed efficiently by the σ^{70} holoenzyme ($E\sigma^{70}$), but not $E\sigma^S$ (Figure 2). We mapped the dominant *rrn* transcription start site using 5'-RACE to a cytidine 8 bp downstream of the -10 consensus (Figure2 – figure supplement 2); while other possible transcription start sites are present within the 300 bp upstream of this site, it is unclear what role they may play in regulation of *P. aeruginosa rrn* transcription. We produced linear templates of 120-170 bp containing *the rrn, pepB,* and *bcn* promoters and 42-50 bp of transcript sequence for use in single-turnover initiation experiments (see materials and methods and supplements to Figure 2 for details).

Because $E\sigma^S$ binds the *rrn* locus *in vivo* during stationary phase in *E. coli* (Raffaelle et al., 2005), we sought to determine whether the SutA-dependent effects on *rrn* transcription we observed previously in *P. aeruginosa* were mediated through $E\sigma^S$, $E\sigma^{70}$ or both. *In vitro*, we found that addition of WT SutA caused increased amounts of *rrn* transcript in both holoenzyme contexts (Figure 2B), but the magnitude of the effect was much larger for $E\sigma^S$ (up to 4-fold increase) than for $E\sigma^{70}$ (up to 70% increase) (Figure 2C, top panels). In both cases, the effect was largest for concentrations of SutA between 125 and 500 nM, and transcript levels decreased again at higher concentrations. The acidic N-tail appears to be strictly required for activation, as the ΔN mutant inhibited transcription in a dose-dependent manner.

The ΔC mutant was still able to enhance transcription, albeit with a small shift in the concentration dependence, especially evident with $E\sigma^S$. These results suggest that the conserved central region containing the α-helix mediates SutA binding to RNAP and that the C-tail may also make a small contribution to this binding.

We also tested $E\sigma^S$ initiation from the *pepB* promoter and $E\sigma^{70}$ initiation from the *bcn* promoter (Figure 2C, bottom panels). For *pepB*, the results were broadly similar to those obtained with $E\sigma^S$ on the *rrn* promoter, although here the C-tail appears just as important as the N-tail. For *bcn*, the effect of SutA was opposite to that for *rrn* and, surprisingly, to what we had observed *in vivo* (Babin et al., 2016). The WT and ΔC proteins inhibited initiation to similar extents in a dose-dependent manner, while the ΔN SutA caused up to a 2-fold increase, with the greatest effect at the highest concentration tested.

To test the relevance of these findings to slow-growth conditions *in vivo*, we generated constructs in which WT, ΔN, or ΔC SutA were under the control of an arabinose-inducible promoter, and integrated them into the chromosome of a Δ*sutA* strain of *P. aeruginosa*. We performed qRT-PCR on the three genes of interest, using cells harvested in stationary phase after growth in minimal media containing pyruvate as a carbon source (Figure 2D). To test the importance of σ^S, we also integrated the WT *sutA* construct into a Δ*sutA* Δ*rpoS* strain (ΔS). For the *rrn* transcript, our *in vivo* qRT-PCR results largely mirrored the *in vitro* results: WT SutA induction led to an increase in transcript, the ΔN protein failed to cause any increase, and the ΔC protein was only mildly defective. In the Δ*rpoS* strain, *rrn* levels were much lower in the absence of SutA, but achieved similar levels to the *rpoS*+ strain background upon SutA induction. This implies that SutA can meaningfully enhance σ^{70}-driven production of *rrn in vivo* even though the magnitude of the *in vitro* effect on this holoenzyme is small, and further suggests that *in vivo,* under slow-growth conditions, σ^{70}-driven *rrn* expression may be even more dependent upon SutA than σ^S-driven *rrn* expression. For *pepB*, the *in vivo* results confirmed its dependence on σ^S and matched

the *in vitro* results, with the ΔC protein showing a stronger defect than the ΔN protein. For *bcn*, the SutA effect was opposite to that observed *in vitro*, as expected based on our published data (Babin et al., 2016), but one aspect was consistent with the *in vitro* results: the N-tail was required for the observed effect, while deletion of the C-tail had little effect. Many cellular factors (absent in our *in vitro* system) could contribute to the difference in behavior of the *bcn* promoter in the two contexts.

SutA binds to the β1 domain of RNAP

The above results demonstrate that SutA has direct effects on initiation. To map the region of RNAP with which SutA interacts, we used cross-linking and protein footprinting. The first cross-linking method used the homobifunctional reagent bis(sulfosuccinimidyl)suberate (BS^3), which cross-links primary amines within about 25 Å of each other (Rappsilber, 2011). BS^3 was added directly to complexes formed with purified core RNAP and SutA (Figure 3 – figure supplement 1), cross-linked complexes were digested with the peptidase Glu-C, and the resulting fragments were subjected to LC-MS/MS. Analysis performed with the software package Protein Prospector (Trnka et al., 2014) identified species that comprised one peptide from SutA and one peptide from RNAP (see materials and methods and Figure 3 – figure supplements 1 and 3 for additional details), thus allowing for mapping of cross-link sites. The second cross-linking method used the photoreactive non-canonical amino acid p-benzoyl-L-phenylalanine (BPA) that, when activated by irradiation with UV light, can form covalent bonds with a variety of moieties within 10 Å (Chin et al., 2002; Kauer et al., 1986). We introduced BPA at 9 different positions of SutA (6, 11, 22, 54, 61, 74, 84, 89, or 100), formed complexes with purified E and each of the BPA-modified SutA proteins, irradiated them with UV light, and visualized cross-linked species following SDS-PAGE (Figure 3 – figure supplement 2). For the most efficient cross-linkers (BPA at positions 54 and 84), we determined the sites of the cross-links on RNAP by identifying cross-linked peptides via StavroX (Götze et al., 2012) analysis of LC-MS/MS data after tryptic digest of the complexes (Figure 3 – figure supplement 4).

Both cross-linking approaches identified interactions between the central region of SutA and the β1 domain or nearby regions of the β subunit of RNAP (Figure 3A and B, green and orange). All SutA residues participating in the cross-links were within (BS^3) or just outside (BPA) the α-helical region. BPA cross-linking is sensitive to the orientations of the interacting residues, so BPA positions within the helix that did not cross-link may not have been oriented optimally for the cross-linking reaction to occur.

To identify the positions of the N- and C-tails, we designed variants of SutA for affinity cleavage experiments. We introduced cysteine residues at SutA position 2, 32, or 98 and conjugated the chelated iron reagent, iron-(S)-1-[*p*-(bromoacetamido)benzyl]EDTA (FeBABE), to these cysteines. FeBABE catalyzes localized (estimated to occur within 12 Å of the FeBABE moiety) hydroxyl radical cleavage reactions following exposure to ascorbate and peroxide (Meares et al., 2003). We assembled complexes with the FeBABE-modified SutA variants and RNAP, initiated the cleavage reactions, and analyzed the cleavage products by SDS-PAGE followed by Western blotting with an antibody against the C-terminus of β. To map the FeBABE cleavage positions, cleavage products were compared to β fragments of known sizes (Figure 3 – figure supplement 5). While the strongest cleavage product of the N-terminal FeBABE (at residue 2; N-Fe) was in the cleft between the β1 domain and the adjacent β2 domain (also called the β lobe), the strongest cleavage products of the C-terminal FeBABE (at residue 98; C-Fe) were in the long α-helix on the inside surface of β1, amongst the BS^3 and BPA cross-linking sites (Figure 3A). The FeBABE at residue 32 was able to cleave at both β positions, suggesting that the N-tail is mobile to some degree even in the context of binding to RNAP.

While most of the cross-links and cleavages mapped to β1 or the adjacent cleft, a cross-link was also detected between the 84 BPA position and β967, a residue located in βi9, an insertion in the β flap domain (Opalka et al., 2010). Additionally, weaker cleavage products for the N-Fe and C-Fe variants were detected at β721 and β1058 respectively, which are situated on either side of the βi9 (Figure 3B). We

consider this to represent a second, weaker site, because β967 is too far from the β residues 484 and 493 that formed BPA cross-links for all of them to be reached from a single, stably bound position of the SutA 84. However, we note that we did not detect more than one shifted band after cross-linking with the 54 or 84 BPA variants (Figure 3 – figure supplement 2), suggesting that two separate sites on β are not likely to be occupied by two SutA molecules at the same time. Instead, it may be that SutA binding to a surface on the outside of the β1 domain, combined with rotation or translation of SutA along that surface and in conjunction with its flexibility, could allow for all of the observed cross-links and cleavages.

To corroborate SutA-β interaction without cross-linking or cleavage and to interrogate which residues of SutA might directly participate therein, we conducted an NMR experiment. We were able to purify only a small amount of soluble β1 domain (colored darker blue in Figure 3C), which we mixed with an equimolar amount of ^{15}N-labeled full-length SutA. As a control to rule out non-specific interactions, we mixed SutA with an equimolar amount of σ^S, which does not appear to bind SutA. Several SutA residues showed chemical shift perturbations in the β1 mixture, compared to the σ^S mixture (Figure 3D). Interestingly, three of these residues, K95, D97 and K99, would be on the same side of an extended peptide chain, supporting the interpretation that the C-tail contributes to SutA binding. The other perturbed residues flank the α-helix, suggesting that the regions at the junctions with the flexible tails may change conformation upon binding to β.

SutA competes with both σ^{70} and DNA for binding to RNAP

Having established the site of SutA interaction with core RNAP, we next examined how the presence of promoter DNA or σ factor might impact SutA binding to β1, and focused on the *rrn* promoter. In the *E. coli rrn* P1 promoter complex, the melted non-template DNA strand is located near β1, and interactions among the DNA, σ and β regulate transcription initiation (Feklistov and Darst, 2011; Haugen et al., 2006;

NandyMazumdar et al.; Winkelman et al., 2015). SutA does not bind to dsDNA on its own, but we considered a possibility that it could change the dynamics of these interactions in the context of RNAP by bringing its flexible acidic N-tail in close proximity to the path of the DNA. We also hypothesized that this binding site could explain the difference in the magnitude of SutA's impact on *rrn* initiation by $E\sigma^{70}$ compared to $E\sigma^{S}$. Both σ factors are highly conserved from *P. aeruginosa* to *E. coli*, and in both organisms, domains 2, 3, and 4 are highly similar between the two σ factors. In addition, both σ^{70} and σ^{S} have unstructured acidic regions near their N-termini (Gowrishankar et al., 2003). However, σ^{70} contains a large (~245 amino acids) insertion, termed the "non-conserved region" or NCR, which is not present in σ^{S} (Figure 4A). Crystal and cryoEM structures show that most of the NCR is situated fairly far from β1, contacting the β' subunit on the opposite side of the main channel of RNAP, but an unusually acidic stretch of ~40 residues within the NCR is too flexible to be resolved in these structures (Basu et al., 2014; Narayanan et al., 2018; Zuo and Steitz, 2015). To investigate possible interactions between this flexible acidic loop (AL) and SutA, we threaded the *P. aeruginosa* sequence onto the β subunit of an *E. coli* RNAP crystal structure (Molodtsov et al., 2017) docked that model into the recent cryoEM structure of the *E. coli* $E\sigma^{70}$ OC (Narayanan et al., 2018) and modelled the missing σ^{70} AL (using the *E. coli* sequence for both the structured and flexible regions of σ^{70}) using the MODELLER software suite (Yang et al., 2012). The highly flexible AL could occupy a wide range of positions (e.g., Figure 4A, top), some of which would stay well above the position of the DNA in the main channel (position 1) and some of which clash with the DNA as they reach into and across the main channel toward β1 (position 2). This modeling shows that σ^{70} AL is long enough and its structurally resolved ends are positioned appropriately to allow it to reach the β1 residues that participate in SutA cross-links and cleavages, especially in the absence of DNA. To determine whether the AL might contribute to the observed differences between $E\sigma^{70}$ and $E\sigma^{S}$ activation by SutA, we constructed and purified a *P. aeruginosa* σ^{70} mutant lacking residues 171-214

(ΔAL), which correspond to the region missing in the *E. coli* structure, and repeated our cross-linking and cleavage assays with or without DNA using $E\sigma^{70}$, $E\sigma^{S}$ or $E\sigma^{70}\Delta AL$ holoenzymes instead of E.

To maximize the sensitivity of our cross-linking assay, we used the SutA L54BPA variant, which gave the most efficient cross-link with the core enzyme alone, and performed Western blots using the β antibody. In the absence of DNA, $E\sigma^{70}$ produced noticeably less cross-linking than E or $E\sigma^{S}$. Interestingly, $E\sigma^{70}\Delta AL$ largely restored the cross-linking to the levels seen with E or $E\sigma^{S}$ (Figure 4C, lanes 1-4). This difference in SutA cross-linking between $E\sigma^{70}$ and $E\sigma^{70}\Delta AL$ decreased at higher SutA concentrations, as might be expected if SutA and AL are competing to occupy a similar space.

To test the effect of DNA on the SutA-β interaction, we used either a double-stranded (ds) *rrn* promoter DNA or a bubble template in which the region of the DNA that forms the transcription bubble in the OC was non-complementary (Figure 4B). The dsDNA requires σ to melt the DNA strands and will support the formation of a native population of DNA-RNAP complexes. By contrast, the bubble template obviates the need for σ and would be expected to stabilize an OC formed with the holoenzyme, but this complex may not represent the dominant native complex; the *E. coli rrn* P1, for example, does not form a stable OC (Ruff et al., 2015a). The addition of the bubble DNA had a large negative effect on SutA binding that was synergistic with the presence of σ (Figure 4C, lanes 5-8). Cross-linking could still be readily detected in the absence of σ, and to a lesser extent when σ^{S} was present, but not with either σ^{70} or $\sigma^{70}\Delta AL$; longer exposures revealed that cross-linking did occur at low efficiency (Figure 4 – figure supplement 1). Addition of dsDNA allowed more SutA binding than the bubble template, but still less than was seen in the absence of DNA (Figure 4C, lanes 9-11), suggesting that the artificial bubble OC lacks the native intermediate to which SutA preferentially binds.

To test the effects of DNA and σ on β interactions with the SutA tails, we used FeBABE cleavage assays with the N-Fe and C-Fe SutA variants (Figure 4D). While the results were consistent with those obtained

by BPA cross-linking, we also observed that the cleavage induced by C-Fe SutA was increased in the ΔAL mutant, whereas the N-Fe cleavages were either unaffected or inhibited. This result suggests that AL may clash specifically with the C-tail of SutA.

We failed to detect either cross-linking to or cleavage of the *E. coli* Eσ^{70} (Figure 4 – figure supplements 1 and 2). This is consistent with our observation that overexpression of SutA in *E. coli* fails to upregulate *rrn* expression and suggests that the interaction between SutA and the *P. aeruginosa* RNAP is species-specific.

SutA enhances RNAP-DNA interaction on the *rrn* promoter, and its tails access the transcription bubble DNA

Given that promoter DNA reduces SutA cross-linking to RNAP, we might predict the corollary: SutA would reduce the RNAP-DNA interaction through its competition with promoter DNA. But this would be counterintuitive for a factor that enhances transcription. To investigate how SutA affects the RNAP-DNA interaction, we measured permanganate reactivity of the template strand of the *rrn* promoter, in the presence of different holoenzymes and SutA variants. Permanganate can oxidize thymines (and to a lesser extent, cytidines and guanines) only when the DNA bases are unstacked, as occurs when it is single-stranded, so reactivity can be used to detect promoter melting by RNAP (Kahle and Paule, 2009). We detected intense bands corresponding to oxidation of bases -12 to -9 upstream of the transcription start site, indicative of the population of OCs in which the σ factor has mediated strand opening (Figure 5A), but because the *P. aeruginosa rrn* promoter template strand lacks any thymines downstream of -9, we cannot distinguish between early and late OC intermediates (see Discussion). We carried out the footprinting experiments in triplicate and quantified the signal from the -12 to -9 footprint to serve as a measure of the steady state amount of strand-separated OCs (Figure 5B); Figure 5A shows one representative set of measurements. The addition of WT SutA did not have a significant negative effect

on the interaction between RNAP and the *rrn* promoter DNA in any of the holoenzyme contexts. For $E\sigma^S$, the addition of either 250 nM or 2 μM SutA actually increased the RNAP-DNA interaction (although the effect is only statistically significant at 2 μM SutA), suggesting that in this context, SutA may even stabilize at least one OC intermediate in which the DNA strands are melted. For $E\sigma^{70}$, the footprints are stronger overall but the effect of SutA is very subtle, and peaks at 250 nM SutA. Also, for both holoenzymes, deletion of the C-tail of SutA has a negative effect on the RNAP-DNA interaction, possibly suggesting that it can contribute to stability of some RNAP-DNA-SutA complexes as well as RNAP-SutA interactions, consistent with its effects on SutA *in vitro* transcription activity (Figure 2). Although the ΔAL had a substantial effect on the RNAP-SutA interaction, it appears to have only very mild effects on the RNAP-DNA interaction, consistent with mild effects on transcription activity (Figure 4 – figure supplement 3).

Based on the positions of the SutA cross-links and evidence that it can enhance RNAP-DNA interactions in some contexts, we expected that we should be able to detect evidence of SutA-DNA proximity in a ternary complex containing holoenzyme, SutA, and DNA. To test this, we measured FeBABE SutA-dependent cleavage of the template and non-template DNA strands using primer extension. We saw stronger cleavage with $E\sigma^S$ than with $E\sigma^{70}$, but in both cases the cleavage was fairly weak, as might be expected for a factor that does not directly bind DNA (Figure 5C). In the $E\sigma^S$ complex, the C-Fe induced cleavage of both strands between residues -8 and -12, suggesting that it remains near the upstream fork junction of the transcription bubble. The N-Fe cleaves the template strand near the upstream junction but also cleaves both strands further downstream. For $E\sigma^{70}$, the cleavage was weaker overall and showed a different pattern; for C-Fe in particular, more cleavage took place on the downstream region of the non-template strand. This difference could reflect the fact that σ^{70} AL seems to compete with the C-terminus of SutA, potentially causing it to favor a slightly different position in the ternary complex.

SutA does not directly stabilize the *rrn* OC formed by Eσ^{70} holoenzyme

In *E. coli*, control of rRNA synthesis is dictated by an inherent instability of the *rrn* P1 OC. DksA/ppGpp further destabilize the complex, inhibiting transcription, whereas the initiating nucleotide (iNTP) exerts an opposite effect (Paul et al., 2004a). Accordingly, we wanted to determine 1) whether the *P. aeruginosa rrn* OC is also unstable and sensitive to these inputs, and 2) whether SutA affects the OC stability. First, we purified the *P. aeruginosa* DksA, and measured transcription from the *rrn* promoter by Eσ^{70}, in the presence or absence of SutA and also DksA plus ppGpp (Figure 6A, Figure 6 – figure supplement 1). As observed in *E. coli*, DksA and ppGpp strongly repressed *rrn* transcription. When SutA and DksA/ppGpp were added together, it appeared that SutA might still have a small positive effect (though this effect is not statistically significant), but it certainly did not reverse the strong repression by DksA/ppGpp, suggesting that SutA functions in a different way. Next, we measured *rrn* transcription at different [iNTPs] (Figure 6B, Figure 6 – figure supplement 2). Also consistent with observations in *E. coli*, transcription was strongly repressed at low [iNTPs], but SutA had no effect at the lowest concentration, and similar small effects at two higher concentrations. Finally, we directly measured the half-life of the (heparin-resistant) Eσ^{70} OC in a transcription-based assay. In contrast to what has been seen in *E. coli*, we detected some OC at standard salt concentrations and on a linear template, but its half-life was quite short, at about 45 seconds. Addition of SutA at 125 or 500 nM had no significant effect (Figure 6C, Figure 6 – figure supplement 3). Taken together, these results suggest that while the *P. aeruginosa rrn* promoter forms an inherently unstable OC, which is sensitive to regulatory inputs that utilize its instability, SutA does not appear to function by directly countering the OC dissociation.

To explore further the relationship between the OC and SutA activity, we used a premelted bubble template (Figure 4B, Figure 6D, Figure 6 – figure supplement 4). Any effects that SutA has on the formation (or stability) of the OC should no longer impact transcription from this template, since the OC

cannot collapse. SutA still had a small effect on initiation by $E\sigma^{70}$ in the context of the bubble template (Figure 6D, black symbols), but less than was observed with the dsDNA template (Figure 6D, black lines), suggesting that it may act both by contributing to formation of the OC (the fraction of the activity that is lost in the bubble template) and by having an additional effect independent of OC formation. We also measured initiation on the bubble template by $E\sigma^{S}$. Interestingly, transcription was much more robust than was seen with the dsDNA template (Figure 6D, compare red symbols to red lines), and the effects of SutA were much smaller. We were unable to reliably measure the effects of SutA on $E\sigma^{S}$ OC stability due to low signal, especially in the absence of SutA, but these results suggest that facilitating OC formation and/or stabilization are the major function for SutA in this context. The residual impact of SutA on the bubble template is similar to that seen for $E\sigma^{70}$.

SutA destabilizes RNAP-DNA interactions on the *bcn* promoter

In contrast to its activation of the *pepB* and *rrn* promoters, SutA directly represses the *bcn* promoter *in vitro* (Figure 2). Even though this effect is different than that observed *in vivo*, we were interested in exploring the mechanistic differences between the *bcn* and *rrn* promoters. We found that *bcn* OC was very stable, with a measured half-life of about 60 minutes (Figure 7A, Figure 7 – figure supplement 1) that was unaffected by SutA. *bcn* behavior in the other assays was very different from the *rrn* promoter — the cross-linking, cleavage, and footprinting results suggest that SutA and the *bcn* promoter DNA are mutually destabilizing for interactions with RNAP. First, SutA seems to interact much less efficiently with $E\sigma^{70}$ in the presence of the *bcn* compared to the *rrn* promoter (Figure 7B; data for *rrn* promoter is the same as in Figure 4C/D and is shown again for direct comparison). Nevertheless, SutA disrupts the interaction between the promoter DNA and RNAP as reported by permanganate footprinting; this effect is mediated by the N-tail and is particularly strong for the ΔAL holoenzyme (Figure 7C, D, and Figure 7 – figure supplement 2). We were unable to detect any significant cleavage of the *bcn* DNA by the SutA

FeBABE variants, as would be expected if the ternary complex were rare or unstable (Figure 7 – figure supplement 3). Taken together, these results suggest that, in contrast to its activity on the *rrn* promoter, SutA inhibits OC formation on the *bcn* promoter, and that this activity is dependent on its N-tail.

DISCUSSION

The advent of inexpensive, high-throughput sequencing has opened a new window into the transcriptional activities of bacteria, many representing previously unknown species, living in a plethora of environments. This information explosion invites reconsideration of how our basic models for mechanisms of transcriptional regulation relate to the conditions experienced by diverse bacteria in nature. In particular, mechanisms for modulating transcriptional dynamics during prolonged starvation for nutrients, a pervasive condition in many environments, have not been extensively studied. We viewed SutA as a vehicle through which to gain insight into such dynamics in *P. aeruginosa*. Our previous work showed that SutA is upregulated specifically under conditions of slow growth or growth arrest, that it binds directly to RNAP, and that it modulates expression of hundreds of genes, including the highly regulated *rrn* operon. Our goal in this study was to investigate how SutA might affect RNAP function, by determining its structural characteristics and binding site on RNAP, and by measuring its direct effects on transcription initiation *in vitro* on *rrn* and two other promoters that appeared strongly affected *in vivo*.

SutA has no homology to any previously described domain but its sequence predicts large regions of intrinsic disorder surrounding a short central α-helix, as we confirmed by NMR. Importantly, its completely disordered N-tail is critical for its function, while the C-tail, which displayed some signs of order but no classical secondary structure elements, contributes to binding RNAP. Although the extreme flexibility of SutA and the relatively large distances over which our cross-linking and cleavage reagents could act (10-25 Å) preclude precise docking of SutA onto RNAP, a binding site on the outside

of the β1 domain is consistent with our data. Most of the β1 residues are identical (72%) or similar (87%) between *E. coli* and *P. aeruginosa*, but two less-conserved loops contain residues involved in BS^3 cross-linking (K45 and K116) and could contribute to the observed species specificity. From such a binding site for the SutA helix, its flexible tails can still reach around either side of the β1 domain into the region occupied by the open transcription bubble. Although the binding site of SutA is distinct from binding sites of previously characterized regulators, recent structures of other highly flexible transcription modulators that bind elsewhere have shown that unstructured elements can reach deep into RNAP to alter its function (Kang et al., 2017).

Transcriptional regulators that do not bind DNA directly must exert their effects by altering the conformation of RNAP and /or DNA and can thus regulate many different promoters either positively or negatively, depending on the promoter properties. Our findings that SutA modulates expression of numerous genes (Babin et al., 2016) and has distinct promoter-dependent effects (this work) conform to general expectations of regulators that do not bind DNA. Our results also suggest that SutA interactions with RNAP are modulated by a long flexible acidic loop present in σ^{70} but not σ^{S}, explaining in part the σ-specific effects of SutA. Although the σ^{70}AL has not been previously implicated in transcription regulation, other mobile elements of the β, β' and σ RNAP subunits have been shown to contribute to OC formation and stability (Hook-Barnard and Hinton, 2009; NandyMazumdar et al.; Ruff et al., 2015a) and to be targeted by regulators that can interrupt the initiation pathway by locking these flexible modules in place (Bae et al., 2013).

A detailed understanding of the manner by which SutA alters the conformations of specific RNAP - promoter complexes, and how these alterations lead to the observed effects on initiation, awaits future studies, but viewing our results in the context of the paradigm established by extensive studies in *E. coli* provides a model for consideration. During initiation, RNAP binds to the promoter DNA through contacts

primarily established by σ to form a closed complex, setting in motion a series of steps in which RNAP bends and opens the DNA duplex to form an initial unstable OC in which σ holds the non-template strand. The initial OC then isomerizes (through a series of intermediates that are likely different for different promoters) into a final OC, in which the bubble encompasses -12 to +1, the downstream DNA is held tightly, and the iNTP can load into the active site (Ruff et al., 2015b). The stability of the final OC varies tremendously among different promoters (Ruff et al., 2015b). Decades of studies of rRNA synthesis in *E. coli* have identified the unique properties of the *rrn* P1 promoter that make it one of the strongest promoters, but also very sensitive to regulation. A combination of suboptimal spacing (16 bp) between the near consensus -35 and -10 hexamers, a GC-rich 8-nt (as compared to the optimal 6-nt) discriminator region that separates the -10 hexamer and the +1 position, and a C residue 2 nt downstream of the -10 hexamer that cannot make productive contacts to σ^{70} lead to very short-lived OCs in which the non-template DNA is scrunched by 2 nts and extruded into solution between β1 and β2 domains (Haugen et al., 2006; Winkelman et al., 2016; Winkelman et al., 2015). Importantly, the *rrn* P1 OC does not appear to undergo the final isomerization steps to reach the stable final OC (Ruff et al., 2015b).

While detailed information is not available for *P. aeruginosa rrn* promoter complexes, they have all the canonical *rrn* P1 features except that the discriminator is 7 instead of 8 nt. Consistently, our data show DksA /ppGpp repression, iNTP sensitivity, and an OC half-life that is quite short (45 s), although not as short as that for *E. coli rrn* (~1 s), a difference that is likely due to the shorter discriminator (Henderson et al., 2017). We note that promoters with 7-nt discriminators also form 1-nt pre-scrunched and unstable OCs; interestingly, the region proposed to accommodate the scrunched non-template strand is the cleft adjacent to β1 where most of our SutA cross-links and cleavages occurred (Winkelman et al., 2015). In contrast, promoters with 6-nt discriminators make favorable contacts to σ and are much more

stable (Henderson et al., 2017); *bcn* is such a promoter, with a 6-nt discriminator and long (~60 min) OC half-life.

Unlike DksA, which exerts its effects by destabilizing OCs (Paul et al., 2004a), our data suggest that SutA does not alter the OC stability at either the *rrn* or *bcn* promoter, perhaps because SutA does not appear to efficiently bind stable $E\sigma^{70}$ OC, represented by the *rrn* bubble template and the naturally stable OC formed on the *bcn* promoter. SutA increases transcription from *rrn*, but represses transcription from *bcn* *in vitro*. As proposed for DksA (Rutherford et al., 2009), these opposing effects could be due to SutA acting to lower the free energy of an OC intermediate or change the activation barriers of different transition steps *en route* to the final OC on these two (and other) promoters. Interestingly, *in vivo*, the effects of SutA on the *bcn* promoter are positive and the strongest that we observed for any gene in the genome (Babin et al., 2016). Several possibilities to explain this discrepancy could fit within the outlines of this model, but broadly, the participation of an additional cellular factor that changes the characteristics of the intermediate with which SutA interacts could have the effect of flipping its influence on transcription from negative to positive. Identifying such a factor is an interesting objective for future work.

SutA effects on the global transcriptome could also be nuanced through its distinct interactions with holoenzymes formed with σ^{70} and σ^{S}, closely related σ factors with partially overlapping promoter specificities (Feklistov et al., 2014; Schulz et al., 2015). The C-tail of SutA may be a key contributor to these differences. Our NMR analysis suggests that residues in the C-tail directly participate in binding to β1, yet the interaction of the C-tail with RNAP is inhibited by the σ^{70} AL in the context of the holoenzyme. Consistent with these observations, the C-tail is more important for activation of *rrn* and *pepB,* and makes a bigger contribution to enhancing the RNAP-DNA interaction in the context of $E\sigma^{S}$. Taken together, these results suggest that SutA may play a more important stabilizing role for some OC

intermediate formed by $E\sigma^S$ than it does in the context of $E\sigma^{70}$ (Figure 8). Interestingly, both σ factors seem to have a small residual positive effect on initiation even when the OC is pre-formed and stabilized, as is the case for the artificial bubble template. We do not know the nature of this effect, but our published ChIP-Seq data (Babin et al., 2016) suggest that SutA can associate with elongating RNAP, and are consistent with the notion that SutA could influence RNA synthesis at stages after the formation of the OC.

In conclusion, this work has provided structural and functional insight into how SutA can impact RNAP in growth-arrested cells. Many intriguing questions remain: First, what are the promoter characteristics that SutA recognizes to favor transcription from some yet disfavor transcription from others and thus redistribute transcriptional resources in energy-limited cells? Second, how does SutA navigate changes in $E\sigma^S$ vs. $E\sigma^{70}$ abundance over different phases of growth and growth arrest so as to efficiently optimize expression of a subset of genes? Third, what other factors interact with SutA during slow growth and dormancy? Fully understanding the regulatory architecture that gives rise to the impressive ability of *P. aeruginosa* to tolerate slow-growth and dormancy is a long-term challenge, yet an improved mechanistic understanding of SutA, a global regulator active in these states, represents an important step towards that end.

ACKNOWLEDGEMENTS

We thank Ben Ramirez (University of Illinois at Chicago) for helping us with preliminary NMR studies of SutA, Jacqueline Barton (Caltech) for giving us access to her lab to perform experiments involving radioactivity, Nate Glasser for help with HPLC measurements to quantify SutA, Hsiau-Wei (Jack) Lee and Aimee Marceau (University of California, Santa Cruz) for help with the NMR binding experiment, Weidong Hu (City of Hope) for help with NMR experiments using the Bruker AV III 700 MHz

spectrometer, and Julia Kardon, Niels Bradshaw (Brandeis University), and members of the Newman lab for feedback on the project at different stages. MB was supported by a post-doctoral fellowship from the Cystic Fibrosis Foundation. Grants from the NIH (GM067153) to IA and grants from the HHMI and NIH (5R01HL117328-03 and 1R01AI127850-01A1) to DKN supported this work. The Proteome Exploration Laboratory is supported by the Beckman Institute and NIH 1S10OD02001301. This work was supported by the Institute for Collaborative Biotechnologies through grant W911NF-09-0001 from the U.S. Army Research Office. The content of the information does not necessarily reflect the position or the policy of the Government, and no official endorsement should be inferred.

MATERIALS AND METHODS

Media and Growth Conditions. All cultures were grown at 37 °C with shaking unless otherwise noted. Liquid media were LB (5 g yeast extract, 10 g tryptone, 10 g NaCl per liter), Terrific Broth (TB) (24 g of yeast extract, 20 g of tryptone, and 4 mL of glycerol per liter, buffered to pH 7.0 with 18.9 mM potassium phosphate), or phosphate buffered minimal medium (35.9 mM K_2HPO_4, 14.2 mM KH_2PO_4, 9.3 mM NH_4Cl, 42.8 mM NaCl, 1.0 mM $MgSO_4$, 7.5 µM $FeCl_2{\cdot}4H_2O$, 0.8 µM $CoCl_2{\cdot}6H_2O$, 0.5 µM $MnCl_2{\cdot}4H_2O$, 0.5 µM $ZnCl_2$, 0.2 µM $Na_2MoO_4{\cdot}2H_2O$, 0.1 µM $NiCl_2{\cdot}6H_2O$, 0.1 µM H_3BO_3, 0.01 µM $CuCl_2{\cdot}2H_2O$) with 40 mM sodium pyruvate added as a carbon source.

Strain and plasmid construction. See Table 2 (strains and plasmids) and Table 3 (primers) for relevant details. In general, standard methods were used for plasmid and strain construction. The strains with constructs for arabinose-inducible overexpression of SutA or its N- or C-tail truncations were made by introducing the relevant pUC18T-mini-Tn7T-Gm^R construct (DKN1639, DKN1876, or DKN1877) into *P. aeruginosa* UCBPP-PA14 *ΔsutA* (DKN1625) or *ΔsutAΔrpoS* (DKN1955) by tetraparental conjugation, as

previously described (Choi and Schweizer, 2006). DKN1876 and DKN1877 were generated using outward-facing primers followed by blunt ligation of the DKN1639 plasmid. To generate the *ΔsutAΔrpoS* strain, the *sutA* gene was cleanly deleted from the *ΔrpoS* strain (Basta et al., 2017) by conjugation with strain DKN1637 and then counterselection as previously described (Babin et al., 2016). For comparing the effects of SutA overexpression in *E. coli* to its effects in *P. aeruginosa*, either the expression plasmid (from strain DKN1640) or the empty vector (from strain DKN548 (Shanks et al., 2006)) was transformed by electroporation into either the *P. aeruginosa ΔsutA* strain (DKN1625) or *E. coli* MG1655 (DKN81). For overexpression and Ni-NTA purification of SutA, a plasmid in which the an HA-tagged *sutA* gene had been amplified and cloned into the multiple cloning site of pQE-80L (Qiagen) between the BamHI and HindIII restriction sites (DKN1643) was amplified using outward-directed primers flanking the sequence for the HA tag (not amplifying it) and encoding the TEV cleavage site. The PCR product was phosphorylated and subjected to a blunt end ligation to generate the plasmid encoding a 6His-TEV-SutA construct, and this was transformed into BL31 DE3 cells to generate strain DKN 1697. This construct was subjected to site directed mutagenesis using outward-facing primers encoding the desired changes to generate all of the SutA variant constructs used in this study (DKN1879-DKN1892), except SutA 46-101 (DKN1878). Sequences of SutA46-101, DksA (DKN1893) and *rpoB* β1 (DKN1895) were cloned out of genomic DNA from *P. aeruginosa* UCBPP-PA14 and into the pQE-80L plasmid from strain DKN1697, replacing the SutA sequence but retaining the TEV cleavage site, using Gibson assembly (Gibson, 2011). The *rpoD* and *rpoS* sequences were cloned from *P. aeruginosa* gDNA and into the pET15b vector (DKN1901 and DKN1894, respectively), as expressing *rpoD*from pQE-80L proved somewhat toxic to *E. coli*. The σ^{70}Δ171-214 construct (DKN1902) was generated using outward facing primers and blunt-end ligation of the plasmid from strain DKN1901. Fragments of βto use as standards in the affinity cleavage experiment were cloned from *P. aeruginosa* gDNA into pQE-80L, removing the sequence for the 6xHis

affinity tag and TEV cleavage site, by Gibson assembly (DKN1896-DKN1900). Template sequences were cloned from *P. aeruginosa* gDNA into the pUC18 vector (DKN1903-DKN1905).

Protein purification.

RNAP: RNAP was purified from the *P. aeruginosa ΔsutA* strain essentially as previously described ((Kuznedelov et al., 2011) and references therein). Briefly, cells were grown in 6 L of TB to an OD_{600} of approximately 1.0. Cells were washed with TBS and pellets were frozen at -80 °C. Cell pellets were resuspended in 90 mL RNAP lysis buffer (50 mM Tris pH 8.0, 100 mM NaCl, 1 mM EDTA, and cOmplete complete Ultra EDTA-free protease inhibitor tablets (Roche)) containing 40 Kunitz units DNAseI and cells were lysed by passage through an EmulsiFlex-C3 (Avestin). Lysates were clarified by centrifugation at 12,000 xg, and nucleic acids and acidic proteins were precipitated by addition of a 10% polyethyleneimine (polymin P; Sigma-Aldrich) solution at pH 7.9 to a final concentration of 0.5%. Precipitated protein was pelleted, washed with TGEB (10 mM Tris pH 8.0, 5% glycerol, 0.1 mM EDTA, 10 mM β-mercaptoethanol) plus 0.3 M NaCl, and the RNAP fraction was eluted with TGEB plus 1 M NaCl. Residual polymin P was removed by ammonium sulfate precipitation (2M). The ammonium sulfate pellet was resuspended in TGEB and loaded onto a 50 mL Heparin Sepharose 6 Fast Flow column (GE Healthcare). The column was washed with 2 column volumes of TGEB plus 0.3 M NaCl, and RNAP was eluted with a step to TGEB plus 0.6 M NaCl. The elution fraction was precipitated with 2 M ammonium sulfate, and resuspended into approximately 1 mL of TGEB plus 0.5 M NaCl. Low molecular weight contaminants were removed via size exclusion chromatography on a HiPrep 16/60 Sephacryl S-300 HR column (GE Healthcare). Fractions containing RNAP were diluted in TGEB to a final NaCl concentration of 0.3 M and loaded onto a HiTrap Q HP 5 mL column (GE Healthcare). RNAP was eluted into TGEB with a gradient between 0.3 M and 0.5 M NaCl over 20 column volumes. RNAP was dialyzed into RNAP storage buffer (20 mM Tris-HCl pH 8.0, 0.1 mM EDTA, 10 mM β-mercaptoethanol, 100 mM NaCl, 20% glycerol),

concentrated to 1.4 mg/mL and frozen at -80 °C. The total yield was approximately 2.9 mg of high purity core enzyme.

6xHis-tagged proteins: For all tagged proteins, the following central steps were in common, and initial protein expression and lysis steps, plus additional purification steps specific to each protein are detailed below: Soluble protein was mixed with His-Pur Ni-NTA beads (Thermo Scientific or Clontech) in batch and binding was allowed to occur for 1h at 4 °C. Beads were washed three times with lysis buffer containing 20 mM imidazole and eluted three times with lysis buffer containing 250-500 mM imidazole. Eluents were combined, loaded onto an Amicon 3 or 10 kDa centrifugal filter (EMD Millipore), and buffer exchanged to TEV-digestion buffer (50 mM Tris pH 8.0, 0.5 mM EDTA, and 1 mM DTT). The 6xHis-tag was cleaved by addition of His-tagged TEV protease in a 1:50 mass ratio and incubation overnight at 4 °C. The digested sample was reapplied to His-Pur Ni-NTA, and washed with lysis buffer containing 20 mM imidazole; the protein of interest remained unbound or was eluted in this wash step, while the cleaved peptide tag and His-tagged TEV protease remained bound to the resin. The cleaved protein product includes the native protein sequence with an additional N-terminal serine (or glycine for σ^{70}purified from the pET15b vector).

SutA (unlabeled): Strain DKN1697 was grown with 200 μg/ml ampicillin. A 20 mL culture grown overnight in LB was distributed between two flasks, each containing one liter of 2xYT and grown at 37 °C to OD_{600}=0.6. Protein expression was induced by addition of 1 mM isopropyl β-D-1-thiogalactopyranoside (IPTG) and expression was allowed to continue for 4 hr. Cells were pelleted and frozen at -80 °C. Pellets were resuspended in lysis buffer (40 mM NaH_2PO_4, 300 mM NaCl, pH 8) containing 5 mM imidazole, 1 mg/mL lysozyme, and cOmplete mini protease inhibitor, EDTA free and lysed by probe sonication. The lysate was treated with Benzonase Nuclease on ice for 30 min and centrifuged. Following TEV cleavage of the SutA protein, the protein was concentrated on an Amicon

Ultra-15 centrifugal filter, applied to a Superdex 75 10/300 column, buffer exchanged to SutA storage buffer (25 mM Tris pH 8, 100 mM NaCl, 20% glycerol, and 2 mM β-mercaptoethanol), and stored at -80 °C.

SutA 46-101 ($^{15}N^{13}C$): Strain DKN1878 was grown overnight in 10 ml LB and then split between two baffled flasks containing M9 minimal salts medium (6 g/L sodium phosphate dibasic, 3 g/L potassium phosphate monobasic, 0.5 g/L NaCl, 1 g/L $^{15}NH_4Cl$ (Cambridge Isotope Laboratories, Cambridge MA), 2.5 g/L ^{13}C glucose(Cambridge Isotope Laboratories)) supplemented with 100 µg/ml carbenicillin (Gold Bio), 1 mM $MgSO_4$, 300 µM $CaCl_2$ and trace metals (7.5 µM $FeCl_2 \cdot 4H_2O$, 0.8 µM $CoCl_2 \cdot 6H_2O$, 0.5 µM $MnCl_2 \cdot 4H_2O$, 0.5 µM $ZnCl_2$, 0.2 µM $Na_2MoO_4 \cdot 2H_2O$, 0.1 µM $NiCl_2 \cdot 6H_2O$, 0.1 µM H_3BO_3, 0.01 µM $CuCl_2 \cdot 2H_2O$). Cultures were grown at 37 °C until they reached mid-exponential phase (8 hrs) and then protein expression was induced by adding IPTG to a final concentration of 1 mM. Cells were harvested after 5 hr of induction and frozen at -80 °C. Pellets were resuspended in lysis buffer (50 mM sodium phosphate, pH 8.0, 300 mM NaCl, 5 mM imidazole) plus 20 Kunitz units DNaseI and EDTA-free cOmplete mini protease inhibitor tablets (Roche) and lysed by passage through an EmulsiFlex-C3. Following TEV cleavage, the protein was concentrated and loaded onto a Hi-Load 16/600 Superdex75 pg size exclusion column, buffer exchanging into the NMR buffer containing 20 mM sodium phosphate pH 7.0 and 100 mM sodium chloride.

SutA WT ($^{15}N^{13}C$): Strain DKN1697 was grown, protein expression induced, and cells lysed as described for the SutA 46-101 ($^{15}N^{13}C$) protein. As an additional purification step following TEV cleavage, the protein was concentrated and buffer exchanged into a buffer containing 20 mM N-methylpiperazine, pH 5.0, and 100 mM NaCl and loaded onto a 5 ml HiTrap Q Sepharose fast flow anion exchange column (GE Healthcare Life Sciences). The protein was eluted with a 20 column-volume gradient to 600 mM NaCl

and then was concentrated to 1 ml before size exclusion chromatography as described for the SutA 46-101 ($^{15}N^{13}C$) protein.

SutA WT (^{15}N): Protein was produced and purified as described for the SutA WT ($^{15}N^{13}C$) protein, except glucose with the natural carbon isotope ratios was used at 4 g/L.

SutAΔN unlabeled: Strain DKN1879 was grown overnight in 5 ml LB then diluted 1:200 into TB plus 100 µg/ml carbenicillin and grown at 37 °C. Expression was induced when the culture reached mid-exponential phase with 1 mM IPTG and cells were harvested after 4 hrs of induction. Lysis and purification steps were the same as described for the SutA 46-101 ($^{15}N^{13}C$) protein, and the final protein storage buffer was 25 mM Tris pH 8, 100 mM NaCl, 20% glycerol, and 2 mM β-mercaptoethanol.

SutAΔC unlabeled: Strain DKN1880 was used, and all expression and purification steps were the same as for the unlabeled SutAΔN protein.

SutAΔN (^{15}N): Strain DKN1879 was used, and all expression and purification steps were the same as for the SutA 46-101 ($^{15}N^{13}C$) protein, except glucose with the natural carbon isotope ratios was used at 4 g/L.

SutAΔC (^{15}N): Strain DKN1880 was used, and all expression and purification steps were the same as for the SutA 46-101 ($^{15}N^{13}C$) protein, except glucose with the natural carbon isotope ratios was used at 4 g/L.

SutA BPA variants: *E. coli* BL21 DE3 was co-transformed with pEVOL-pBpF (Chin et al., 2002) and the plasmids from strains DKN1881-DKN1889 (pQE80L-6xHis-TEV-SutA amber mutants). Approximately 20 colonies were scraped from the agar plate and grown at 33 °C in LB to OD600 = 0.6. Cultures were treated with 1 mM BPA (Iris-Biotech, Marktredwitz, Germany) and 1 mM IPTG and incubated in the dark for 20 h. Cells were pelleted and frozen at -80 °C. Pellets were resuspended in lysis buffer (40 mM

NaH2PO4, 300 mM NaCl, pH 8) containing 5 mM imidazole, 1 mg/mL lysozyme, and cOmplete mini protease inhibitor, EDTA free and lysed by probe sonication. The lysate was treated with Benzonase Nuclease on ice for 30 min and centrifuged. Following TEV cleavage, SutA fractions were pooled and loaded onto an Amicon 10 kDa centrifugal filter, and buffer exchanged to SutA storage buffer (25 mM Tris pH 8, 100 mM NaCl, 20% glycerol), and stored at -80°C.

SutA FeBABE variants: Plasmids from strains DKN1890-DKN1892 were transformed into BL21(DE3) cells by electroporation. Expression and purification steps were the same as for the SutAΔN unlabeled protein.

β1: Strain DKN1895 was used. An overnight culture was grown in LB plus 100 µg/ml carbenicillin and 10 µg/ml gentamicin at 37 °C. The culture was diluted 1:100 into TB and grown for 3 hrs without antibiotics at 30 °C. The culture was cooled to 13 °C and expression was induced for 24 hrs with 400 µg/ml IPTG. Cell pellets were collected and frozen at -80 °C. Pellets were resuspended in a modified RNAP purification buffer (20 mM Tris pH 7.6, 5% glycerol, 3 mM 2-mercaptoethanol, 200 mM NaCl, 10 mM imidazole) plus 20 Kunitz units DNaseI and EDTA-free cOmplete mini protease inhibitor tablets (Roche) and lysed by passage through an EmulsiFlex-C3 (Avestin). Much of the expressed protein was not soluble, but the soluble fraction was bound in batch to Ni-NTA beads, washed, eluted, and its TEV tag cleaved as described above, except TEV was used at a mass ratio of 1:25. Following TEV cleavage, the protein was concentrated to 1 ml in SEC buffer (30 mM Tris pH 7.6, 120 mM NaCl, 0.1 mM EDTA, 5% glycerol, 2.1 mM 2-mercaptoethanol) and passed over a HiLoad 16/600 Superdex 200 pg column. Fractions containing the protein of interest were collected and concentrated, and the glycerol concentration was brought to 20% before storage at -80 °C.

σ^{70}: Strain DKN1901 was grown overnight in LB containing 100 µg/ml carbenicillin, then diluted 1:1000 into TB. After 4 hr growth, the culture was cooled to 16 °C and expression was induced with 400 µg/ml

IPTG for 18 hr. Cell pellets were collected, and lysis and purification was carried out as described for the RpoB B1 protein.

σ^S: Strain DKN1894 was used. Expression and purification were carried out as described for the unlabeled WT SutA, except TEV cleavage was not performed and an addition size exclusion step using a Superdex 200 column was added. Final protein storage buffer included 25 mM Tris pH 8, 100 mM NaCl, 20% glycerol, and 2 mM β-mercaptoethanol.

DksA: Strain DKN1893 was used. Expression and purification were carried out as described for the unlabeled WT SutA.

σ^{70} Δ171-214: Strain DKN1902 was used. Expression and purification steps were carried out as for the full-lengthσ^{70}.

FeBABE conjugation. FeBABE was conjugated to the purified SutA S2C, S32C, and S98C proteins as described (Meares et al., 2003). Briefly, the purified proteins were de-metallated and fully reduced by incubating in a buffer containing 20 mM sodium phosphate pH 7.0, 100 mM NaCl, 20 mM EDTA, and 1 mM DTT overnight. They were then buffer exchanged into conjugation buffer (20 mM MOPS pH 8.0, 100 mM NaCl, 2 mM EDTA, 5% glycerol) using Amicon 3 kDa centrifugal filters, with care taken to reduce DTT concentrations to sub-micromolar levels. The concentration of free cysteines was measured using Ellman's reagent (see below) and this measurement was used as the SutA concentration for the FeBABE variant proteins. SutA concentrations in the labeling reactions were 25-30 µM. The FeBABE reagent (Dojindo Molecular Technologies, Rockville MD) was dissolved in DMSO to 20 mM and added to a final concentration of 300 µM in a reaction volume of 1 ml. The reaction was incubated for 1 hr at 37°C and then quenched by dilution of the FeBABE reagent via dialysis into protein storage buffer (20 mM Tris, pH 7.6, 100 mM NaCl, 20% glycerol, 0.1 mM EDTA). The concentration of free cysteines was measured again

using Ellman's reagent to determine the efficiency of FeBABE conjugation, which was as follows: S2C variant (N-Fe): 57.4% labeled; S32C variant: 37.9%; S98C variant (C-Fe): 76.3%.

Protein quantification. As we characterized SutA, it became clear that standard methods for protein quantification were very inaccurate for this protein, and that the degree and direction of the inaccuracy was different for the N- and C-terminal SutA mutants. This is likely due to the unusual amino acid composition of SutA compared to the bovine serum albumin (BSA) standard that is usually used for calibration in Bradford and BCA assays. We found that the Bradford assay (and coomassie staining of gels) greatly underestimated SutA concentration (likely due to a lack of aromatic amino acids and overabundance of acidic amino acids), and that the ΔC mutation exacerbated this problem by removing one of the two aromatic amino acids. The BCA assay slightly overestimated SutA concentration, likely due to the high accessibility of protein backbone, and this was also exacerbated in the ΔC protein, perhaps because a higher percentage of the remaining protein was the completely unstructured N-tail. Accordingly, we quantified the concentrations of our unmodified SutA proteins using total acid hydrolysis, derivatization of the resulting free amino acids, and HPLC as described below (Vendrell and Aviles, 1986). The FeBABE SutA variants were quantified using Ellman's reagent to measure their free cysteines (one per protein) before FeBABE conjugation as described below. The BPA SutA variants were quantified using the BCA assay (Thermo Fisher) according to the manufacturer's instructions, which was reasonably accurate for the full-length protein. All other proteins (RNAP core enzyme and β1 fragment, σ factors, and DksA) were quantified using the Quick Start Bradford Protein Assay (Bio-Rad) with BSA as a standard.

Ellman's reagent assay: Ellman's reagent (5,5-dithio-bis-(2-nitrobenzoic acid)) (Thermo Fisher) was dissolved in FeBABE conjugation buffer at 4 mg/ml. This stock was further diluted 1:50 into the buffer containing the protein to be assayed and distributed to the wells of a 96-well plate at 200 µl per well. 20

µl protein sample or cysteine hydrochloride monohydrate calibration standard was added, and absorbance at 412 nm was measured on a plate reader after incubation for 15 min at room temperature.

Amino acid hydrolysis and HPLC: SutA proteins prepared for NMR, which were stored in 20 mM sodium phosphate, 100 mM NaCl buffer without glycerol, were used for quantification by amino acid hydrolysis. Subsequently, the concentrations of the glycerol stocks of the corresponding unlabeled proteins were determined by quantifying the intensity of Coomassie staining on an SDS-PAGE gel of the quantified NMR protein stocks and the glycerol stocks, run side by side. Vacuum hydrolysis of the SutA protein stocks was carried out by continuous boiling for 24 hr at 105 °C in 6 N HCl in a Thermo Scientific Pierce 1 ml vacuum hydrolysis tube (Thermo Fisher), according to the manufacturer's instructions. After hydrolysis, the protein was dried *in vacuo* and resuspended in 100 µl 150 mM $NaHCO_3$ pH 9.0. 100 µl 15 mM dabsyl chloride (Sigma) in acetonitrile was added and the samples were incubated at 70 °C for 15 min. The reaction was quenched by the addition of 800 µl of a 1:1 mixture of ethanol and water. Debris were removed by centrifugation at top speed in a microfuge and the sample was transferred to an HPLC vial. 5 µl of the sample was injected onto a Waters Alliance HPLC system, composed of an e2695 separation module, 2998 PDA detector, and Acquity QDa detector, and fitted with a 3x100 mm XBridge BEH C18 reversed-phase chromatography column, 2.5 µm particle size. Buffer A contained 0.04% NH_4OH in water, and Buffer B contained 0.04% NH_4OH in acetonitrile. Each sample was loaded onto the column in a mixture of 8% buffer B and 92% buffer A, and a gradient from 8-30% buffer B was run over 40 min, followed by a gradient from 30-90% buffer B over 10 min. The column was then cleaned for 2 min with 90% buffer B, and returned to 8% buffer B over 8 min. A 2.5 mM amino acid standard mix in 0.1 N HCl (Sigma) was subjected to the same hydrolysis and derivatization protocol and used to calibrate amino acid peak areas. The identity of each peak was confirmed by mass spectrometry. Quantifications of

alanine, glycine, isoleucine, leucine, lysine, methionine, phenylalanine, proline, and serine were averaged for each sample to estimate the concentration of the SutA variant.

NMR experiments

Proteins were purified as described above. Except where noted, protein concentrations were 300 µM and the buffer contained 20 mM sodium phosphate, pH 7.0, 100 mM sodium chloride, and 10% D_2O.

46-101: 2D and 3D NMR spectra were collected on a Varian Inova 600 MHz NMR with a triple resonance inverse probe running VnmrJ 4.2A. The optimal temperature for minimizing the linewidth of ^{15}N HSQC peaks was found to be 7 °C. Although SutA was stable in solution at fairly high concentration at a range of temperatures, the peaks showed concentration-dependent broadening that was only alleviated by decreasing the concentration and acquiring the spectra below ambient temperature. The following spectra were acquired: ^{15}N HSQC, ^{13}C HSQC, HNCO, HNCA, HNCACB, CBCACONH, HNCOCA, HNCACO, CCONH, and ^{15}N HSQC experiments modified for measurement of T_2 and of ^{15}N-^{1}H NOE. These experiments were all done with standard Varian/Agilent pulse programs included in the Biopack extension of VnmrJ. The processed spectra were imported into the CcpNmr Analysis program (Vranken et al., 2005), and Assign-derived peak lists from the spectra were submitted to the PINE web server assignment program maintained by NMRFAM at the University of Wisconsin, pine.nmrfam.wisc.edu (Bahrami et al., 2009). Assignments proposed by the PINE output were validated or corrected in the Analysis software.

Full-Length SutA: Spectra were acquired at 7 °C on a Bruker AV III 700 MHz spectrometer with a TCI cryoprobe running Topspin 3.2. The spectra (^{15}N HSQC, ^{13}C HSQC, HNCACB, and CBCACONH) were all acquired with standard Bruker pulse programs. ^{15}N HSQC experiments modified for measurement of T_2 and of ^{15}N-^{1}H NOE were performed on a Varian Inova 600 MHz NMR with a triple resonance inverse probe running VnmrJ 4.2A, at 7 °C, with standard Varian/Agilent pulse programs included in the Biopack

760 extension of VnmrJ. Standard ^{15}N HSQC spectra were also collected at 7 °C, 16 °C and 25 °C. The spectra were imported into CcpNmr Analysis and partially assigned via the PINE web server as described previously.

Additional ^{15}N HSQC experiments: ^{15}N HSQC spectra for the SutA ΔN and SutA ΔC SutA proteins were collected on a Varian Inova 600 MHz NMR with a triple resonance inverse probe running VnmrJ 4.2A, with standard Varian/Agilent pulse programs included in the Biopack extension of VnmrJ, to test whether the truncations influenced the overall structure of the protein.

Stretched gel preparation for residual dipolar coupling measurements: ^{15}N^{13}C-labeled SutA was embedded in a stretched polyacrylamide gel using the "Gel NMR Starter Kit" (cat. #NE-373-B-5.4/4.2, New Era, Vineland NJ), according to the manufacturer's instructions. Briefly, a cylindrical 8%
770 polyacrylamide gel of about 300 µl, with a diameter of 5.4 mm (29:1 acrylamide:bisacrylamide ratio) was prepared. After polymerization, the gel was dialyzed 3 times against nanopure water, then dried overnight at 37 °C, and then returned to the cylindrical chamber in which it was cast. 300 µl ^{15}N^{13}C-labeled SutA at a concentration of 300 µM in a buffer containing 20 mM sodium phosphate, pH 7.0, 100 mM sodium chloride, and 10% D_2O was added to the dried gel and allowed to soak into it overnight at room temperature. The SutA-impregnated gel was then pushed into an NMR tube with a diameter of 4.2 mm, resulting in its stretching. Spectra were collected on a Varian Inova 600 MHz NMR with a triple resonance inverse probe running VnmrJ 4.2A. To extract ^{1}J(^{15}N, ^{1}H) coupling constants, the pulse sequence gNhsqc_IPAP was used to acquire the in-phase and antiphase spectra alternately. The sum and difference spectra were generated in VnmrJ with appropriate 2D transform coefficients and
780 imported into CcpNmr Analysis for overlay with the conventional ^{15}N HSQC spectrum.

NMR binding experiment: ^{15}N-labeled SutA and β1 fragment purified as described above were buffer exchanged into 20 mM sodium phosphate, pH 7.0, 100 mM sodium chloride, at an approximate

concentration of 30 µM each. To increase the chances that most of the SutA would be bound to β1 fragment, the mixture was run over a HiLoad Superdex 200 pg size exclusion column (GE Healthcare Life Sciences, Marlborough MA) and fractions representing the complex were retained and concentrated to 270 µl before adding D_2O to 10%. The final concentration of the complex was approximately 25 µM. In addition, ^{15}N-labeled SutA was mixed with σ^S at 50 µM each and buffer exchanged into 20 mM sodium phosphate, pH 7.0, 100 mM sodium chloride, and 10% D_2O. ^{15}N HSQC spectra were acquired on a Bruker 800 MHZ AV III HD spectrometer with a TCI cryoprobe at 25 °C using the standard Bruker pulse sequence hsqcetfpf3gpsi.

Data analysis: Secondary shifts were calculated by the TALOS software package as part of the PINE output. RDC values were evaluated manually by comparing the overlaid sum and difference spectra in the CcpNmr Analysis Suite, and the presence or absence of a peak in the positive (^{1}H-^{15}N) NOE was also evaluated manually for each assigned residue in the CcpNmr Analysis Suite. R_2 values were calculated by fitting a single exponential to the series of peak integral values collected with different T_2 relaxation times for each assigned residue. To generate structural models based on the chemical shift and RDC values we collected, these values were uploaded to the Robetta Fragment Server (Kim et al., 2004), and 3- and 9-residue fragment libraries were picked. Each library contained 200 fragments per SutA amino acid position. Using these fragment libraries, 16,000 decoy structures were generated using the PyRosetta suite (Chaudhury et al., 2010), following a folding protocol based on the PyRosetta folding tutorial published by the Gray lab (Bradley et al., 2005). Briefly, the SutA protein sequence was set to a linear structure, then 1000-1500 cycles of fragment insertion and energy minimization were performed to generate each decoy. Each cycle consisted of 3 short fragment (3 residues) and 1 long fragment (9 residues) insertions, followed by a low-resolution Monte Carlo scoring. As is perhaps unsurprising for a protein that has large regions of intrinsic disorder, the decoys did not converge to a single family of lowest-energy structures. We calculated the RMSD for each decoy compared to an ab initio structural

prediction for SutA that was produced by the Robetta Server (Kim et al., 2004). In general, decoys with lower RMSDs compared to this ab initio prediction also contained some version of the α helix that is supported by our NMR data; some other decoys (and some with the lowest energy scores) did not have the α helix. We arbitrarily chose several decoys to show a range of conformations that SutA might adopt; the strongest predictions of our NMR data are that residues 56-76 adopt an α-helix secondary structure and that the N- and C-tails are disordered, and all of the chosen models conform to those predictions. To color the model shown in Figure 1D according conservation, the alignment shown in Figure 1 Supplement 1 was opened in Chimera (Pettersen et al., 2004), and the "Render by conservation" function was used.

***In vitro* transcription experiments**

Experiments were carried out broadly as described in (Artsimovitch and Henkin, 2009). In general, RNAP holoenzyme was prepared by mixing core enzyme with a 3-fold (σ^{70}) or 5-fold (σ^{s}) excess of σ factor and incubating for 15 min at 37 °C. dsDNA templates were prepared by PCR from plasmids carrying the relevant promoter sequences or directly from *Pseudomonas aeruginosa* UBCPP-PA14 genomic DNA, using the Kappa high-fidelity hot-start 2x master mix according to the manufacturer's instructions (see strain and primer tables for plasmid and primer details). PCR products were checked by electrophoresis on 2% agarose gels to ensure that they consisted of a single product, purified from primers and residual dNTPs using the DNA Clean and Concentrator kit (Zymo Research, Irving CA), and quantified by NanoDrop (Thermo Fisher). The *rrn* bubble template was prepared by annealing the template strand and non-template strand oligos as follows: 80-mer oligos (Integrated DNA Technologies) were resuspended at a concentration of 100 µM in 0.1x TE and mixed together in 10X annealing buffer to give final concentrations of 45 µM duplex, 10 mM Tris-Cl ,100 mM NaCl, and 1 mM EDTA, then heated to 95 °C for 5 min and allowed to cool from 95 °C to 70 °C at a rate of 0.1 °C/ second, incubated at 70 °C for 20

min, then allowed to cool to 22 °C at a rate of 0.1 °C/second. All pre-incubations and reaction incubations took place at 37 °C, and all reactions used TGA buffer (20 mM Tris-acetate pH 8.0, 2 mM Na-acetate, 2 mM Mg-acetate, 4% glycerol, 0.1 mM DTT, 0.1 mM EDTA). Water used in reaction and running buffer preparation was treated with diethyl pyrocarbonate (DEPC). Reactions were quenched with an equal volume of urea stop buffer (8 M urea, 10 mM EDTA, 0.8x TBE, 2 mg/ml bromophenol blue, 2mg/ml xylene cyanol FF, 2 mg/ml amaranth), and heated to 95 °C for 2 min immediately before gel loading. 20% acrylamide denaturing Urea-TBE gels were prepared using the Sequa-gel system (National Diagnostics) according to the manufacturer's instructions except TBE was added to 0.5x instead of 1x. A 60-well comb was used and gels were run using the Owl S3 vertical sequencing gel system (Thermo Fisher). 2 µl sample was loaded per lane. After electrophoresis, one glass plate was removed and the gel was covered with plastic wrap and exposed directly to the phosphorimager screen (Molecular dynamics) for 12-48 hr.

Single turnover initiation experiments: For SutA titrations on the *rrn* and *bcn* promoters, reactions were assembled as follows: RNAP holoenzyme (20 nM final concentration), DNA template (15 nM final concentration), TGA buffer, and water were mixed in a volume of 3 µl and added to 1 µl SutA (at 5x the final concentration) or storage buffer on ice. These 4 µl reactions were incubated for 6 min to allow open complex to form. 1 µl NTP mix (375 µM initiating dinucleotide, 250 µM each NTP not carrying ^{32}P label (ATP, UTP, and either CTP or GTP), 100 µM cold NTP of the same type as that carrying the label (either CTP or GTP), 0.75 µCi α^{32}P GTP or CTP (3000 Ci/mmol, 10 mCi/ml, Perkin Elmer, Waltham MA), and 100 µg/ml heparin) was added and transcription was allowed to continue for 8 minutes before reactions were quenched. Initiating nucleotides were CpU for the *rrn* promoter and ApC for the *bcn* promoter (IBA Lifesciences, Göttingen, Germany). For the *pepB* promoter, 40 nM Eσ^S was and the transcription reactions were allowed to proceed for 16 min in an effort to ensure sufficient signal. The final NaCl concentration in these reactions (due to NaCl in protein storage buffers) was 26 mM for the

rrn and *bcn* promoters and 32 mM for the *pepB* promoter. For the iNTP titration experiments, no dinucleotides were included, and instead the NTP mix contained 50, 500, or 5000 µM CTP and UTP (for the 10, 100, and 1000 µM iNTP conditions), 250 µM ATP, 100 µM GTP, and 0.75 µCi α^{32}P GTP per 1 µl NTP mix. For the DksA/ppGpp experiments, 0.5 µl 5 µM SutA (or 0.5 µl storage buffer) and 0.5 µl of a mixture containing 2.5 µM DksA and 25 µM ppGpp (Sigma) in storage buffer (or 0.5 µl storage buffer) were distributed to tubes. The remainder of the experimental set-up was the same as for the SutA titration experiments.

Multiple turnover initiation experiments (bubble template): Reactions were assembled and run as described above for single turnover assays, but no heparin was included in the NTP mix. This was to allow both abortive and processive initiation to occur according to their natural rates in a multiple turnover context, since complexes leading to abortive initiation are heparin resistant and thus abortive initiation would occur in a multiple turnover context regardless of heparin addition.

Open complex stability assays: A 7x reaction master mix containing RNAP holoenzyme (for 20 nM final concentration in transcription reactions) template (15 nM final), SutA at the indicated concentration, or storage buffer and water in a volume of 27.5 µl was mixed on ice. 1 µl NTP mix (at the same concentrations as described for single turnover reactions, but without heparin) was distributed to each of 6 reaction tubes. The reaction master mix was incubated for 6 min to allow open complex to form, and then 0.5 µl of heparin at 1.5 mg/ml was added. Immediately, 4 µl of the master mix was removed and added to 1 µl NTP mix for the time 0 point. At the indicated time points after the addition of heparin, additional 4 µl aliquots were removed and added to tubes containing 1 µl NTP mix. Each reaction was quenched 8 min after mixing the reaction mix with the NTP mix.

Gel image acquisition and analysis: Phosphorimager screens were scanned on a Typhoon FLA 9000 gel imaging system (GE Healthcare Life Sciences), at the maximum PMT setting and with each pixel

representing 200 μm. Images were analyzed using the gel lane analysis tool of the FIJI open-source image analysis suite (Schindelin et al., 2012). First, images were rotated, background-subtracted, and contrast-adjusted (ensuring that no pixels were saturated), then pixel densities in the relevant regions of each lane were plotted, and the areas under each peak quantified. For the SutA titration experiments, 2-3 bands spanning a length range of about 4-8 nucleotides represented the run-off transcripts (RNAP terminates inefficiently on a linear transcript, sometimes producing multiple bands), and all of the major bands in this range were quantified (the ratios of each band to the total were not generally affected by SutA). The most prominent higher band likely represents the product of transcription initiating at one end of the linear transcript and running to the other end, and was ignored. For the iNTP titrations, the major products were the same as those seen for initiation with the CpU dinucleotide, but at the highest [iNTP], additional bands within the 8 nucleotide range appeared, and all bands in this range were quantified. For initiation on the bubble template, abortive products were much more prominent, and their relative abundances were affected by the σ used. In order to calculate a value representing the number of initiation events, all major bands in each lane were quantified and the signal intensity for each band was divided by the number of G bases in the sequence corresponding to that band to obtain a value proportional to the number of transcripts represented by the band. The sum of the values for each band in the lane was used as a measure of the total number of transcripts initiated. Whenever possible, values were normalized and compared within the same gel. Where comparisons across gels were necessary, values from each gel were normalized to the values obtained for reactions containing 0 nM SutA and $E\sigma^{70}$ on that gel.

Transcription start site mapping: *P. aeruginosa* UCBPP-PA14 culture was collected in mid-exponential, early stationary, and late stationary phases, cells were pelleted, and pellets were frozen in liquid nitrogen. RNA was extracted from the pellets using the RNeasy kit (Qiagen, Hilden, Germany) according to the manufacturer's instructions. Genomic DNA was depleted using the Turbo DNA-free kit

(Ambion/Invitrogen, Carlsbad CA) according to instructions. cDNA corresponding to the 5' ends of nascent rRNA transcripts was generated by reverse transcription using 10 µg total RNA, 4 pmol rRNA-specific primer, 500 µM dNTPs, 5µM DTT, 1x reverse transcriptase buffer, and 300 units SuperScript reverse transcriptase in a 40 µl reaction. Primer binding was allowed to occur for 5 min at 65 °C, then the reverse transcriptase was added and the reaction allowed to proceed for 45 min at 55°C, then the reaction was stopped by incubation for 15 min at 70 °C. 2 units RNaseH were added and the reactions were incubated at 37 °C for 20 min to degrade RNA-DNA hybrids, and the cDNA was cleaned up using the Qiaquick PCR clean-up kit (Qiagen). Poly-T tails were added to the 3' ends of the cDNA using terminal transferase (Promega) according to instructions. The resulting T-tailed cDNA was then used as a template in a first round PCR reaction with a primer against the rRNA transcript and one against the poly-T tail that adds an additional specific sequence. This PCR product was then used as the template in a second round PCR reaction with primers against the rRNA transcript and the newly added specific sequence that was part of the primer in the first round PCR. Two different DNA polymerases were tried (GoTaq, Promega; or Q5, NEB), according to instructions, and gave similar results (Figure 2, – figure supplement 2). The resulting PCR products from the stationary phase time points were cloned into the pUC18 plasmid using Gibson assembly and approximately 40 individual clones were sequenced. Many of the products turned out to represent the site that is cleaved by RNAse III in the first step of 16S rRNA maturation, which is very similar in sequence and distance upstream of the mature 16S rRNA start (Steitz and Young, 1979) to the *E. coli rrn* RNAse III cleavage site (these correspond to the strong, lowest band in Figure 2 – figure supplement 2). However, a number of the products corresponded to the proximal putative transcription initiation site (second lowest band) and most of these initiated at the cytidine 8 bp downstream of the -10 motif, although a few also initiated at a cytidine 7 bp downstream of the -10 motif. Although we detected some fainter bands potentially corresponding to start sites further upstream, we were unable to recover any sequences corresponding to these start sites, even

after the higher faint bands were gel-purified before cloning into pUC18. We also tested a promoter corresponding to the next putative start site upstream of this start site *in vitro* and found that it drove initiation more weakly than the proximal start site (data not shown). Together, these data suggest that this proximal start site is the dominant one in *P. aeruginosa*, at least under the conditions we investigated.

qRT-PCR: For all experiments, total RNA was extracted from frozen cell pellets using the RNeasy kit (Qiagen), genomic DNA was removed using the Turbo DNA-free kit (Ambion/Invitrogen), cDNA was generated using the iScript reverse transcriptase kit (Bio-Rad), and qPCR reactions were carried out using the iTaq Universal SYBR Green Supermix (Bio-Rad) in an Applied Biosystems 7500 Real-time PCR system, all according to instructions. For experiments comparing *rrn* expression in *E. coli* and *P. aeruginosa*, either the empty vector pMQ72 or pMQ72 carrying *sutA* under control of the pBAD arabinose-inducible promoter was transformed into the *ΔsutA* strain of *P. aeruginosa* UBCPP-PA14 or *E. coli* MG1655 by electroporation (see strains). Overnight cultures in LB plus 100 or 20 µg/ml gentamicin respectively were diluted into fresh LB plus 20 mM arabinose and allowed to grow for 16 hr into stationary phase before harvesting cells and freezing cell pellets in liquid nitrogen. Nascent *rrn* transcripts were measured using primers that hybridize to the leader region upstream of the start of the 16S rRNA gene, which is degraded during ribosome maturation, and normalized to *hcaT* transcripts in *E. coli* (Zhou et al., 2011) or to *oprI* transcripts in *P. aeruginosa* (see primers). Standard curves relating the primer efficiencies of the *rrn* and control genes were generated using genomic DNA from the respective organisms. *oprI* is a much more abundant transcript than *hcaT*, resulting in lower normalized values for the *P. aeruginosa rrn* transcript than for the *E. coli* normalized transcript. For experiments evaluating the effects of WT or mutant SutA on expression of *rrn, pepB, or bcn in vivo*, in the presence or absence of *rpoS*, constructs for expressing WT or mutant *sutA* under the control of the pBAD arabinose-inducible promoter were integrated into the *attB* site of the *P. aeruginosa* chromosome, in the *ΔsutA* strain, so

that arabinose-induced SutA expression was the only source of SutA in these strains. Additionally, the WT *sutA* construct was introduced into the *attB* site of a *ΔrpoSΔsutA* strain. These strains were grown overnight in LB, then diluted 1:1000 into minimal medium containing 40 mM pyruvate as a sole carbon source, and either containing 20 mM arabinose or not. The pyruvate minimal medium cultures were allowed to grow for 24 hr, during which they slowly reached stationary phase (pyruvate minimal medium imposes a doubling time of approximately 4 hr), and then cells were harvested and cell pellets were frozen in liquid nitrogen. Primers for the *rrn* transcript were to the leader region of the transcript as described above, and primers for *pepB* and *bcn* were directed against the coding sequence of those genes. These transcripts of interest were normalized to *oprI* transcript levels using standard curves generated from genomic DNA.

Cross-linking and Affinity Cleavage

BS^3 cross-linking: Bis(sulfosuccinimidyl) suberate (BS^3) d_0 and d_4 isotopologs were purchased from Thermo Scientific. RNAP and SutA were mixed in a 1:10 molar ratio (0.5 µM RNAP, 5.0 µM SutA) in 10 mM HEPES pH 8, 100 mM potassium acetate and incubated on ice for 1.5 hr. Cross-linking was initiated by addition of 5 mM of a 4:1 molar ratio of BS^3 d_0:d_4 and the reaction was incubated on ice for 2 hr. Cross-linking was quenched by addition of ammonium bicarbonate to a final concentration of 50 mM. Proteins were digested in solution by incubation with 500 ng GluC overnight at 37 °C. Digestion was quenched by addition of 5% formic acid. Digested peptides were desalted by HPLC using a C8 microtrap (Optimize Technologies, Oregon City OR), using a gradient of buffer A: 0.2% formic acid in H_2O and buffer B: 0.2% formic acid in acetonitrile) and concentrated *in vacuo*. Samples were resuspended in 0.2% formic acid and analyzed on the Orbitrap Elite Hybrid Ion Trap MS equipped with an Easy 1000 nanoUHPLC (Thermo Scientific). Solvent A consisted of 97.8% H_2O, 2% ACN, and 0.2% formic acid and

solvent B consisted of 19.8% H_2O, 80% ACN, and 0.2% formic acid. Digested peptides were directly loaded at a flow rate of 500 nL/min onto a 16-cm analytical HPLC column (75 µm ID) packed in-house with ReproSil-Pur C_{18}AQ 3 µm resin (120 Å pore size, Dr. Maisch, Ammerbuch, Germany). The column was enclosed in a column heater operating at 45 °C. After 30 min of loading time, the peptides were separated with a 50 min gradient at a flow rate of 350 nL/min. The gradient was as follows: 2% B for five min, 2–40% B (60 min), and 100% B (10 min). The Orbitrap was operated in data-dependent acquisition mode to automatically alternate between a full scan (*m*/*z*=300–1600) in the Orbitrap and subsequent 5 HCD MS/MS scans in the Orbitrap. Normalized collision energy was 30% and activation time was 100 ms. Resolution on MS was set to 120,000 and MS/MS was 15,000. The experiment was performed with two replicates.

Raw files were first searched using MaxQuant to identify precursor mass pairs, differing by 4.02 Da, that represent cross-links made by both of the BS^3 linker isotopologs. Raw files were converted to peak lists with ProteoWizard (Kessner et al., 2008) and subset for only those spectra that were identified as mass pairs. Subset peak lists were analyzed with Protein Prospector online, version 5.12.4, following reported protocols with modifications below (Trnka et al., 2014). The protein database contained the sequences for purified SutA, RpoA, RpoB, RpoC, RpoD, and RpoZ. 80 peaks from each spectrum were searched using a tolerance of 10 ppm for precursor ions and 25 ppm for product ions. Enzyme specificity was GluC, and up to two missed cleavages per peptide were allowed. Carbamidomethylation of cysteines was specified as a constant modification, and protein N-terminal acetylation, oxidation of methionine, and dead-end modification with the cross-linker at lysine positions and protein N-termini were set as variable modifications. Additionally, incorrect monoisotopic peak assignments were considered as variable modifications. The analysis was run twice for each set of peak lists to search for both cross-linker isotopologs.

For cross-links detected between RNAP proteins, we used a reported structural model of the *E. coli* RNAP complex (PDB: 3LU0) to calculate the inter α-carbon distance between amino acids (Opalka et al., 2010). We used this calculated distance as a metric to distinguish "quality" cross-links from all others. Based on the length of the linker, the maximum inter α-carbon distance between lysines cross-linked by BS3 is 24.6 Å, so we considered cross-links with distances near or below this value to be reasonable. Like the study by Trnka et al., we found Score Difference to be the best discriminant for making this distinction. A Score Difference cutoff of 8.0 (similar to the value of 8.5 found by Trnka et al.) separated high-distance and low-distance cross-links (Figure 3 supplement). The final criteria for assigning quality cross-links were: (i) found as a precursor mass pair and (ii) Score Difference greater than 8.0. These cross-links were aggregated to determine the number of spectra from each replicate and the maximum Score Difference for each amino acid linkage (Figure 3 supplement). To visualize cross-link spectra, peak lists subset for matched pairs were analyzed by StavroX (Götze et al., 2012) using the same settings described for Protein Prospector. The best spectra used to match the cross-links between SutA and RNAP are shown in Figure 3 supplement.

BPA cross-linking for LC-MS/MS analysis: 20 µl cross-linking reactions contained 500 nM core RNAP, 2 µM SutA (BPA54 or BPA84 variant), 100 mM NaCl, and TGA buffer (4% glycerol, 20 mM Tris-acetate pH 8.0, 2 mM sodium acetate, 2 mM magnesium acetate, 100 µM DTT, and 100 µM EDTA). Complexes were allowed to form for 6 min at 37 °C and were then UV-irradiated for 1 min at 1W/cm^2 using the Omnicure S2000 lamp (Excelitas, Waltham MA). Cross-linked complexes were dried *in vacuo*, resuspended in 40 µl 8 M urea and 100 mM Tris-HCl, reduced with 3 mM TCEP, alkylated with 10 mM iodoacetamide, digested with 100 ng lysyl endopeptidase for 4 hr, and then digested with 500 ng trypsin overnight in 2 M urea and 1 mM $CaCl_2$. Formic acid was added to 5% and then the sample was desalted by HPLC using a C8 microtrap (Optimize Technologies), with a gradient of buffer A: 0.2% formic acid in H_2O and buffer B: 0.2% formic acid in acetonitrile), concentrated *in vacuo*, and resuspended in 0.2% formic acid.

Samples were resuspended in 0.2% formic acid and run on the Q Exactive HF Orbitrap MS, equipped with an Easy 1200 nanoUHPLC (ThermoFisher Scientific). Solvent A consisted of 97.8% H_2O, 2% ACN, and 0.2% formic acid and solvent B consisted of 19.8% H_2O, 80% ACN, and 0.2% formic acid. Digested peptides were directly loaded at a flow rate of 220 nL/min onto a 20-cm analytical HPLC column (50 µm ID) packed in-house with ReproSil-Pur C_{18}AQ 1.9 µm resin (120 Å pore size, Dr. Maisch, Ammerbuch, Germany). The column was enclosed in a column heater operating at 65 °C. After 45 min of loading time, the peptides were separated with a 60 min gradient at a flow rate of 220 nL/min. The gradient was as follows: 2–6% B (4 min), 6-25% B (41 min), 25-40% B (15 min), and 100% B (10 min). The Orbitrap was operated in data-dependent acquisition mode to automatically alternate between a full scan (*m*/*z*=300–1650) in the Orbitrap and subsequent 7 HCD MS/MS scans. Normalized collision energy was 28 and max injection time of 250 ms. Resolution on MS was set to 60,000 and MS/MS was 30,000. Raw files were converted to mzXML files by msConvert (Adusumilli and Mallick, 2017) and analyzed using StavroX (Götze et al., 2012) with a precursor and fragment ion tolerance of 5 ppm and a 1% FDR.

FeBABE cleavage experiments: FeBABE cleavage experiments were based on protocols described in (Meares et al., 2003).Our initial determination of SutA-FeBABE cleavage sites (as shown in Figure 3) utilized a large-format gel and Western blotting apparatuses (16x16 cm) to allow for higher resolution in calculating the cleavage site. 20 µl Reactions contained 250 nM RNAP (E, Eσ^S, or Eσ^{70}), 250 nM *rrn* template, 2 µM SutA (WT or FeBABE variant), 100 mM NaCl, in 1x TGA buffer (yielding a final glycerol concentration of 8% including enzyme storage buffers). Holoenzyme complexes were formed by mixing a 3-fold molar excess of σ^S or σ^{70} with E and incubating at 37 °C for 15 min. After assembling the rest of the reaction mixture, it was incubated at 37 °C for 10 min. to allow SutA and DNA-containing complexes to form, and then cleavage was initiated by the addition of 2.5 µl 50 mM sodium ascorbate, 10 mM EDTA then 2.5 µl 50 mM hydrogen peroxide (J.T. Baker Ultrex grade (Avantor, Radnor PA)), 10 mM

EDTA. Reactions were incubated for 7 min and then quenched by the addition of 8.3 µl 4x LDS loading buffer (Bio-Rad, Hercules CA).

FeBABE protein cleavage reactions of open complexes: containing different σ factors and promoter DNA were carried out on a smaller scale for SDS-PAGE and western blotting on mini gels, which allowed for more efficient transfer. 10 µl reactions contained 100 nM RNAP, 100 nM template, 2µM SutA, and 100 mM NaCl, in 1x TGA buffer, and sodium ascorbate, hydrogen peroxide, and loading buffer were added to the same final concentrations as described above.

FeBABE DNA cleavage reactions: were also 10 µl but contained 100 nM RNAP, 15 nM template DNA, and 2 µM SutA in 1x TGA buffer. The final NaCl concentration in these reactions (derived from the protein storage buffers) was 40 mM. The reactions were quenched by the addition of 37.5 µl 100 mM thiourea, then treated with proteinase K, ethanol precipitated, and subjected to primer extension, before running them on Urea-TBE denaturing PAGE gels as described below for $KMnO_4$ footprinting.

SDS-PAGE and Western blotting

For FeBABE initial large-format gels, markers for calibrating the observed cleavage positions were generated by cloning C-terminal fragments of β (aa 355-1357, 450-1357, 520-1357, 626-1357, and 1062-1357) into the pQE80L expression vector, and transforming into *E. coli* (see strain list). 5 ml cultures of these strains in LB were grown to late exponential phase and high levels of expression were induced by incubating with 1 mM IPTG for 4 hr. 100 µl aliquots of these cultures were pelleted by centrifugation and stored at -80 °C. Pellets were resuspended in 25 µl BugBuster (Novagen) and mixed together as follows: for 6% gels, 2 µl each of fragments 355, 450, and 520, plus 12 µl of fragment 626 were brought to a final volume of 200 µl 1x SDS loading buffer, and 10-15 µl were loaded; for 8% gel, 36 µl 1062 fragment was added to the mixture. 6% or 8% Tris-glycine-SDS gels were cast in the PROTEAN II xi Cell system using a 19:1 acrylamide: bisacrylamide mixture (Bio-Rad). Samples were denatured by heating in

LDS sample buffer for 5 min at 80 °C and 1 mM DTT was added to the upper buffer to minimize protein oxidation during the 6-8 hr run time at 150 V. Following electrophoresis, gels were stained with Instant Blue colloidal Coomassie stain (Expedeon, San Diego CA) for 1 hr, briefly rinsed in water, and transferred to a nitrocellulose membrane using 1x Towbin transfer buffer containing 20% methanol and 0.03% SDS, for 4-6 hr at 250 mA using a Hoefer TE62 transfer apparatus (Hoefer, Holliston MA). Membranes were blocked for 1 hr in 2.5% non-fat dry milk in TBST, then incubated in primary antibody (EPR18704, Abcam, Cambridge MA) at a 1:1500 dilution for 8 hr, washed in TBST and incubated in the secondary antibody (goat anti-rabbit HRP, Sigma, St. Louis) at a dilution of 1:5000 for 1 hr before washing in TBST and developing with SuperSignal™ West Pico PLUS Chemiluminescent Substrate (ThermoFisher, Waltham MA) according to instructions. Blots were exposed to x-ray film for 5-15 min. For the FeBABE reactions to analyze the effects of different σ factors and DNA templates, samples were run on 4-20% gradient Tris-glycine SDS mini-gels (Bio-Rad) for 1 hr. at 150 V, then stained with Coomassie Colloidal Blue and transferred to pre-cut nitrocellulose membranes (Bio-Rad) for 8 hr at 20 V in 1X Towbin transfer buffer without methanol or SDS added. The membranes were cut to separate region containing the uncleaved β subunit band from the region containing the cleavage products, which were of much lower abundance. Western blotting for the membrane region containing the cleavage products was the same as described above for the large-format gel, but the region containing the uncleaved band was incubated with primary antibody diluted 1:2000 and secondary antibody diluted 1:20,000. The two regions of the membrane were then placed next to each other for exposure to X-ray film. The cutting of the membrane occasionally resulted in the appearance of a second band immediately below the uncleaved band (especially in the outer lanes of the gel), which was just the edge of the uncleaved band. For analysis and Western blotting of BPA cross-linking in various holoenzyme/DNA contexts, reaction volumes were 10 µl and contained 100 nM RNAP core or holoenzyme, the concentrations of the BPA54 variant listed in the figures, 100 nM template DNA, 100 mM NaCl, and TGA buffer. Cross-linking was

carried out as described above for LC-MS/MS analysis, and then samples were added to LDS loading buffer. 3-8% Tris-acetate gels and Tris-acetate-SDS running buffer (NuPAGE) were used to maximize separation of the cross-linked β+SutA band from the uncross-linked β only band. Subsequent steps of the Western blotting protocol were the same as for the FeBABE mini-gels, using the same antibody dilutions as for the uncleaved portion, described above.

$KMnO_4$ footprinting and FeBABE DNA cleavage analysis

Footprinting was carried out essentially as described in (Kahle and Paule, 2009). Briefly, 10 µl reactions containing 100 nM RNAP holoenzyme, 15 nM template DNA, and the amounts of SutA or SutA mutant indicated in the figures in 1x TGA buffer were incubated for 6 min to allow complexes to form and then 1 µl of 110 mM $KMnO_4$ was added and the oxidation reaction was allowed to proceed for 5 min. Reactions were quenched by the addition of 1 µl 1 M 2-mercaptoethanol. Reaction volumes were brought to 50 µl with water and then 50 µl of a solution of 0.2% SDS and 2 mg/ml proteinase K was added and the reactions were incubated for 1 hr at 50 °C. 1 µl of linear acrylamide at a concentration of 10 mg/ml (as a carrier for nucleic acid precipitation), 10 µl of 3 M sodium acetate pH 5.2, and 275 µl of ethanol were added and DNA was precipitated overnight. Nucleic acid pellets were washed once with 70% ethanol, dried, and resuspended in 8 µl water. 12.5 µl primer extension reactions contained 10 mM Tris, 50 mM KCl, 1.5 mM $MgCl_2$, 5% DMSO, 2 M betaine, 250 µM dNTPs (TaKaRa, Kusatsu, Shiga Prefecture, Japan), 2.5 pmol Cy3 or Cy5 labeled primer (Integrated DNA Technologies, Coralville IA), 2.5 µl template, and 1 unit (0.2µl) Taq polymerase (NEB, Ipswich MA). After heating to 95 °C for 3 min, 15 cycles of 30 seconds at 95 °C, 30 seconds at 53 °C, and 30 seconds at 72 °C were carried out, followed by a final 3 min incubation at 72 °C. Reactions were mixed with an equal volume of formamide loading buffer (97% formamide, 10 mM Tris, 10 mM EDTA, 0.05% SDS), heated to 98 °C for 2 min, snap cooled on ice, and 8 µl were loaded onto a 12% Urea-TBE denaturing PAGE gel (Sequa-gel system, National

Diagnostics, Atlanta GA) prepared with 0.5x TBE. Samples were run at 50 W (approx.. 2500 V) with 0.5x TBE running buffer on a vertical sequencing gel apparatus (Ellard Instrumentation, Monroe WA). Sequencing ladders showing the positions of C or G bases in the template sequence were generated in 10 µl reactions containing 1x Thermopol reaction buffer (NEB), 1 µl Therminator polymerase (NEB), 250 µM dNTPs (TaKaRa), 25 µM ddGTP or ddCTP (TriLink Biotechnologies, San Diego CA), 100 nM template DNA (same as used in FeBABE cleavage or $KMnO_4$ footprinting assays), 1 µM Cy3 or Cy5 labeled primer (same as used for primer extension), and 2 M betaine. Reactions were incubated at 95 °C for 3 min, then 5 cycles of 95 °C for 30 seconds, 50 °C for 1 min, 72 °C for 1 min, followed by a final incubation at 72 °C for 3 min. Sequencing reactions were mixed with 30 µl formamide loading buffer and heated and cooled before loading as described for the samples. Sample lanes did not include loading dye, which is fluorescent in both Cy3 and Cy5 channels, but empty lanes were run with formamide loading buffer containing both Bromophenol Blue and Xylene cyanol FF. Following electrophoresis, gels were scanned directly using the fluorescence mode of a Typhoon Trio variable mode imaging system (GE Healthcare Life Sciences), using a PMT setting of 600 and each pixel representing 200 µm. Image analysis was carried out using the FIJI analysis suite (Schindelin et al., 2012). Images were background subtracted and contrast-adjusted and all major bands of interest in each lane were quantified. For $KMnO_4$ footprinting, the intensities of the footprint bands were normalized to the intensity of the band corresponding to the full-length primer extension product for comparison across multiple gels. For the FeBABE cleavage, the intensities of each band in the lanes containing N-Fe or C-Fe SutA were normalized by dividing by the intensities of the corresponding bands in the negative control lanes containing WT SutA.

Data visualization

Unless otherwise noted, molecular structures were visualized using the Chimera suite (Pettersen et al., 2004). Graphs were produced using the ggplot2 library in R (Wickham, 2016). Gel images were

background-subtracted and contrast adjusted using the FIJI suite (Schindelin et al., 2012). NMR spectra were visualized using the CcpNmr Analysis suite (Vranken et al., 2005). LC-MS/MS spectra for cross-linked peptides were shown using StavroX software (Götze et al., 2012). Figures were assembled using Adobe Acrobat CC2018.

REFERENCES

Adusumilli, R., and Mallick, P. (2017). Data Conversion with ProteoWizard msConvert. Methods in molecular biology *1550*, 339-368.

Artsimovitch, I., and Henkin, T.M. (2009). In vitro approaches to analysis of transcription termination. Methods *47*, 37-43.

Babin, B.M., Atangcho, L., van Eldijk, M.B., Sweredoski, M.J., Moradian, A., Hess, S., Tolker-Nielsen, T., Newman, D.K., and Tirrell, D.A. (2017). Selective Proteomic Analysis of Antibiotic-Tolerant Cellular Subpopulations in *Pseudomonas aeruginosa* Biofilm. mBio *8*, 16.

Babin, B.M., Bergkessel, M., Sweredoski, M.J., Moradian, A., Hess, S., Newman, D.K., and Tirrell, D.A. (2016). SutA is a bacterial transcription factor expressed during slow growth in *Pseudomonas aeruginosa*. Proceedings of the National Academy of Sciences of the United States of America *113*, E597-605.

Bae, B., Davis, E., Brown, D., Campbell, E.A., Wigneshweraraj, S., and Darst, S.A. (2013). Phage T7 Gp2 inhibition of *Escherichia coli* RNA polymerase involves misappropriation of σ70 domain 1.1. Proceedings of the National Academy of Sciences of the United States of America *110*, 6.

Bahrami, A., Assadi, A.H., Markley, J.L., and Eghbalnia, H.R. (2009). Probabilistic interaction network of evidence algorithm and its application to complete labeling of peak lists from protein NMR spectroscopy. PLoS Comput Biol *5*, e1000307.

Basta, D.W., Bergkessel, M., and Newman, D.K. (2017). Identification of Fitness Determinants during Energy-Limited Growth Arrest in *Pseudomonas aeruginosa*. mBio *8*.

Basu, R.S., Warner, B.A., Molodtsov, V., Pupov, D., Esyunina, D., Fernandez-Tornero, C., Kulbachinskiy, A., and Murakami, K.S. (2014). Structural basis of transcription initiation by bacterial RNA polymerase holoenzyme. The Journal of biological chemistry *289*, 24549-24559.

Bergkessel, M., Basta, D.W., and Newman, D.K. (2016). The physiology of growth arrest: uniting molecular and environmental microbiology. Nature reviews Microbiology *14*, 549-562.

Bowers, P.M., Strauss, C.E., and Baker, D. (2000). De novo protein structure determination using sparse NMR data. J Biomol NMR *18*, 311-318.

Bradley, P., Misura, K.M., and Baker, D. (2005). Toward high-resolution de novo structure prediction for small proteins. Science *309*, 1868-1871.

Buchan, D.W., Minneci, F., Nugent, T.C., Bryson, K., and Jones, D.T. (2013). Scalable web services for the PSIPRED Protein Analysis Workbench. Nucleic acids research *41*, W349-357.

Burgess, R.R., and Jendrisak, J.J. (1975). A procedure for the rapid, large-scale purification of *Escherichia coli* DNA-dependent RNA polymerase involving Polymin P precipitation and DNA-cellulose chromatography. Biochemistry *14*, 4634-4638.

Chaudhury, S., Lyskov, S., and Gray, J.J. (2010). PyRosetta: a script-based interface for implementing molecular modeling algorithms using Rosetta. Bioinformatics *26*, 689-691.

Chin, J.W., Martin, A.B., King, D.S., Wang, L., and Schultz, P.G. (2002). Addition of a photocrosslinking amino acid to the genetic code of *Escherichia coli*. Proceedings of the National Academy of Sciences of the United States of America *99*, 11020-11024.

Choi, K.H., and Schweizer, H.P. (2006). mini-Tn7 insertion in bacteria with single attTn7 sites: example *Pseudomonas aeruginosa*. Nature protocols *1*, 153-161.

Ciofu, O., Tolker-Nielsen, T., Jensen, P.O., Wang, H., and Hoiby, N. (2015). Antimicrobial resistance, respiratory tract infections and role of biofilms in lung infections in cystic fibrosis patients. Adv Drug Deliv Rev *85*, 7-23.

Dennis, P.P., Ehrenberg, M., and Bremer, H. (2004). Control of rRNA synthesis in *Escherichia coli*: a systems biology approach. Microbiology and molecular biology reviews : MMBR *68*, 639-668.

Drozdetskiy, A., Cole, C., Procter, J., and Barton, G.J. (2015). JPred4: a protein secondary structure prediction server. Nucleic acids research *43*, W389-394.

Feklistov, A., and Darst, S.A. (2011). Structural basis for promoter-10 element recognition by the bacterial RNA polymerase sigma subunit. Cell *147*, 1257-1269.

Feklistov, A., Sharon, B.D., Darst, S.A., and Gross, C.A. (2014). Bacterial sigma factors: a historical, structural, and genomic perspective. Annu Rev Microbiol *68*, 357-376.

Gibson, D.G. (2011). Enzymatic assembly of overlapping DNA fragments. Methods in enzymology *498*, 349-361.

Götze, M., Pettelkau, J., Schaks, S., Bosse, K., Ihling, C.H., Krauth, F., Fritzsche, R., Kühn, U., and Sinz, A. (2012). StavroX—A Software for Analyzing Crosslinked Products in Protein Interaction Studies. J Am Soc Mass Spectrom *23*, 12.

Gowrishankar, J., Yamamoto, K., Subbarayan, P.R., and Ishihama, A. (2003). In Vitro Properties of RpoS (σ^S) Mutants of *Escherichia coli* with Postulated N-Terminal Subregion 1.1 or C-Terminal Region 4 Deleted. Journal of bacteriology *185*, 2673-2679.

Hager, D.A., Jin, D.J., and Burgess, R.R. (1990). Use of Mono Q high-resolution ion-exchange chromatography to obtain highly pure and active *Escherichia coli* RNA polymerase. Biochemistry *29*, 7890-7894.

Haugen, S.P., Berkmen, M.B., Ross, W., Gaal, T., Ward, C., and Gourse, R.L. (2006). rRNA promoter regulation by nonoptimal binding of sigma region 1.2: an additional recognition element for RNA polymerase. Cell *125*, 1069-1082.

Henderson, K.L., Felth, L.C., Molzahn, C.M., Shkel, I., Wang, S., Chhabra, M., Ruff, E.F., Bieter, L., Kraft, J.E., and Record, M.T., Jr. (2017). Mechanism of transcription initiation and promoter escape by *E. coli* RNA polymerase. Proceedings of the National Academy of Sciences of the United States of America, 9.

Hook-Barnard, I.G., and Hinton, D.M. (2009). The promoter spacer influences transcription initiation via sigma70 region 1.1 of *Escherichia coli* RNA polymerase. Proceedings of the National Academy of Sciences of the United States of America *106*, 737-742.

Ishihama, A. (2000). Functional Modulation of *Escherichia coli* RNA Polymerase. Annu Rev Microbiol *54*, 19.

Jones, D.T., and Cozzetto, D. (2015). DISOPRED3: precise disordered region predictions with annotated protein-binding activity. Bioinformatics *31*, 857-863.

Kahle, B.F., and Paule, M.R. (2009). The Use of Diethyl Pyrocarbonate and Potassium Permanganate as Probes for Strand Separation and Structural Distortions in DNA. Methods in molecular biology *543*, 13.

Kang, J.Y., Olinares, P.D., Chen, J., Campbell, E.A., Mustaev, A., Chait, B.T., Gottesman, M.E., and Darst, S.A. (2017). Structural basis of transcription arrest by coliphage HK022 Nun in an *Escherichia coli* RNA polymerase elongation complex. eLife *6*.

Kauer, J.C., Erickson-Viitanen, S., Wolfe, H.R., and DeGrado, W.F. (1986). p-Benzoyl-L-phenylalanine, A New Photoreactive Amino Acid. The Journal of biological chemistry *261*, 6.

Kessner, D., Chambers, M., Burke, R., Agus, D., and Mallick, P. (2008). ProteoWizard: open source software for rapid proteomics tools development. Bioinformatics *24*, 2534-2536.

Kim, D.E., Chivian, D., and Baker, D. (2004). Protein structure prediction and analysis using the Robetta server. Nucleic acids research *32*, W526-531.

Kuznedelov, K., Semenova, E., Knappe, T.A., Mukhamedyarov, D., Srivastava, A., Chatterjee, S., Ebright, R.H., Marahiel, M.A., and Severinov, K. (2011). The antibacterial threaded-lasso peptide capistruin inhibits bacterial RNA polymerase. J Mol Biol *412*, 842-848.

Meares, C.F., Datwyler, S.A., Schmidt, B.D., Owens, J., and Ishihama, A. (2003). Principles and Methods of Affinity Cleavage in Studying Transcription. Methods in enzymology *371*, 25.

Meyer, A.S., and Grainger, D.C. (2013). The *Escherichia coli* Nucleoid in Stationary Phase. Adv Appl Microbiol *83*, 69-86.

Mohana-Borges, R., Goto, N.K., Kroon, G.J., Dyson, H.J., and Wright, P.E. (2004). Structural characterization of unfolded states of apomyoglobin using residual dipolar couplings. J Mol Biol *340*, 1131-1142.

Molodtsov, V., Scharf, N.T., Stefan, M.A., Garcia, G.A., and Murakami, K.S. (2017). Structural basis for rifamycin resistance of bacterial RNA polymerase by the three most clinically important RpoB mutations found in *Mycobacterium tuberculosis*. Molecular microbiology *103*, 1034-1045.

Murray, H.D., Appleman, J.A., and Gourse, R.L. (2003a). Regulation of the *Escherichia coli rrnB* P2 Promoter. Journal of bacteriology *185*, 28-34.

Murray, H.D., and Gourse, R.L. (2004). Unique roles of the *rrn* P2 rRNA promoters in Escherichia coli. Molecular microbiology *52*, 1375-1387.

Murray, H.D., Schneider, D.A., and Gourse, R.L. (2003b). Control of rRNA Expression by Small Molecules Is Dynamic and Nonredundant. Molecular cell *12*, 125-134.

NandyMazumdar, M., Nedialkov, Y., Svetlov, D., Sevostyanova, A., Belogurov, G.A., and Artsimovitch, I. (2016). RNA polymerase gate loop guides the nontemplate DNA strand in transcription complexes. Proceedings of the National Academy of Sciences of the United States of America *113*, 6.

Narayanan, A., Vago, F.S., Li, K., Qayyum, M.Z., Yernool, D., Jiang, W., and Murakami, K.S. (2018). Cryo-EM structure of *Escherichia coli* sigma(70) RNA polymerase and promoter DNA complex revealed a role of sigma non-conserved region during the open complex formation. The Journal of biological chemistry *293*, 7367-7375.

Olivares, J., Bernardini, A., Garcia-Leon, G., Corona, F., M, B.S., and Martinez, J.L. (2013). The intrinsic resistome of bacterial pathogens. Frontiers in microbiology *4*, 103.

Opalka, N., Brown, J., Lane, W.J., Twist, K.A., Landick, R., Asturias, F.J., and Darst, S.A. (2010). Complete structural model of *Escherichia coli* RNA polymerase from a hybrid approach. PLoS biology *8*.

Paul, B.J., Barker, M.M., Ross, W., Schneider, D.A., Webb, C., Foster, J.W., and Gourse, R.L. (2004a). DksA: a critical component of the transcription initiation machinery that potentiates the regulation of rRNA promoters by ppGpp and the initiating NTP. Cell *118*, 311-322.

Paul, B.J., Ross, W., Gaal, T., and Gourse, R.L. (2004b). rRNA transcription in Escherichia coli. Annu Rev Genet *38*, 749-770.

Pettersen, E.F., Goddard, T.D., Huang, C.C., Couch, G.S., Greenblatt, D.M., Meng, E.C., and Ferrin, T.E. (2004). UCSF Chimera--a visualization system for exploratory research and analysis. Journal of computational chemistry *25*, 1605-1612.

Raffaelle, M., Kanin, E.I., Vogt, J., Burgess, R.R., and Ansari, A.Z. (2005). Holoenzyme switching and stochastic release of sigma factors from RNA polymerase in vivo. Molecular cell *20*, 357-366.

Rappsilber, J. (2011). The beginning of a beautiful friendship: cross-linking/mass spectrometry and modelling of proteins and multi-protein complexes. Journal of structural biology *173*, 530-540.

Reddy, T., and Rainey, J.K. (2010). Interpretation of biomolecular NMR spin relaxation parameters. Biochemistry and cell biology = Biochimie et biologie cellulaire *88*, 131-142.

Rohl, C.A., and Baker, D. (2002). De novo determination of protein backbone structure from residual dipolar couplings using Rosetta. J Am Chem Soc *124*, 2723-2729.

Ross, W., Sanchez-Vazquez, P., Chen, A.Y., Lee, J.H., Burgos, H.L., and Gourse, R.L. (2016). ppGpp Binding to a Site at the RNAP-DksA Interface Accounts for Its Dramatic Effects on Transcription Initiation during the Stringent Response. Molecular cell *62*, 811-823.

Ruff, E.F., Drennan, A.C., Capp, M.W., Poulos, M.A., Artsimovitch, I., and Record, M.T., Jr. (2015a). *E. coli* RNA Polymerase Determinants of Open Complex Lifetime and Structure. J Mol Biol *427*, 2435-2450.

Ruff, E.F., Record, M.T., Jr., and Artsimovitch, I. (2015b). Initial events in bacterial transcription initiation. Biomolecules *5*, 1035-1062.

Rutherford, S.T., Villers, C.L., Lee, J.H., Ross, W., and Gourse, R.L. (2009). Allosteric control of *Escherichia coli* rRNA promoter complexes by DksA. Genes & development *23*, 236-248.

Schindelin, J., Arganda-Carreras, I., Frise, E., Kaynig, V., Longair, M., Pietzsch, T., Preibisch, S., Rueden, C., Saalfeld, S., Schmid, B*., et al.* (2012). Fiji: an open-source platform for biological-image analysis. Nature methods *9*, 676-682.

Schulz, S., Eckweiler, D., Bielecka, A., Nicolai, T., Franke, R., Dotsch, A., Hornischer, K., Bruchmann, S., Duvel, J., and Haussler, S. (2015). Elucidation of sigma factor-associated networks in *Pseudomonas aeruginosa* reveals a modular architecture with limited and function-specific crosstalk. PLoS pathogens *11*, e1004744.

Shanks, R.M., Caiazza, N.C., Hinsa, S.M., Toutain, C.M., and O'Toole, G.A. (2006). *Saccharomyces cerevisiae*-based molecular tool kit for manipulation of genes from gram-negative bacteria. Applied and environmental microbiology *72*, 5027-5036.

Stallings, C.L., Stephanou, N.C., Chu, L., Hochschild, A., Nickels, B.E., and Glickman, M.S. (2009). CarD is an essential regulator of rRNA transcription required for *Mycobacterium tuberculosis* persistence. Cell *138*, 146-159.

Steitz, J.A., and Young, R.A. (1979). Tandem Promoters Direct *E. coli* Ribosomal RNA Synthesis. Cell *17*, 10.

Tamura, K., Stecher, G., Peterson, D., Filipski, A., and Kumar, S. (2013). MEGA6: Molecular Evolutionary Genetics Analysis version 6.0. Molecular biology and evolution *30*, 2725-2729.

Trnka, M.J., Baker, P.R., Robinson, P.J., Burlingame, A.L., and Chalkley, R.J. (2014). Matching cross-linked peptide spectra: only as good as the worse identification. Mol Cell Proteomics *13*, 420-434.

Udikovic-Kolic, N., Wichmann, F., Broderick, N.A., and Handelsman, J. (2014). Bloom of resident antibiotic-resistant bacteria in soil following manure fertilization. Proceedings of the National Academy of Sciences of the United States of America *111*, 15202-15207.

Vendrell, J., and Aviles, F.C. (1986). Complete Amino Acid Analysis of Proteins by Dabsyl Derivatization and Reversed-Phase Liquid Chromatography. J Chromatogr A *358*, 13.

Vranken, W.F., Boucher, W., Stevens, T.J., Fogh, R.H., Pajon, A., Llinas, M., Ulrich, E.L., Markley, J.L., Ionides, J., and Laue, E.D. (2005). The CCPN data model for NMR spectroscopy: development of a software pipeline. Proteins *59*, 687-696.

Waterhouse, A.M., Procter, J.B., Martin, D.M., Clamp, M., and Barton, G.J. (2009). Jalview Version 2--a multiple sequence alignment editor and analysis workbench. Bioinformatics *25*, 1189-1191.

Wickham, H. (2016). ggplot2: Elegant Graphics for Data Analysis (New York: Springer-Verlag New York).

Williams, K.P., Gillespie, J.J., Sobral, B.W., Nordberg, E.K., Snyder, E.E., Shallom, J.M., and Dickerman, A.W. (2010). Phylogeny of gammaproteobacteria. Journal of bacteriology *192*, 2305-2314.

Winkelman, J.T., Chandrangsu, P., Ross, W., and Gourse, R.L. (2016). Open complex scrunching before nucleotide addition accounts for the unusual transcription start site of *E. coli* ribosomal RNA promoters. Proceedings of the National Academy of Sciences of the United States of America *113*, E1787-1795.

Winkelman, J.T., Winkelman, B.T., Boyce, J., Maloney, M.F., Chen, A.Y., Ross, W., and Gourse, R.L. (2015). Crosslink Mapping at Amino Acid-Base Resolution Reveals the Path of Scrunched DNA in Initial Transcribing Complexes. Molecular cell *59*, 768-780.

Wishart, D.S., Sykes, B.D., and Richards, F.M. (1991). Relationship between nuclear magnetic resonance chemical shift and protein secondary structure. J Mol Biol *222*, 311-333.

Wurtzel, O., Yoder-Himes, D.R., Han, K., Dandekar, A.A., Edelheit, S., Greenberg, E.P., Sorek, R., and Lory, S. (2012). The single-nucleotide resolution transcriptome of *Pseudomonas aeruginosa* grown in body temperature. PLoS pathogens *8*, e1002945.

Yang, Z., Lasker, K., Schneidman-Duhovny, D., Webb, B., Huang, C.C., Pettersen, E.F., Goddard, T.D., Meng, E.C., Sali, A., and Ferrin, T.E. (2012). UCSF Chimera, MODELLER, and IMP: an integrated modeling system. Journal of structural biology *179*, 269-278.

Zhou, K., Zhou, L., Qing, E., Zou, R., Stephanopoulos, G., and Too, H. (2011). Novel reference genes for quantifying transcriptional responses of *Escherichia coli* to protein overexpression by quantitative PCR. BMC molecular biology *12*.

Zuo, Y., and Steitz, T.A. (2015). Crystal structures of the *E. coli* transcription initiation complexes with a complete bubble. Molecular cell *58*, 534-540.

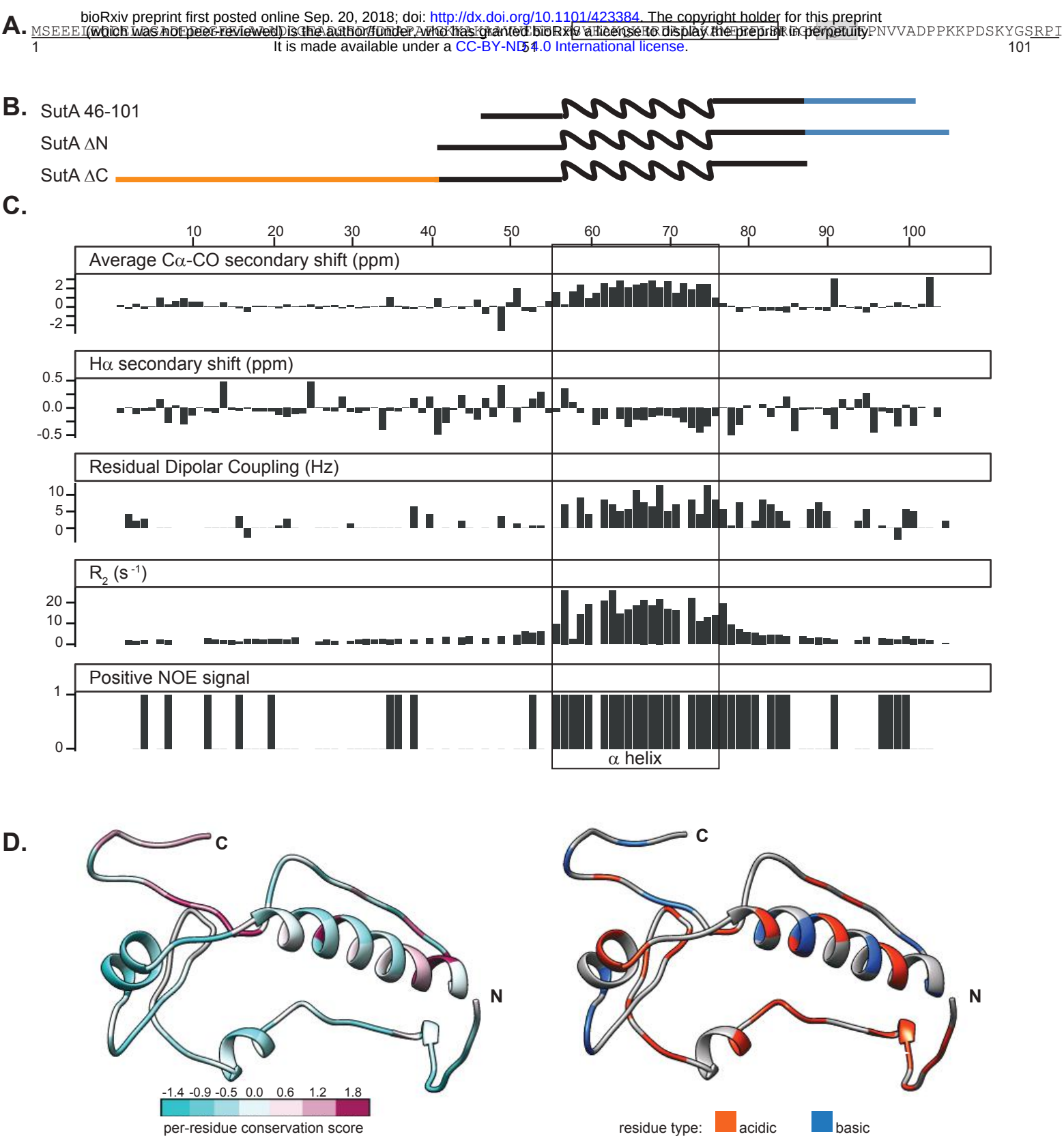

Figure 1. NMR data confirm presence of alpha helix from aa 56-76 and flexible N- and C-terminal tails. A. Primary amino acid sequence for SutA, with computational predictions indicated: underlining = intrinsic disorder; boxing = α-helix; gray shading = β-strand. **B.** Schematic of constructs used; wavy line = α-helix region; blue = C-tail; orange = N-tail. Schematics are aligned with residue numbers and NMR data in (C). **C.** Secondary chemical shift indices, residual dipolar coupling values, transverse relaxation rates, and peaks present in the positive amide NOE spectra following assignment of most backbone resonances for the full-length SutA. Secondary shifts were calculated using TALOS as part of the PINE automated assignment server. RDCs were measured by manual comparison of in-phase-anti-phase spectra between stretched gel and aqueous solution conditions. R_2 values were calculated by fitting single exponential decay curves to peak integrals from spectra with increasing T_2 delays. Positive NOE signal indicates that a peak was detected in the positive (^1H-^{15}N) NOE. The box indicates the location of the α-helix. **D.** One of many possible SutA structures modelled using the Robetta fragment server to incorporate chemical shift and RDC data, and PyRosetta. On the left, residues are colored by per-residue conservation score following alignment of 25 representative homologs (see materials and methods for details). On the right, residues are colored by chemical properties.

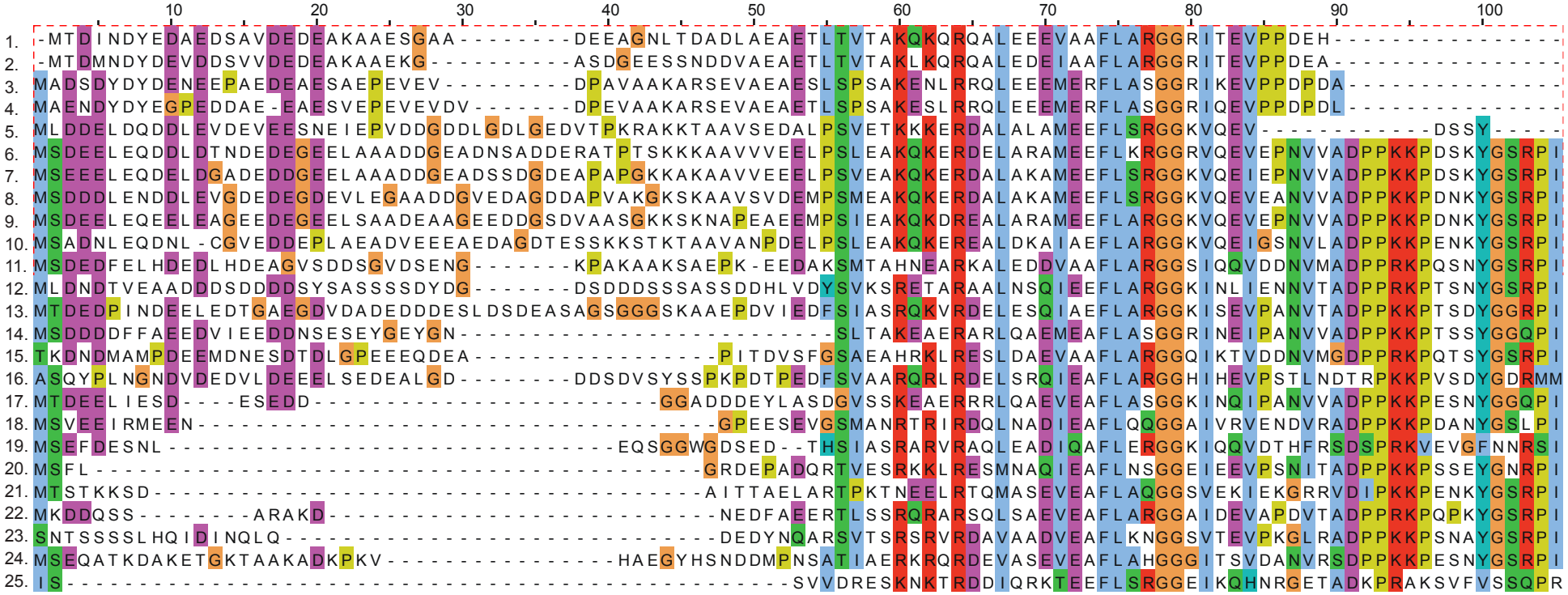

1. *Acinetobacter baumannii*
2. *Acinetobacter equi*
3. *Perlucidibaca piscinae*
4. *Perlucidibaca aquatica*
5. *Oblitimonas alkaliphila*
6. *Pseudomonas stutzeri*
7. *Pseudomonas aeruginosaUCBPP-PA14*
8. *Pseudomonas putida*
9. *Azotobacter vinelandiiDJ*
10. *Ventosimonas gracilis*
11. *Oceanobacter kriegii*
12. *Simiduia agarivorans*
13. *Cellvibrio japonicus*
14. *Saccharophagus degradans*
15. *Thalassolituus oleivorans*
16. *Marinimicrobium agarilyticum*
17. *Teredinibacter turnerae*
18. *Mangrovitalea sediminis*
19. *Marinobacter lutaoensis*
20. *Endozoicomonas numazuensis*
21. *Reinekea blandensis*
22. *Microbulbifer agarilyticus*
23. *Gynuella sunshinyii*
24. *Oleispira antarctica*
25. *Gamma proteobacterium HTCC2207*

Figure 1- figure supplement 1. *P. aeruginosa* UBCPP-PA14-centric alignment of representative SutA homologs. SutA homologs were detected by BLAST, and representatives were selected from multiple families in each of the four orders in which SutA could be found (Alteromonadales, Cellvibrionales, Oceanospirillales, and Pseudomonadales). After alignment using the MEGA6 software suite (Tamura et al., 2013), gaps in the *P. aeruginosa* UBCPP-PA14 sequence were removed and the aligment was visualized using the Jalview2 applet(Waterhouse et al., 2009).

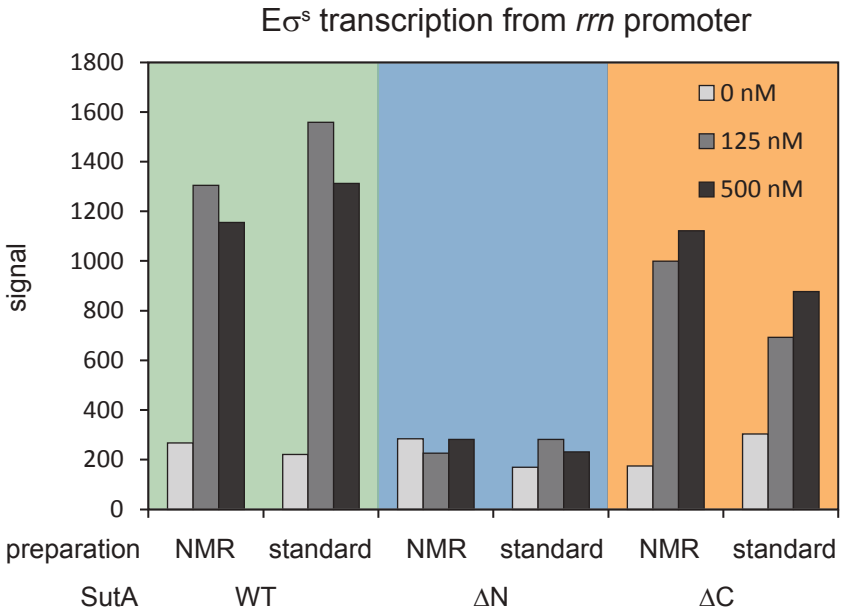

Figure 1 - figure supplement 2. *In vitro* transcriptional activity of SutA proteins prepared for NMR, compared to the same proteins prepared using standard methods. Activity of proteins produced for NMR was tested using the single-turnover initiation assay with $E\sigma^S$ as described for Figure 2.

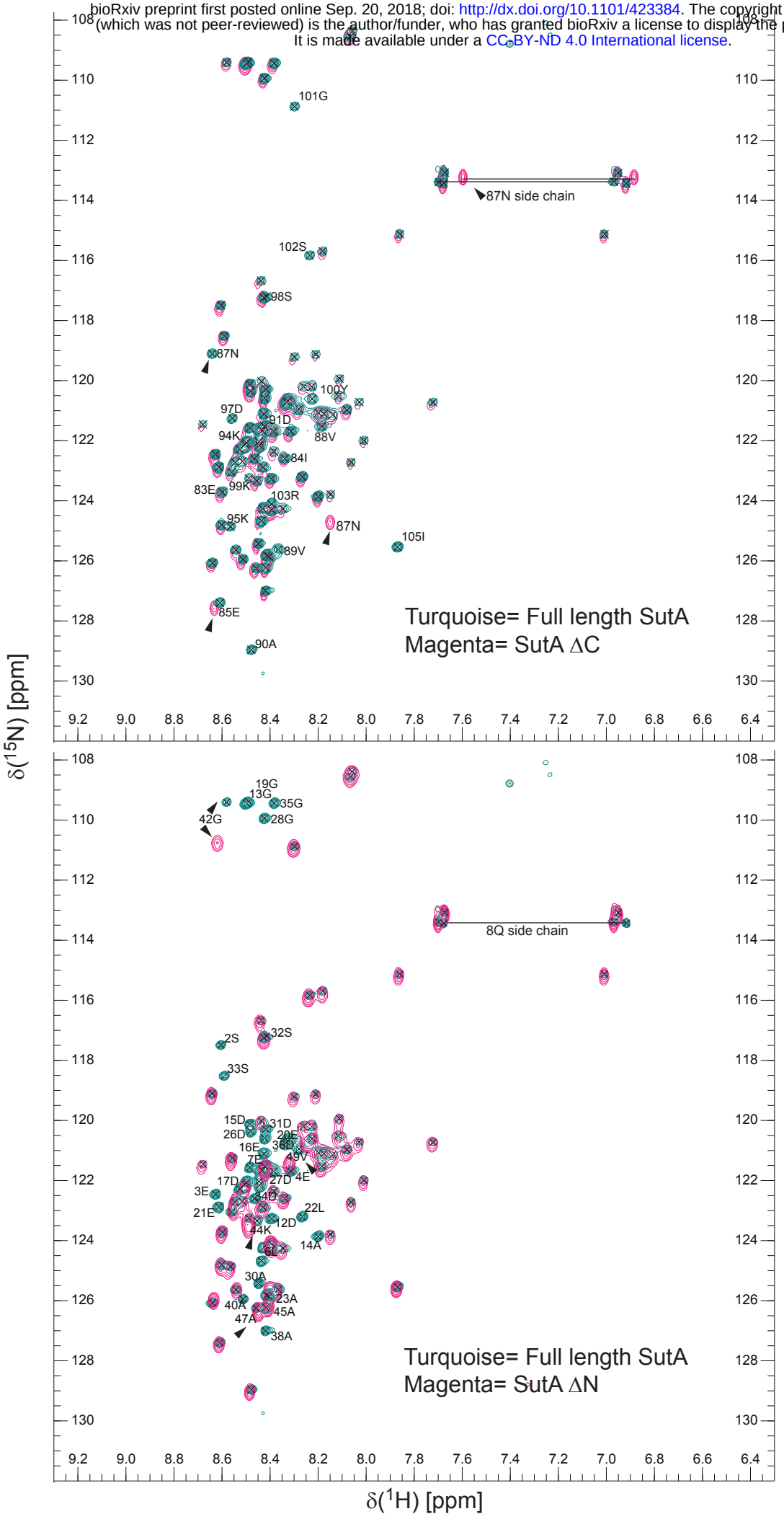

Figure 1 - figure supplement 3. ^{1}H-^{15}N HSQC spectra comparing the full-length WT SutA to ΔN and ΔC proteins. ^{1}H-^{15}NHSQC spectra for SutAΔC (top) and SutAΔN (bottom) (both in magenta) were overlaid on the ^{1}H-^{15}N HSQC for the full-length SutA (turquoise). Apart from the loss of the truncated residues, only a few peaks near the newly created C- or N-terminus are perturbed.

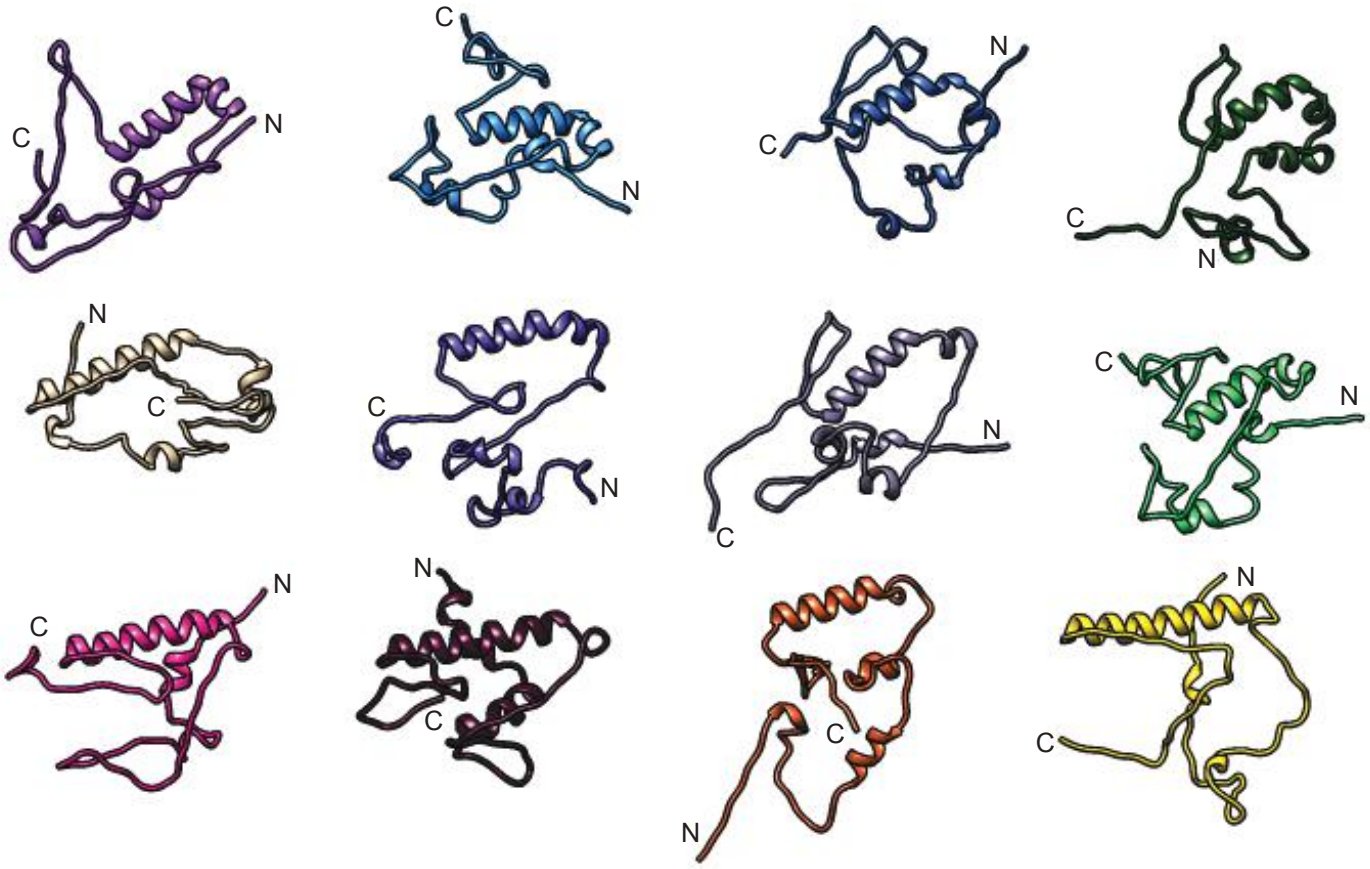

Figure 1 - figure supplement 4. A selection of low-resolution SutA decoys generated by PyRosetta modeling utilizing NMR chemical shift and RDC data. The model used for Figure 1D is in the second row, first column. SutA is a very flexible protein, with its only secondary structural feature being an α-helix encompassing residues 56-76, and even that helix displays some predicted possible flexibility. We did not detect a peak for the Gln61 residue, the point in the helix that shows the most variation in these models.

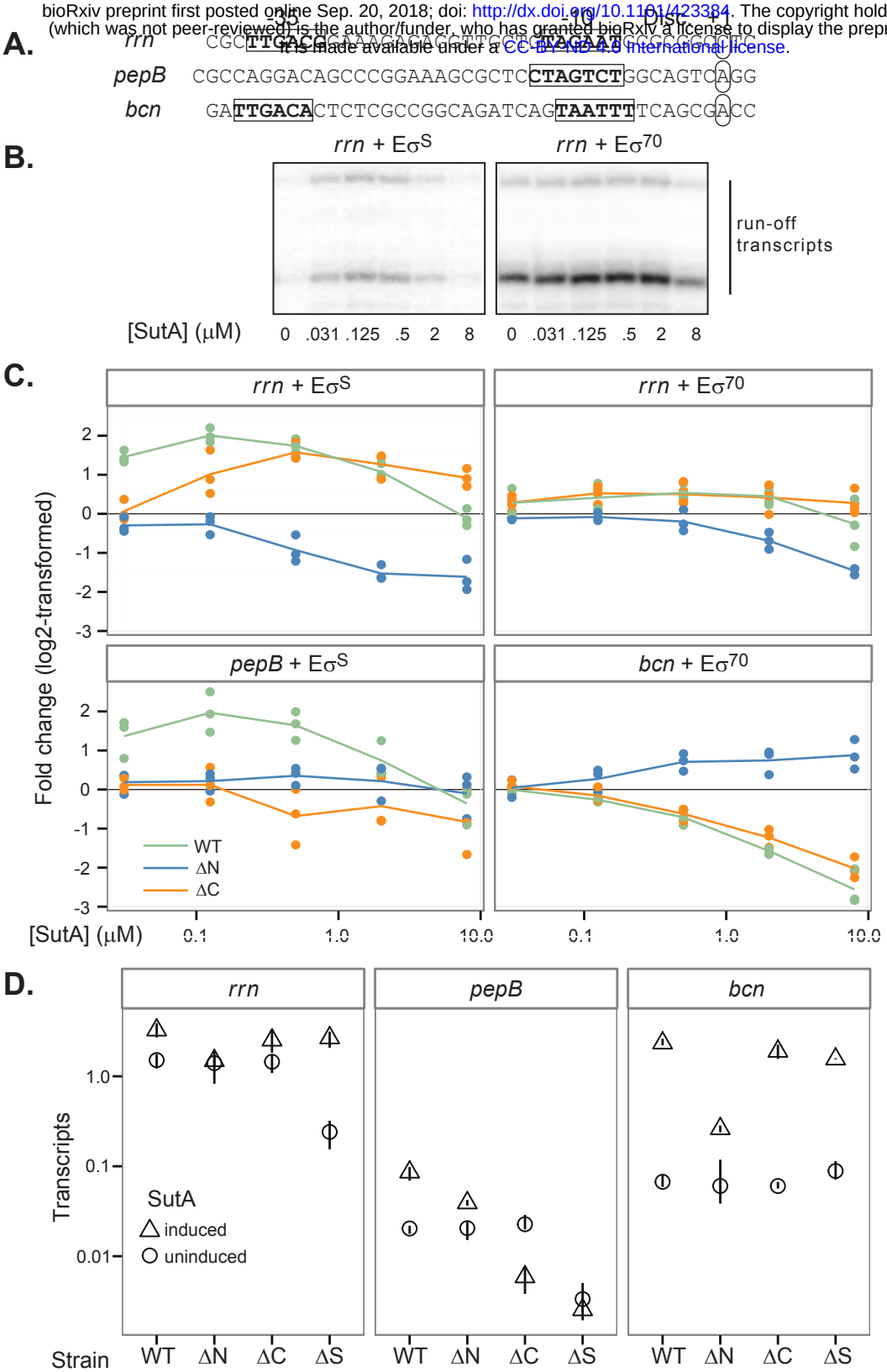

Figure 2. Effects of SutA variants on transcription initiation. A. Promoter sequences. -10 and -35 motifs are indicated in bold and boxed (no consensus -35 motif has been defined for σS in P. aeruginosa), transcription start sites are indicated by circles, and the discriminator region is noted (Disc.). **B.** Representative gel images for single-turnover reactions containing 20 nM RNAP holoenzyme, 15 nM linear template, 20 μg/ml heparin, 75 μM initiating dinucleotide, 50 μM NTPs for the bases not labeled in the experiment, 20 μM cold NTP for the base carrying the ^{32}P label, and 0.75 μCi α^{32}P labeled GTP or CTP per 5 μl reaction, in TGA buffer. Reactions were quenched and loaded onto 20% denaturing polyacrylamide gels. Both bands are productive transcripts that arise from termination near the end of the linear template. Contrast was adjusted according to signal; σ^S activity was much less than σ^{70} activity. **C.** Amount of transcript produced in the presence of varying concentrations of SutA, compared to the amount produced in the absence of SutA, expressed as a log2-transformed ratio. Reactions were as described above, except for reactions including pepB promoter and σS holoenzyme, which contained 40 nM RNAP. Individual replicate values are plotted (n≥ 3), and lines connect the average of all replicates at each concentration. **D.** SutA effects *in vivo*. WT, ΔN, or ΔC SutA were expressed from an arabinose-inducible promoter in a Δ*sutA* strain or Δ*sutA* Δ*rpoS* strain (WT SutA only, "ΔS"). Strains were grown overnight in LB and diluted 1:1000 into minimal medium containing 40 mM pyruvate as a carbon source ± 20 mM arabinose. After 24 hours, during which cultures slowly reached stationary phase, transcript levels were measured by qRT-PCR. Each transcript of interest was normalized to the number of *oprI* transcripts in the same sample. Symbols represent average values for triplicate measurements, and lines represent the range of values.

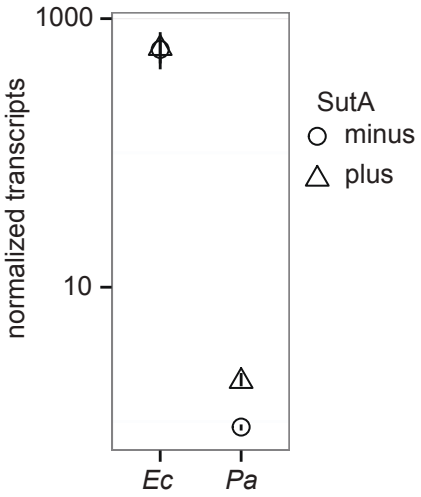

Figure 2 - figure supplement 1. Induction of SutA overexpression in *E. coli* does not cause upregulation of rrn expression. SutA under control of an arabinose-inducible promoter on the pMQ72 plasmid backbone, or the empty vector, was introduced into either *E. coli* MG1655 or *P. aeruginosa* UBCPP-PA14 Δ*sutA*, and cells were grown into late stationary phase in LB in the presence of 20 mM arabinose before harvesting them, extracting RNA, and measuring nascent rrn transcript levels by qRT-PCR. Symbols represent the average value from 3 biological replicates, and vertical lines represent the range of values observed.

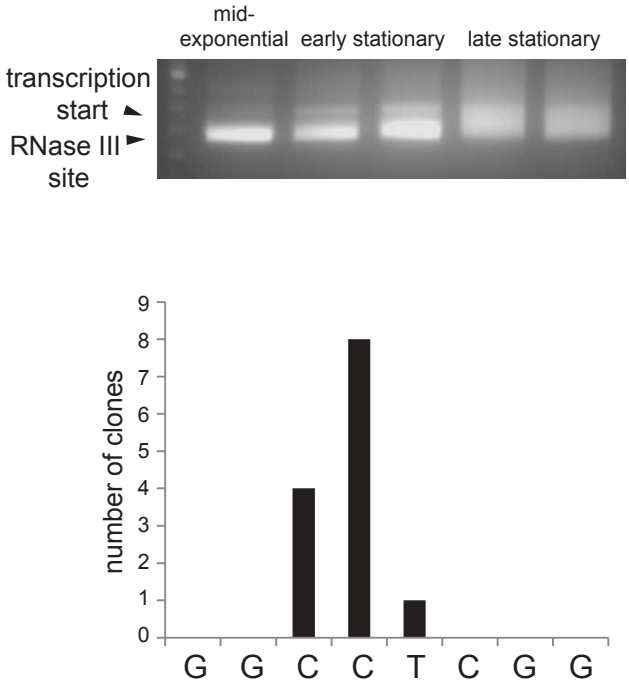

Figure 2 - figure supplement 2. 5'RACE to determine the transcription start site for *rrn* in *P. aeruginosa*. Total RNA was extracted from P. aeruginosa UCBPP-PA14 in exponential, early stationary, or late stationary phase, and the leader sequence of the rrn transcript was reverse transcribed, T-tailed, PCR-amplified, and cloned into pUC18. Several clones from the stationary phase time points were from transcripts whose 5' ends corresponded to the RNase III cleavage site in the rrn leader, based on comparison to the *E. coli* sequence, but clones whose 5' ends corresponded to putative transcription start sites were distributed as shown.

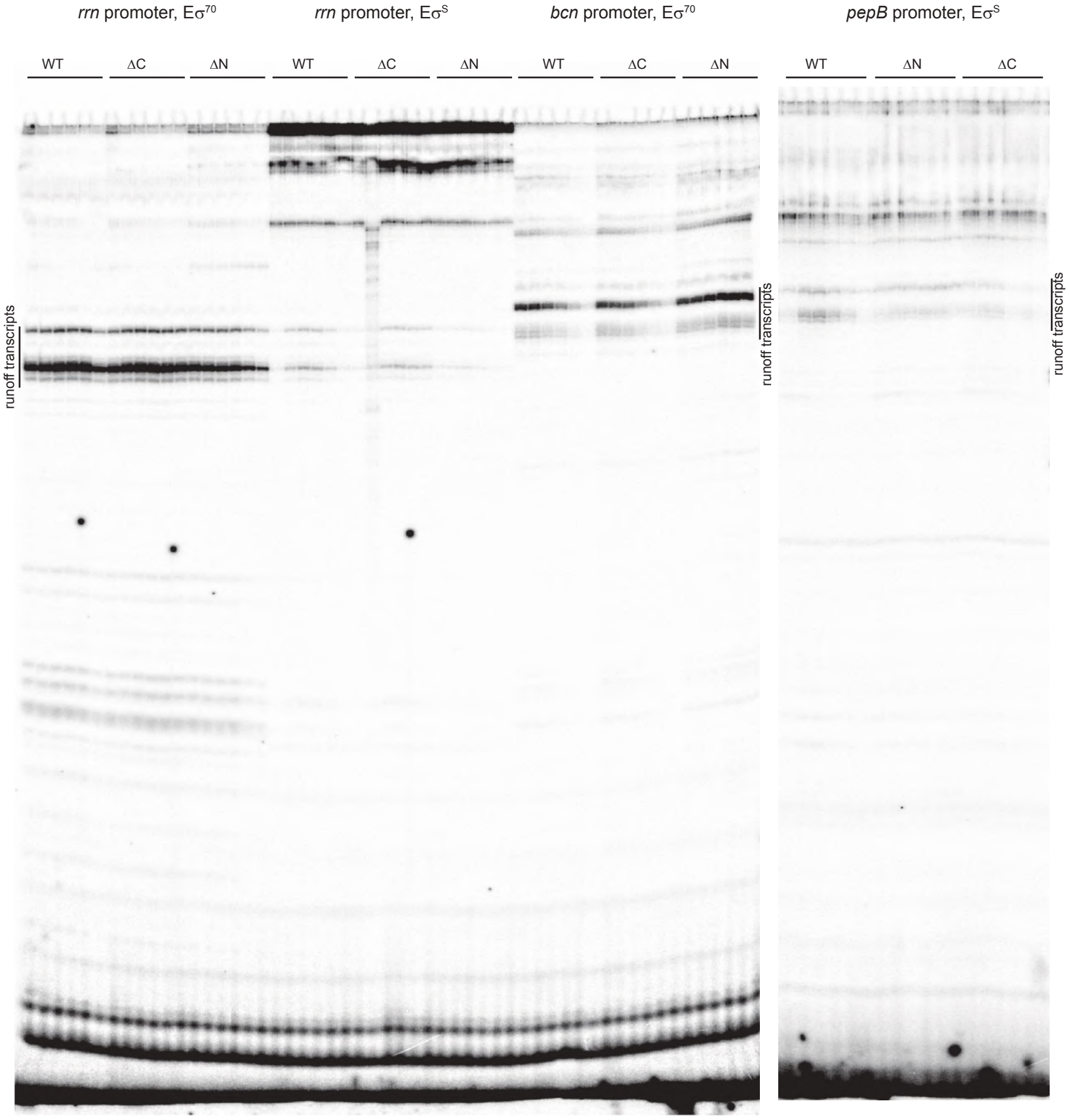

Figure 2 - figure supplement 3. Full length gels for one replicate of each promoter/holoenzyme/SutA combination shown in Figure 2. The rrn/Eσ^S/31 nM SutA ΔC sample was degraded, and an additional replicate of this sample was run on a subsequent gel.

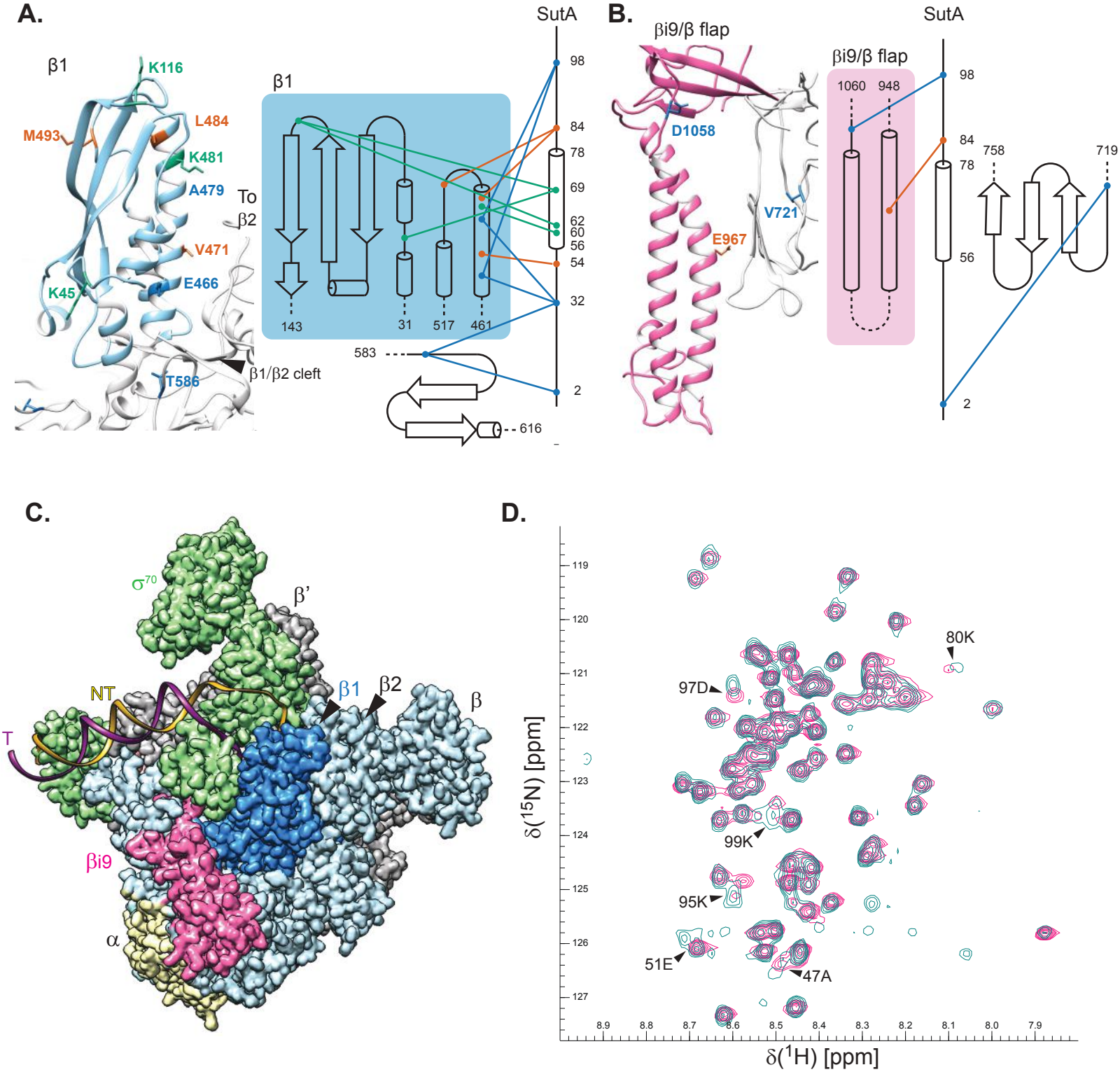

Figure 3. Crosslinking and affinity cleavage suggest that SutA binds to the β subunit of RNAP. A. Contacts with the β1 domain. *P. aeruginosa* sequence was threaded onto a structural model of the *E. coli* β (PDB ID: 5UAG) for interpretation of cross-linking results. A topology diagram of the contacts inferred by cross-linking (BS^3, green lines; BPA, orange lines) and FeBABE-mediated cleavage (blue lines). The contact residues on β1 are colored accordingly. Crosslinked residues were identified by LC-MS/MS, cleavage sites were determined by SDS-PAGE and Western blotting of the cleaved complexes, using a large-format gel system and an antibody raised against a peptide at the extreme C-terminus of the E. coli β. See text, supplemental figures, and materials and methods for further details. **B.** Contacts around the βi9 and β flap domains. Distances from the β1 cross-links suggest this may be a secondary, weaker site. **C.** Cryo-EM structure of E. coli $E\sigma^{70}$ (PDB: 6CA0), indicating relative positions of β1 (darker blue, same as region shown in (A), and fragment purified for (D)) and βi9/β flap regions (pink, same as region shown in (B)). **D.** ^{1}H-^{15}N HSQC spectra showing that chemical shifts for a handful of residues are perturbed when ^{15}N-labeled SutA is mixed with unlabeled β1 domain (pink) vs unlabeled σ^S (turquoise). A small number of extra peaks show up only in the σ^S mixture (turquoise, lower right quadrant); these are most likely due to very low levels of protein cleavage in the C-terminal disordered tail of SutA caused by a minor protease contaminant present in the σ^S protein preparation which occurred during an extended period of exposure to ambient temperatures.

Figure 3 - figure supplement 1

BS³ crosslinking:

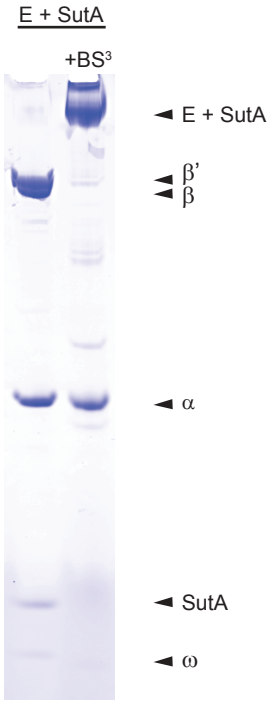

Evaluation of crosslinks among RNAP subunits:

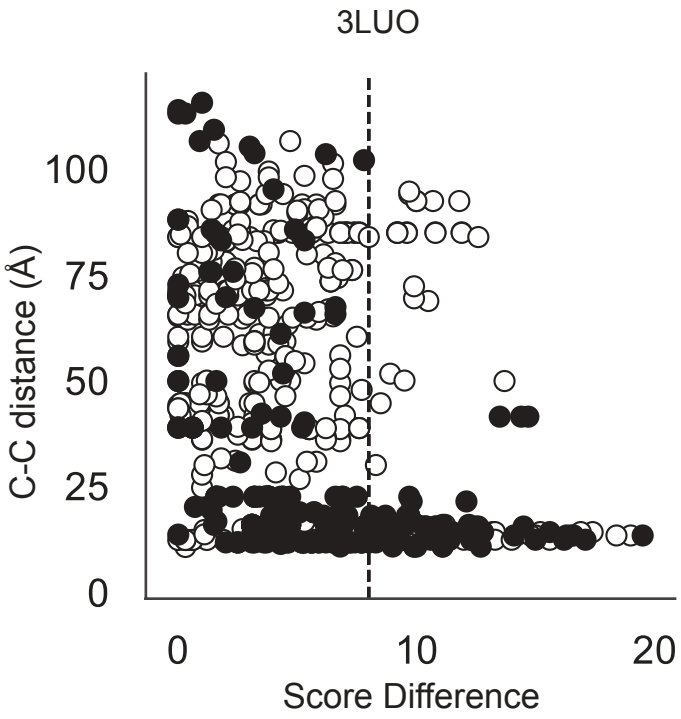

crosslink	# spectra	score diff.
SutA 62-β 116	15	15.6
SutA 69-β 116	11	18.8
SutA 62-β 481	1	8.2
SutA 69-β 45	1	11.4

Figure 3 - figure supplement 2

BPA crosslinking:

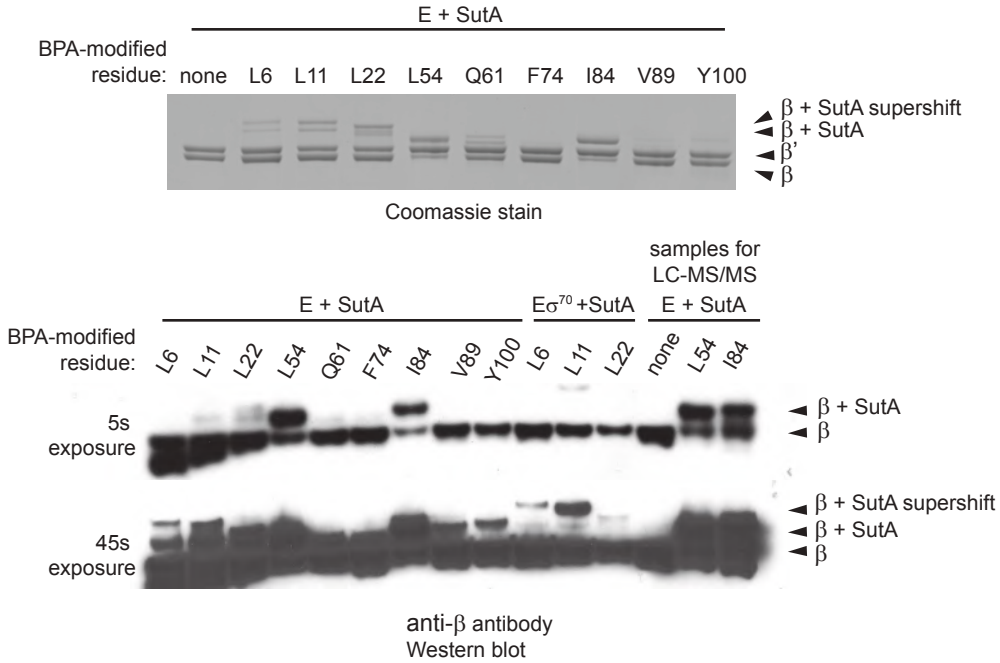

Figure 3 - figure supplement 1.BS³ crosslinking visualization and analysis. A Coomassie-stained SDS-PAGE gel showing BS³ cross-linking of RNAP-SutA complexes, a comparison of the score differences calculated for intra-RNAP cross-links versus the distances between the cross-links in a published RNAP structure that was used to determine an appropriate score difference cut-off for likely real cross-links, and a list of SutA-RNAP cross-links, the number of spectra in which they were detected, and the maximum score difference observed.

Figure 3 - figure supplement 2. A Coomassie stained SDS-PAGE gel and a Western blot using an anti-β antibody showing the formation of shifted β bands following SutA BPA variant crosslinking to β.

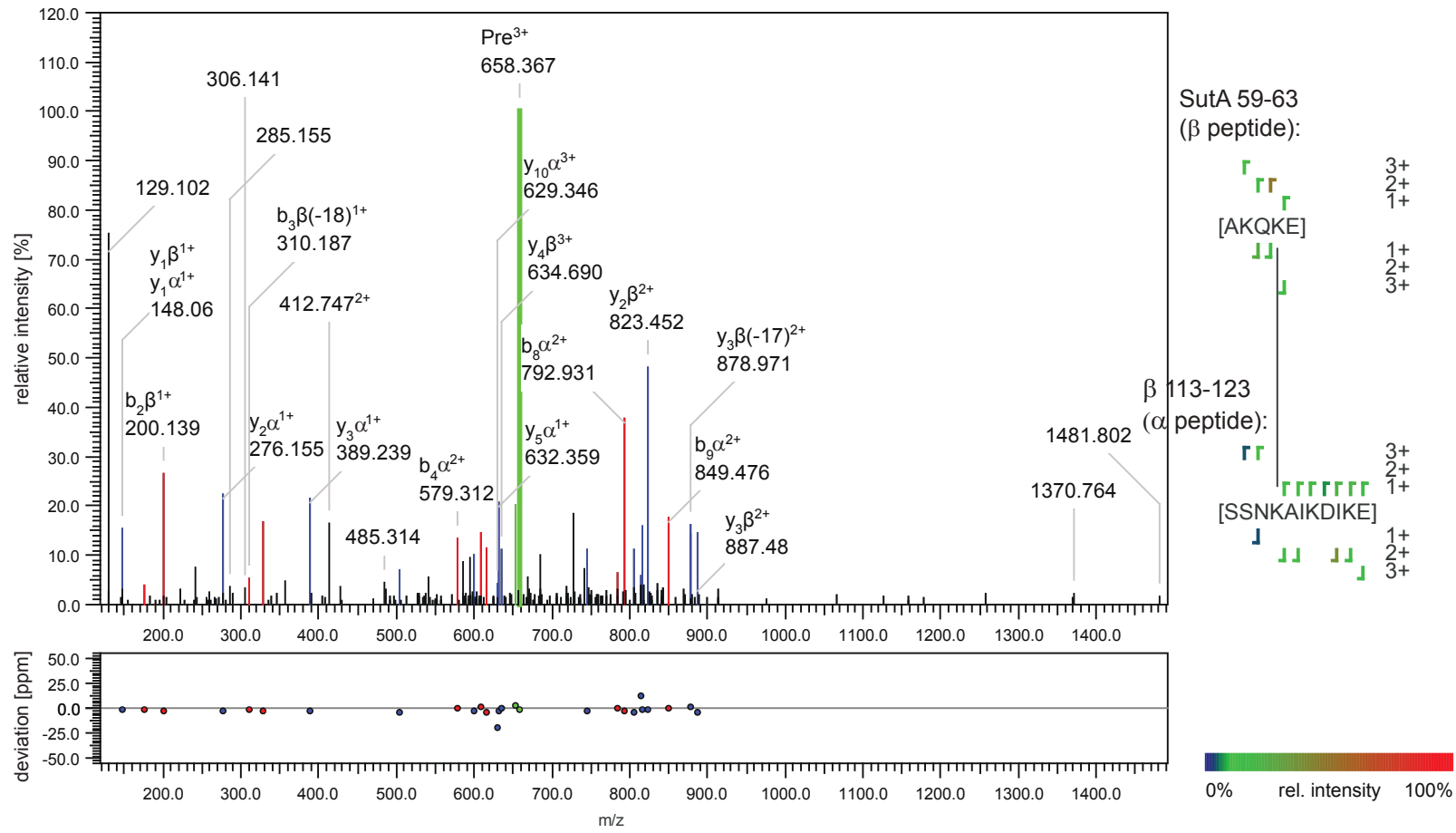

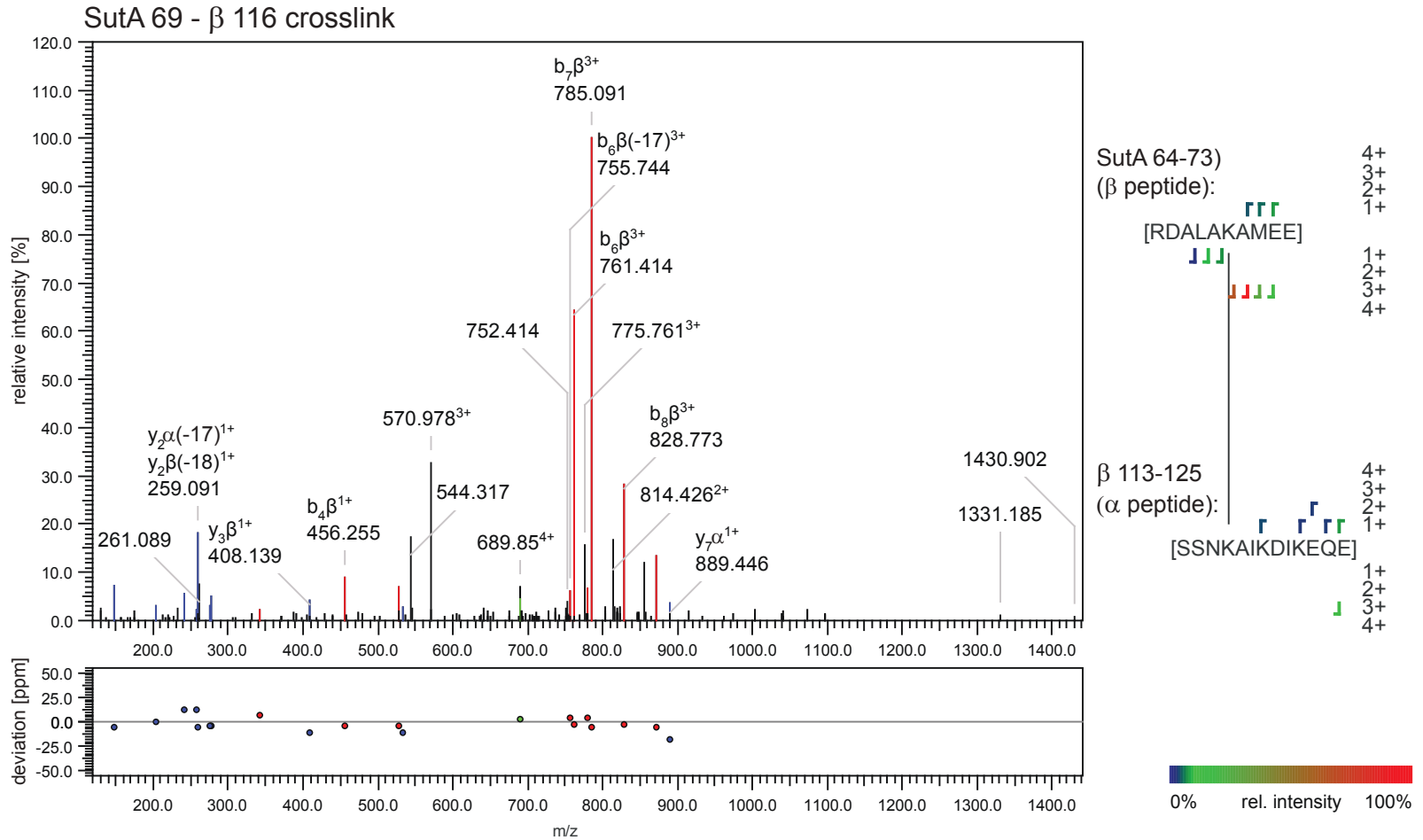

Figure 3 Supplement 3. LC-MS/MS spectra from crosslinked peptides detected in the BS3 experiment. Output from StavroX analysis software shows multiple detected fragment ions from both component peptides, indicating high-quality identifications of crosslinked peptides.

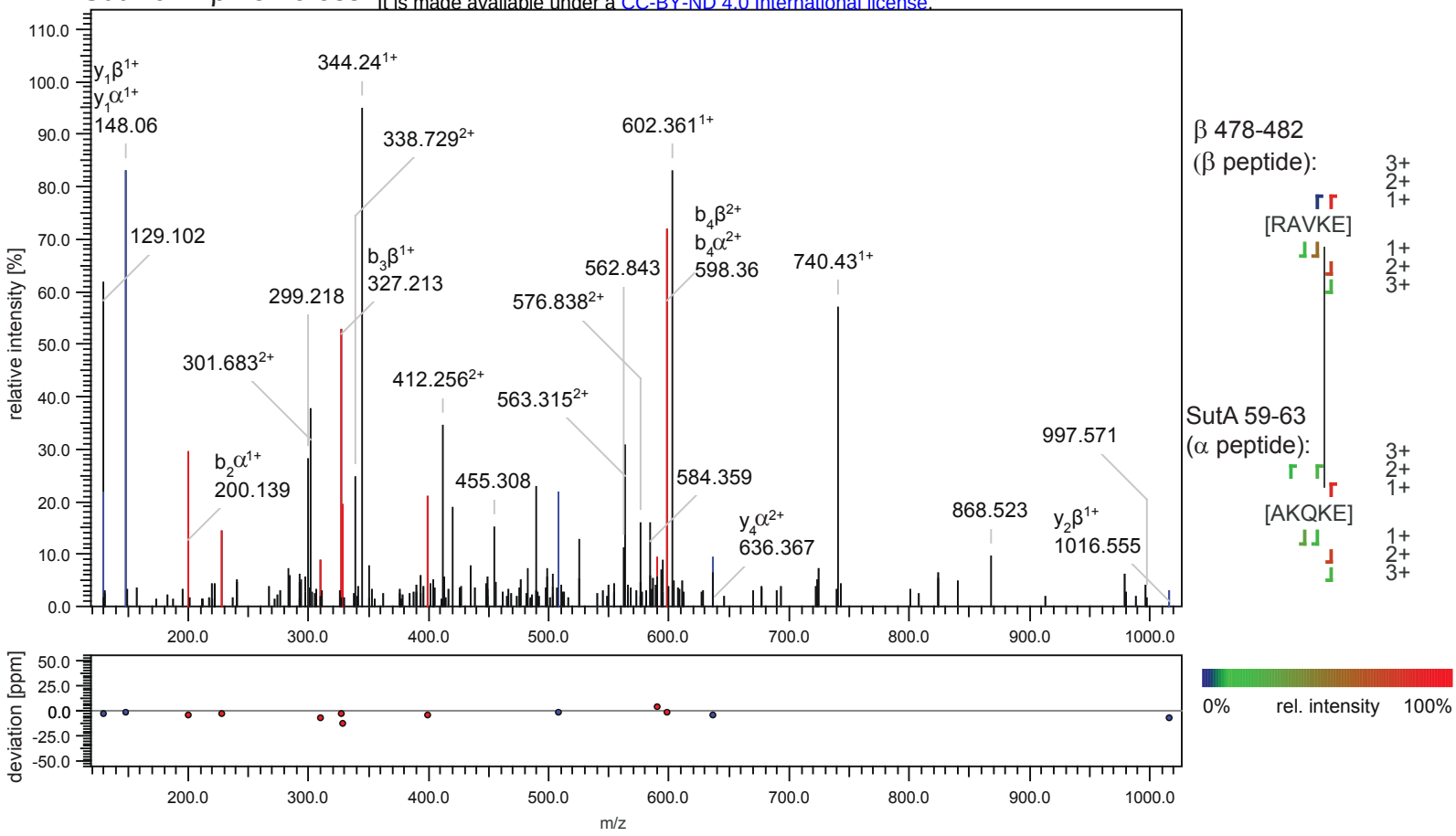

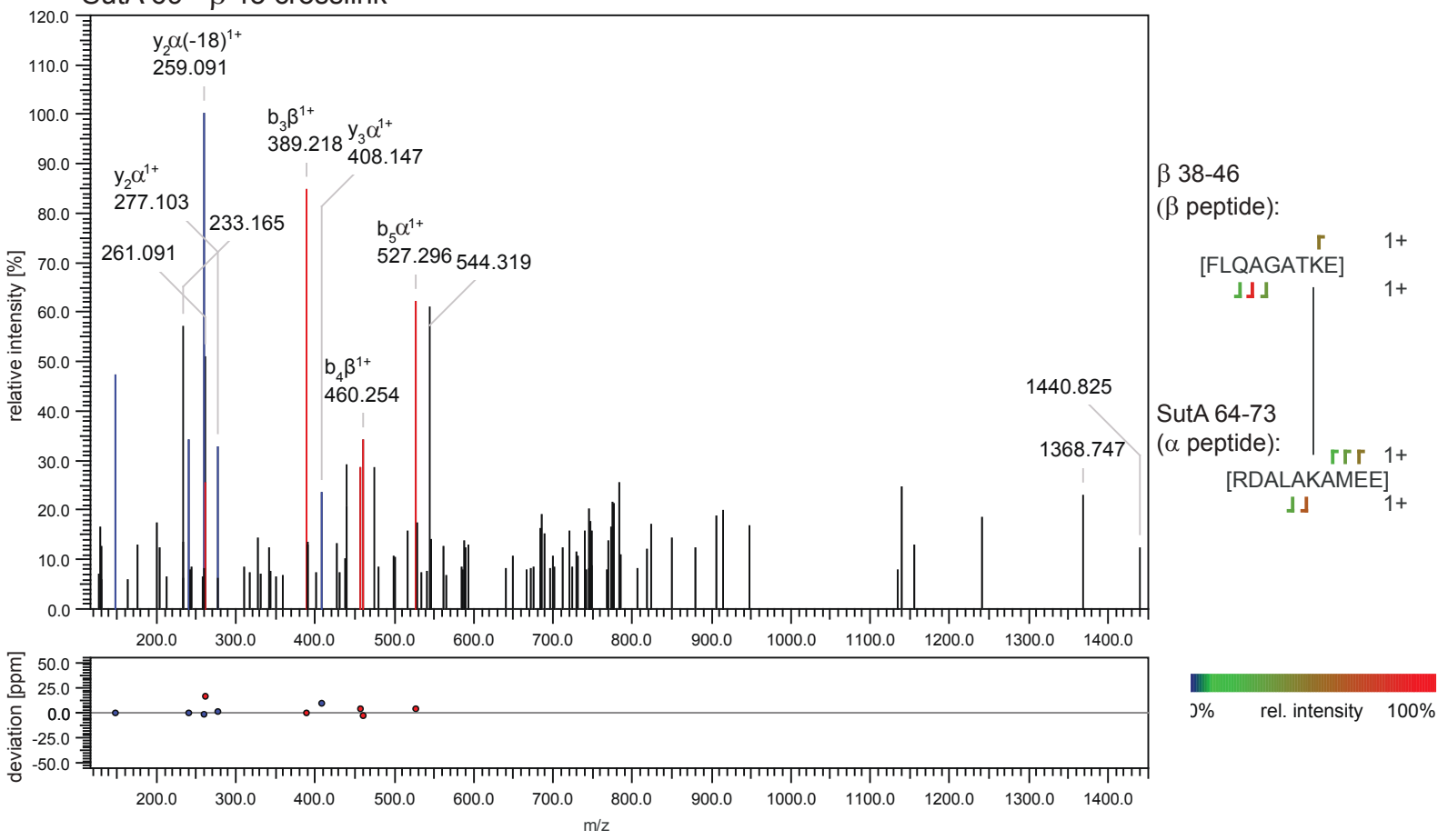

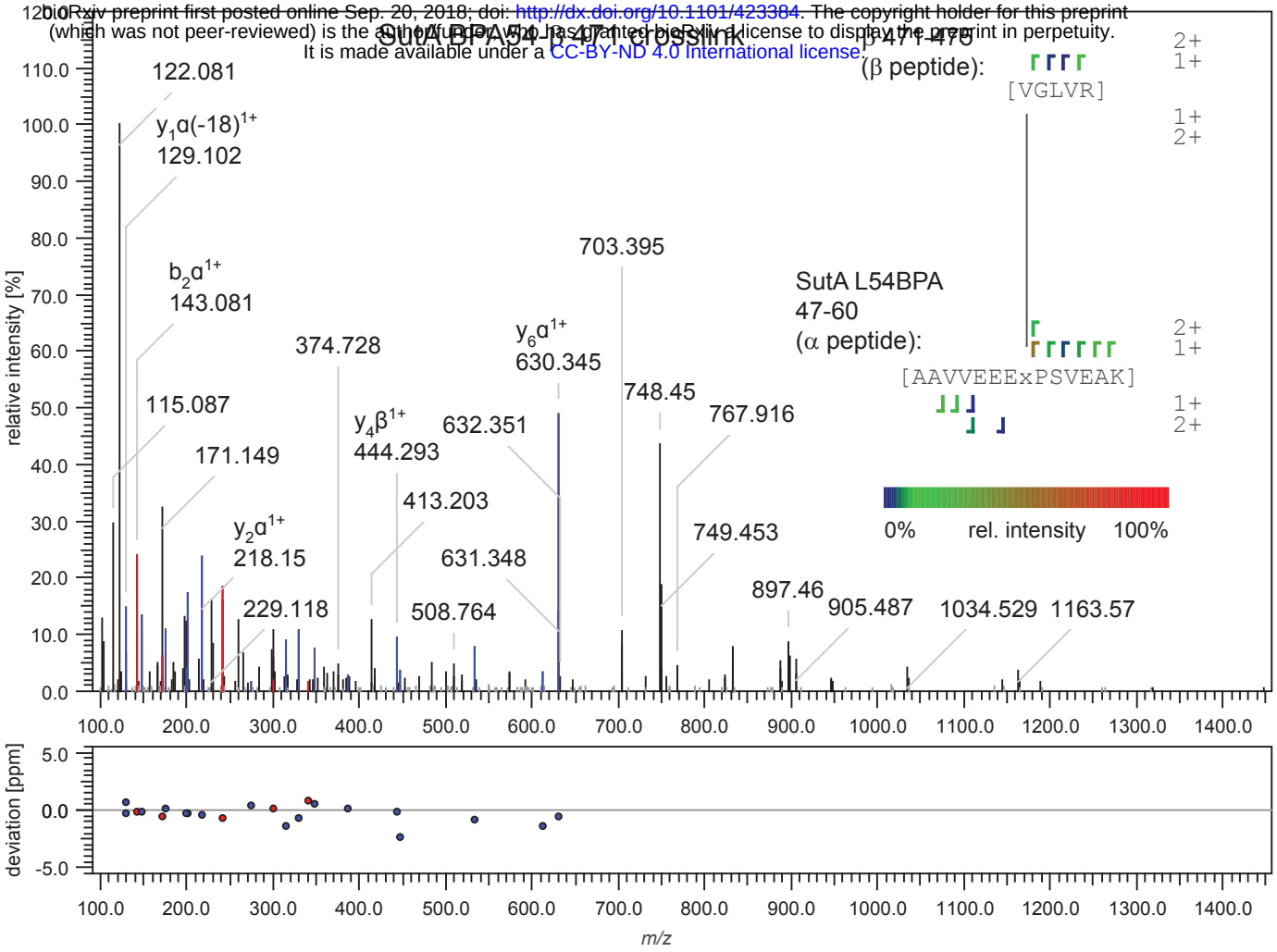

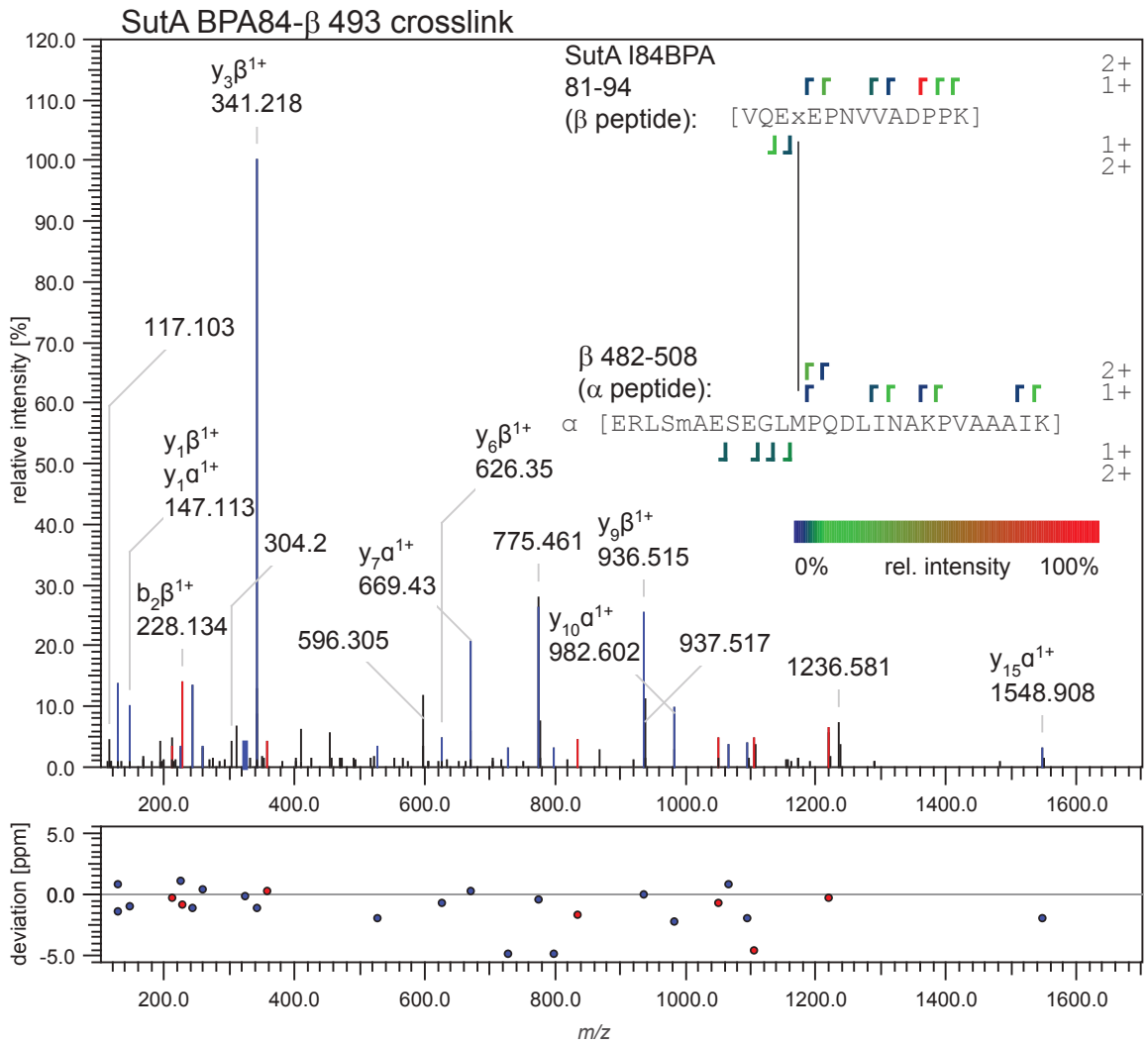

Figure 3 Supplement 4. LC-MS/MS spectra from crosslinked peptides detected in the BPA experiments. Output from StavroX analysis software shows multiple detected fragment ions from both component peptides, indicating high-quality identifications of crosslinked peptides.

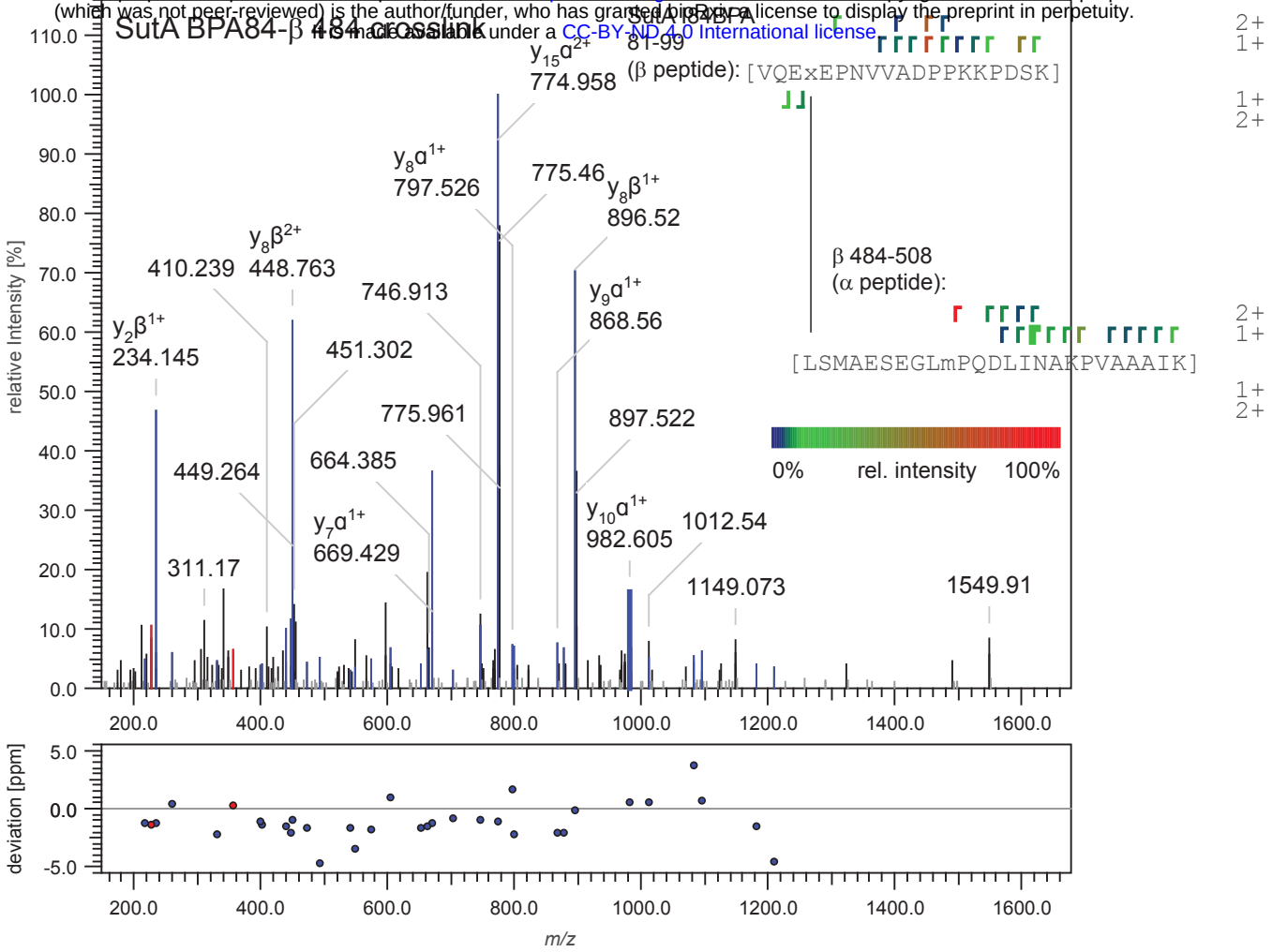

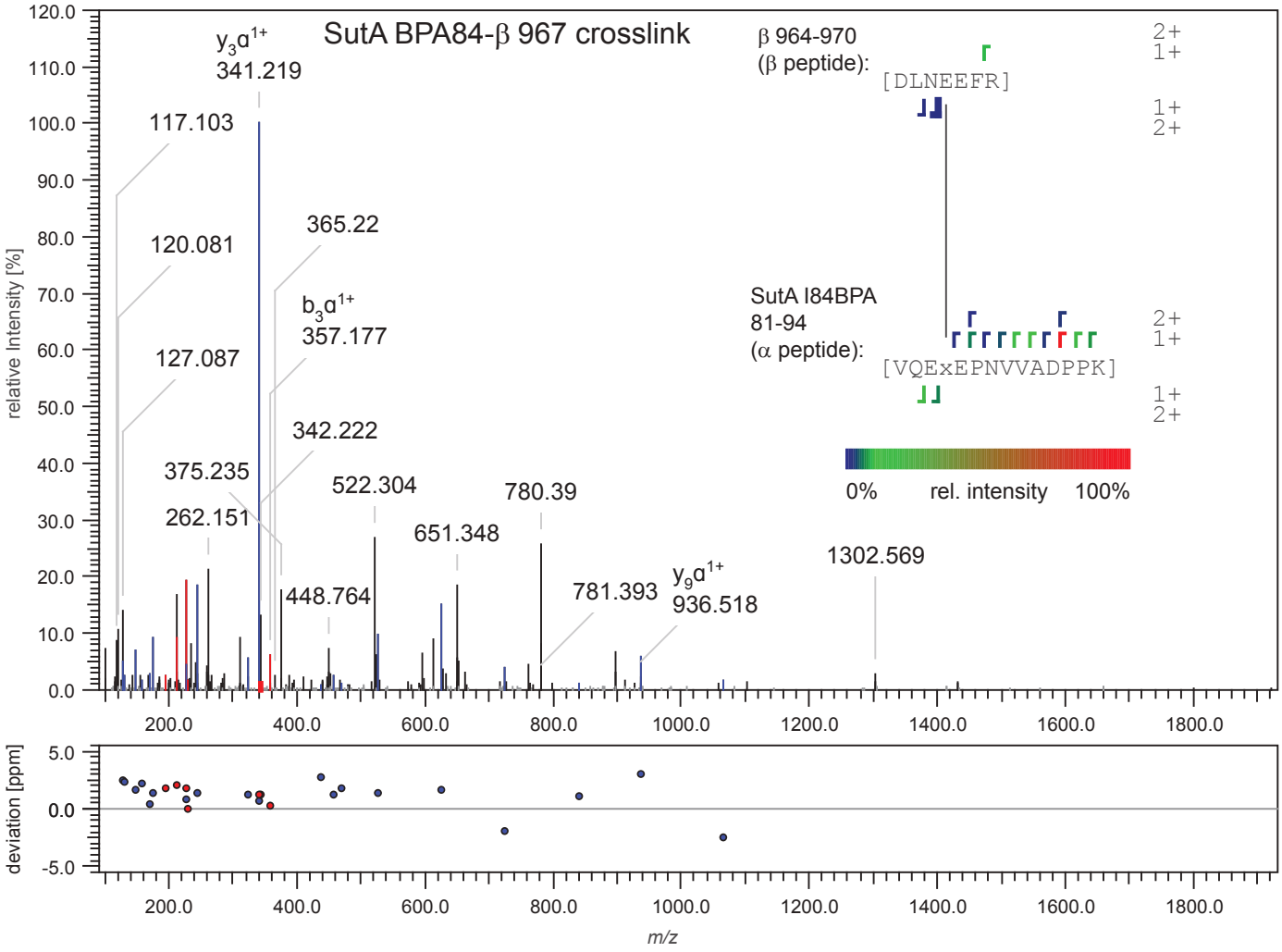

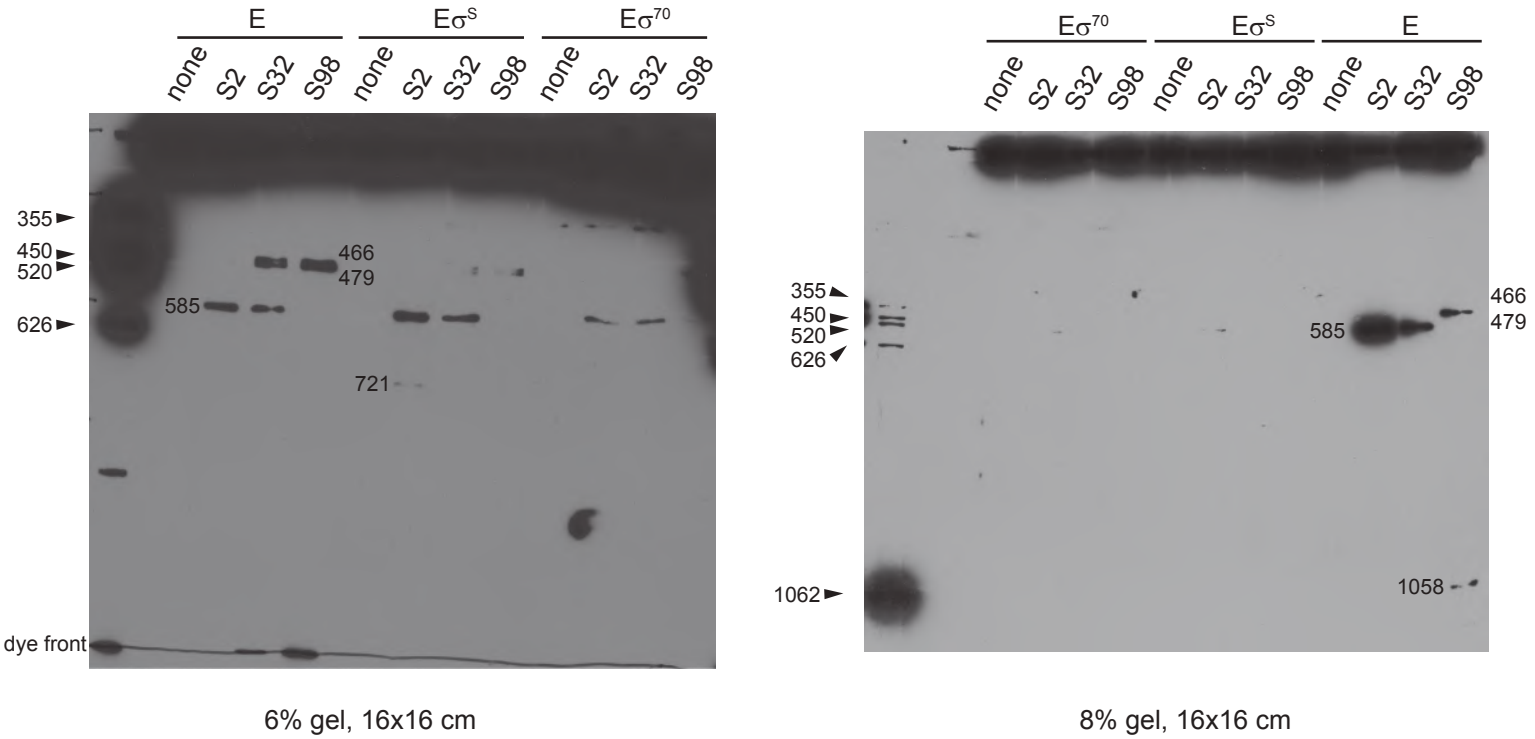

Figure 3 - figure supplement 5. 16x16 cm Western blots from two different percentages of acrylamide, for calculation of FeBABE cleavage positions. Western blotting of FeBABE cleavage products was performed in a large format to allow for accurate calculation of the molecular weights of the cleavage products. For each known fragment, generated by overexpressing a cloned fragment of P. aeruginosa β in E. coli, the molecular weight was calculated using the ExPASy Compute pI/Mw tool, and the log of this value was plotted against the ratio: (distance traveled by band/distance traveled by dye front). The linear relationship established was used to calculate the molecular weights of the FeBABE cleavage products based on their band/dye front ratios, and those molecular weights were used to determine the amino acid position at which the cleavage occurred.

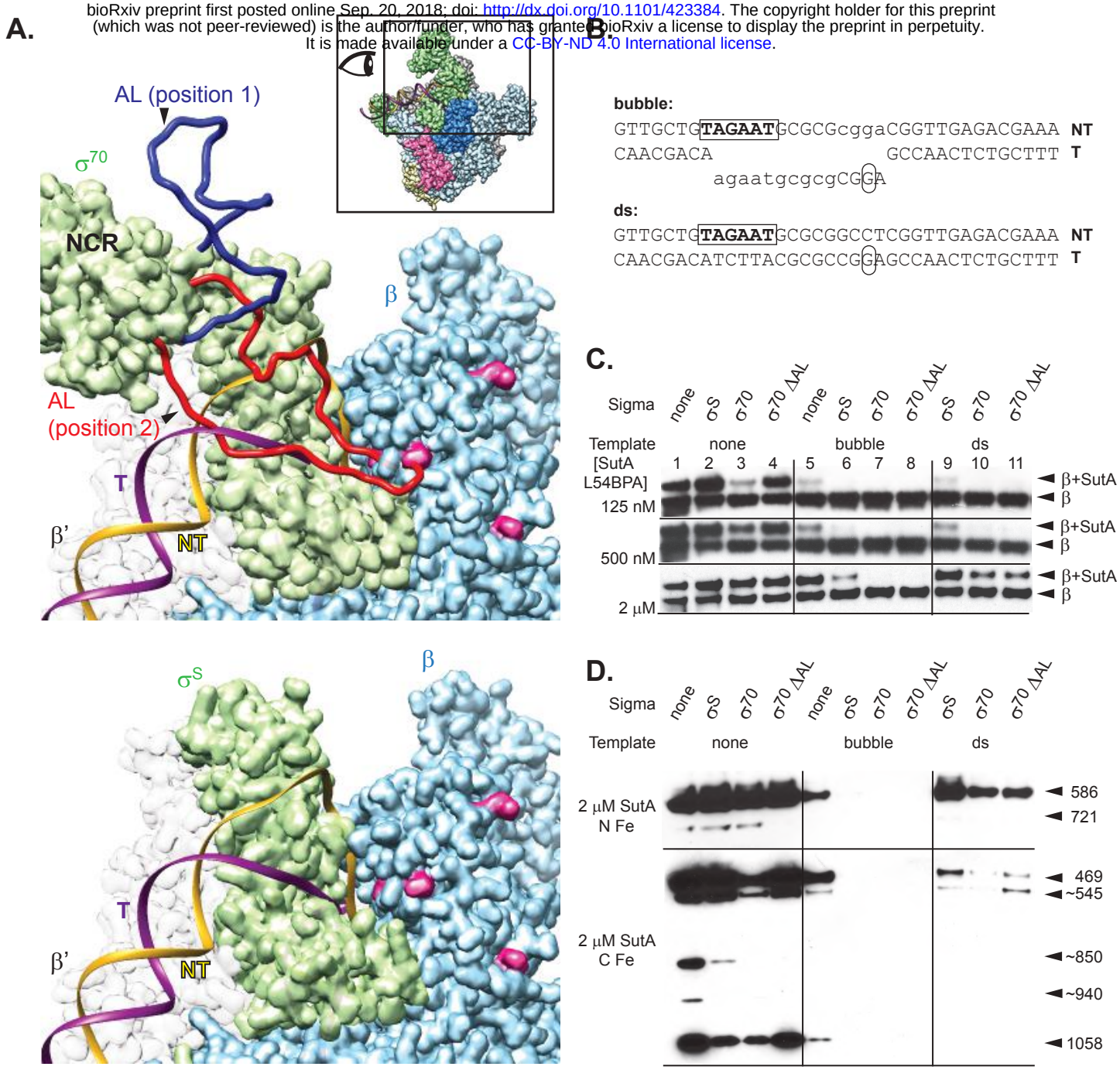

Figure 4. Both σ factor and DNA compete with SutA for binding to the core RNAP. A. Models based on E. coli σ70 and σS holoenzyme structures show potential interactions between σ factors and SutA. The inset shows the perspective and extent of this view relative to the holoenzyme structure shown in (3C). The *P. aeruginosa* β sequence was threaded onto an *E. coli* crystal structure (PBD: 5UAG), and then the β subunit from this was docked into the Eσ^{70} cryoEM structure (top) (PDB:6CA0) or the Eσ^{S} crystal structure (bottom) (PDB:5IPN). Residues showing crosslink or cleavage reactivity with SutA (Fig. 3) are colored magenta. Residues 168-212 of σ^{70}, which are not visualized in the cryoEM structure, were modelled in as a flexible loop. Two different possible positions are shown (red and dark blue), one of which (red) could clearly clash with both the DNA and SutA positions (top). In contrast, σ^{S} does not appear likely to directly contact SutA (bottom). **B**. Sequence and structure of template DNA surrounding transcription start site. **C.** Western blot showing cross-linking of a SutA variant in which L54 has been replaced by BPA to β, in the context of different σ factors and promoter DNA. Reactions contained 100 nM RNAP, 100 nM DNA, 100 mM NaCl, and the indicated amounts of L54BPA SutA in TGA buffer. "ΔAL" refers to a mutant of σ^{70} lacking amino acids 171-214 (*P. aeruginosa* sequence). **D.** Western blots showing β cleavage mediated by N-Fe or C-Fe SutA FeBABE conjugates. Reactions components besides SutA variant were the same as in (C). Sizes of cleavage products were estimated by comparison to β fragments of known sizes analyzed on large non-gradient gels (see supplements to figures 3 and 4); for some products (~), only approximate sizes can be determined. The blot for C-Fe was exposed for longer (4 minutes) than the blot for N-Fe (30 seconds).

Figure 4 - figure supplement 1

SutA L54BPA crosslinking, longer exposure

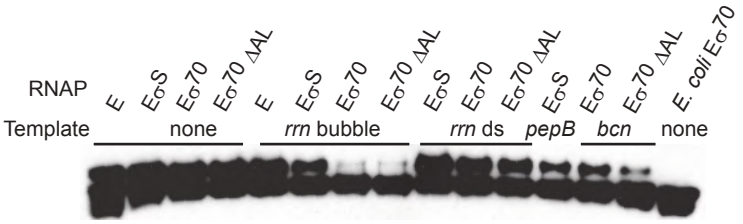

Figure 4 - figure supplement 1. Longer exposure of Western blot showing crosslinking of 2 μM L54BPA SutA to β. A low level of crosslinking is detectable in the presence of Eσ^{70} and the rrn bubble template, but no crosslinking is detected in the presence of *E. coli* Eσ^{70}, even in the absence of DNA.

Figure 4 - figure supplement 2

FeBABE cleavage with β markers and *E. coli* Eσ^{70}

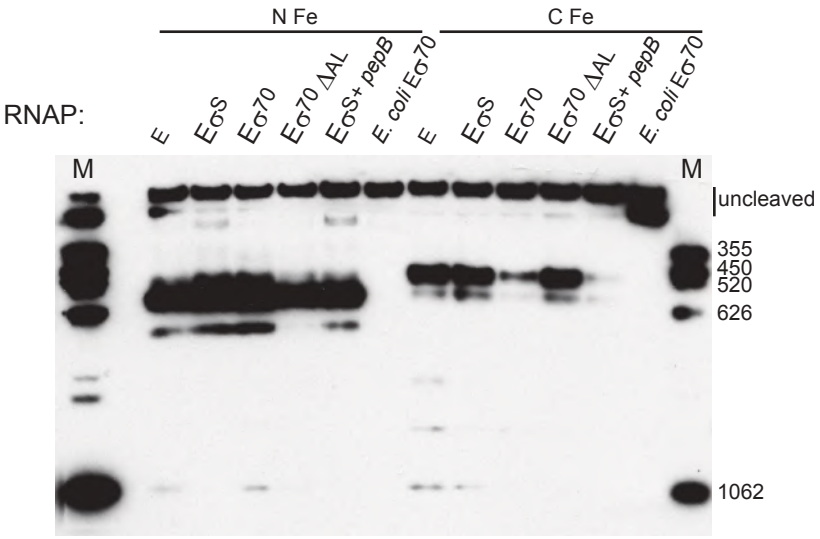

Figure 4 - figure supplement 2. Western blot showing FeBABE cleavage experimental controls. β fragment standards used to determine cleavage positions were run on the mini-gel format for direct comparison to cleavage products observed in open complex contexts, and *E. coli* Eσ^{70} FeBABE cleavage experiments were also run and showed no detectable cleavage.

Figure 4 - figure supplement 3. *In vitro* transcription experiments using Eσ^{70}ΔAL, with the transcription level of the Eσ^{70} holoenzyme in the absence of SutA shown for comparison. Single-turnover initiation assays were performed as described in Figure 2. Eσ^{70}ΔAL appears to have a mild transcription initiation defect, and causes SutA to have more muted effects on initiation.

Figure 4 - figure supplement 3

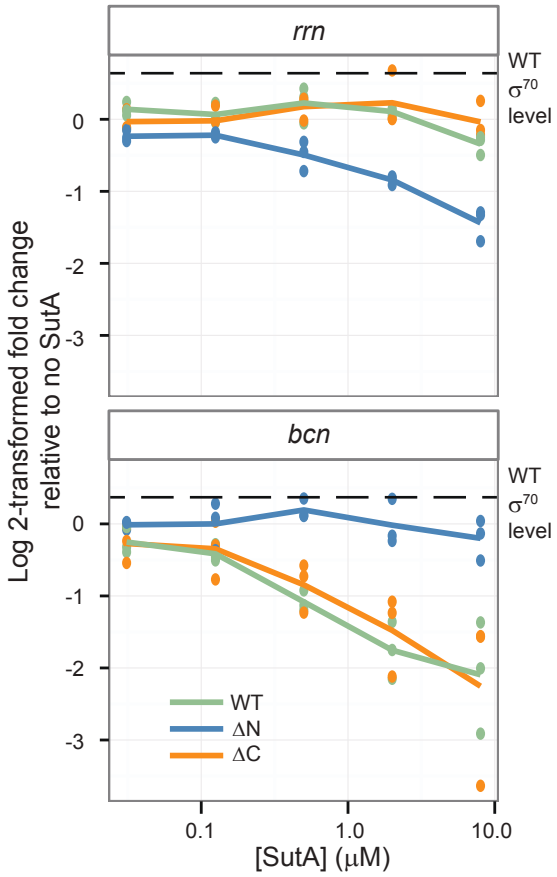

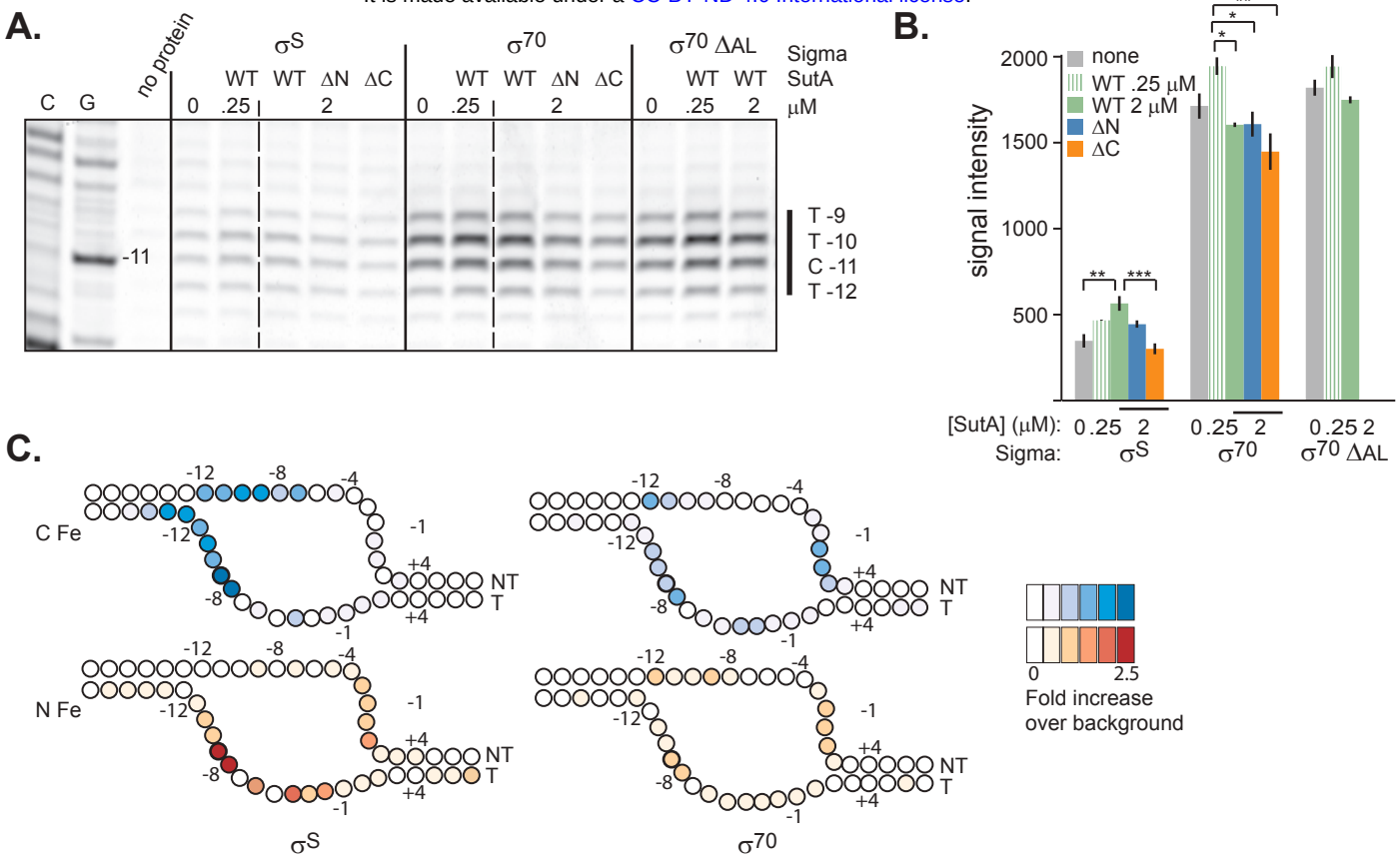

Figure 5. SutA enhances RNAP-DNA interaction, and its tails access the transcription bubble DNA. A. Representative potassium permanganate ($KMnO_4$) footprinting experiment followed by primer extension shows the effects of WT, ΔN, or ΔC SutA on the amount of OC formed upon interaction between the *rrn* DNA and the holoenzyme. Reactions contained 100 nM RNAP holoenzyme, 15 nM template DNA, and the indicated amounts of SutA. The template strand was probed using a Cy5-labeled primer. **B.** Signal intensity from triplicate measurements of the "TTCT" bands (-9 through -12), normalized to the total intensity in each lane (dominated by uncut DNA extension product; see supplement), is shown (right). Error bars are standard error of the mean. P-values for significant differences, as calculated by one-way ANOVA and Tukey's HSD, are indicated by asterisks: *≤ 0.05, **≤ 0.01, ***≤ 0.001. **C**. Cleavage of the DNA in the rrn OCs formed by $E\sigma^{70}$ or $E\sigma^{S}$ in the presence of N-Fe or C-Fe SutA, revealed by primer extension. Average log2-transformed enrichment in signal between the FeBABE reaction and a negative control reaction containing unmodified SutA, from triplicate measurements, is represented by color intensity for each base.

Figure 5 - figure supplement 1: Full-length representative gel of replicate of $KMnO_4$ footprinting assay.

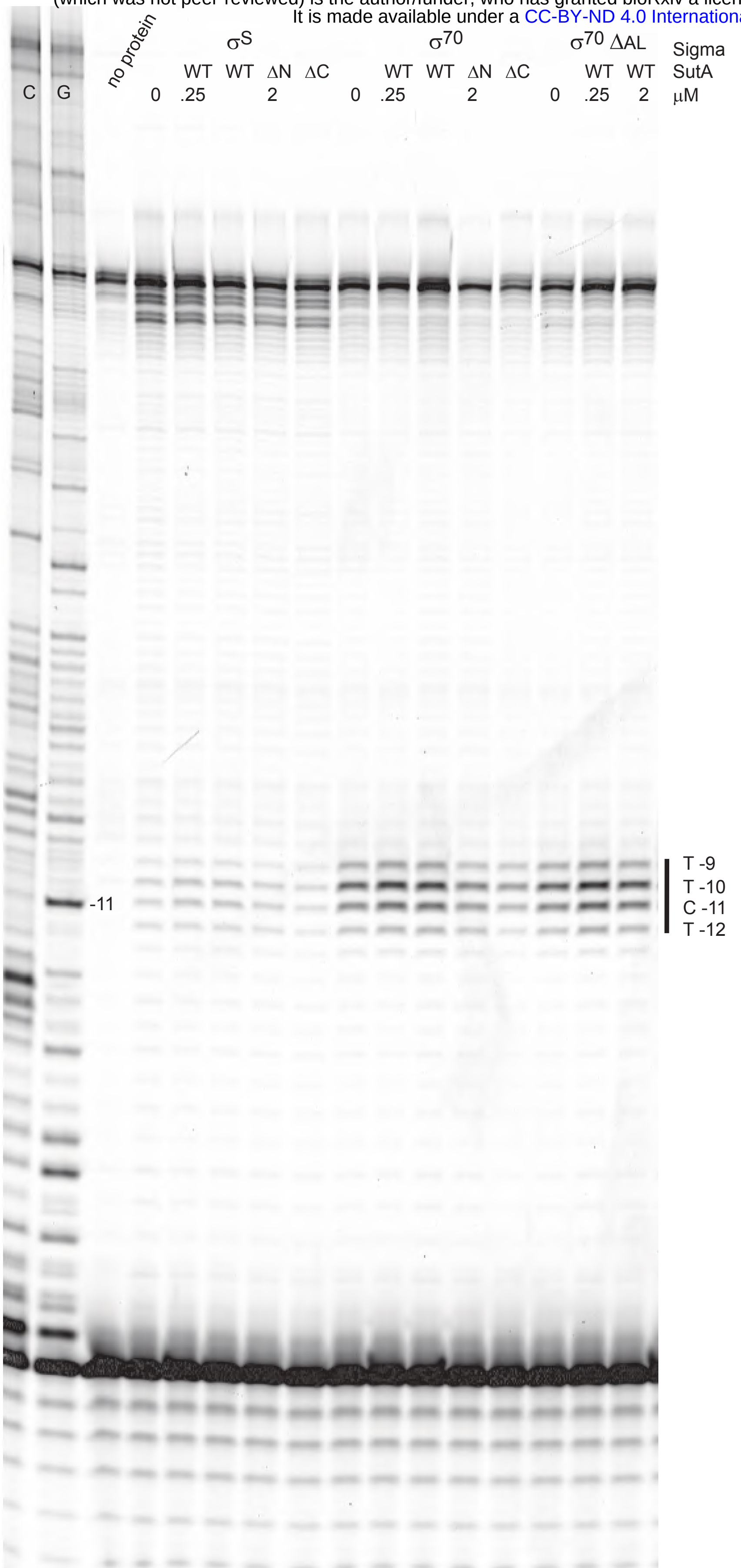

Figure 5 - figure supplement 2. Full length gels for triplicate measurements of FeBABE DNA cleavage for rrn promoter with Eσ^S and Eσ^{70}. Regions represented by color scales in Figure 5C are outlined with red boxes. Images were contrast-adjusted to make signal more visible; cleavage was much stronger for Eσ^S.

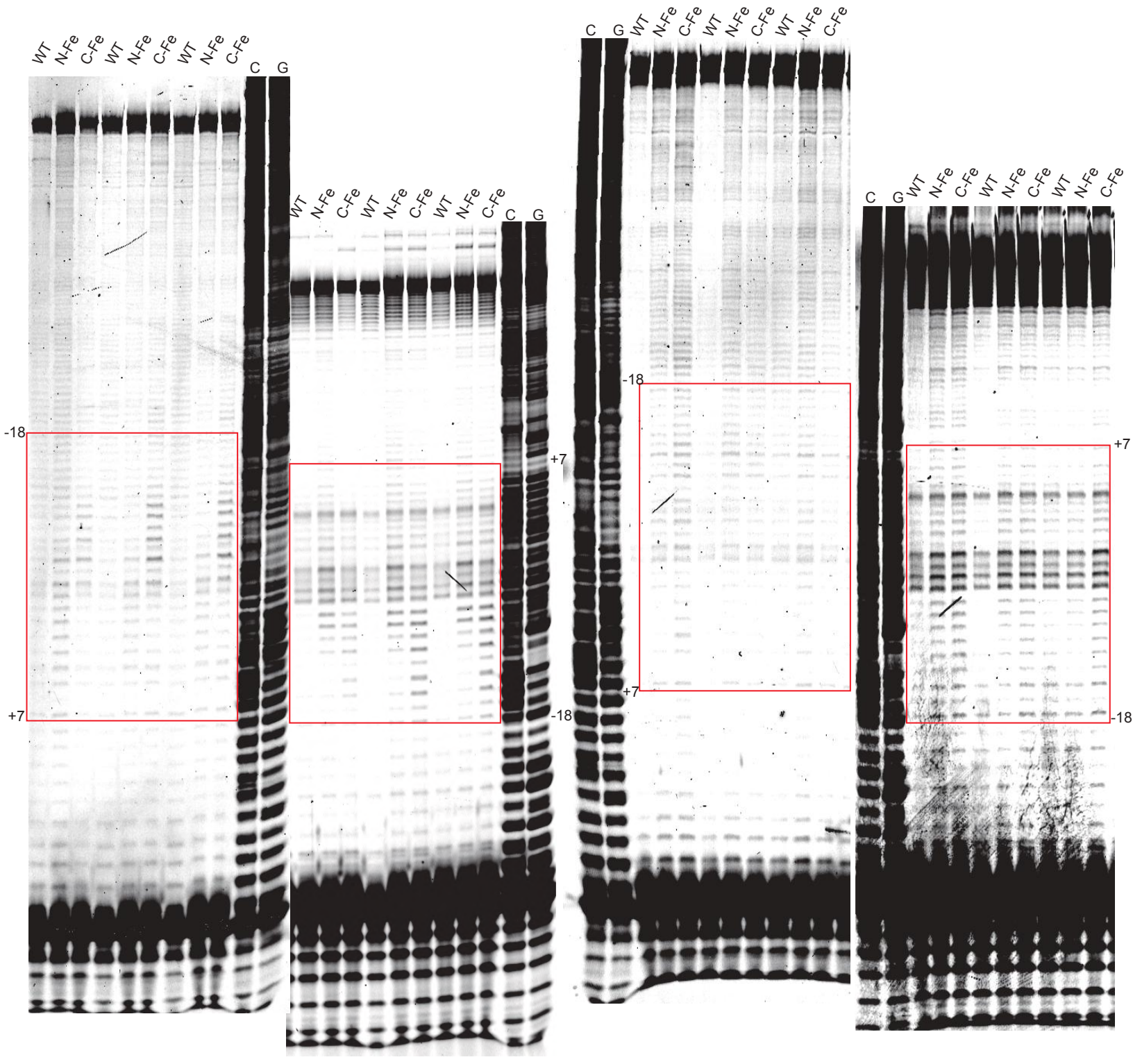

Cy3-labeled primer against NT strand | Cy5-labeled primer against T strand | Cy3-labeled primer against NT strand | Cy5-labeled primer against T strand

Eσ^s | Eσ^{70}

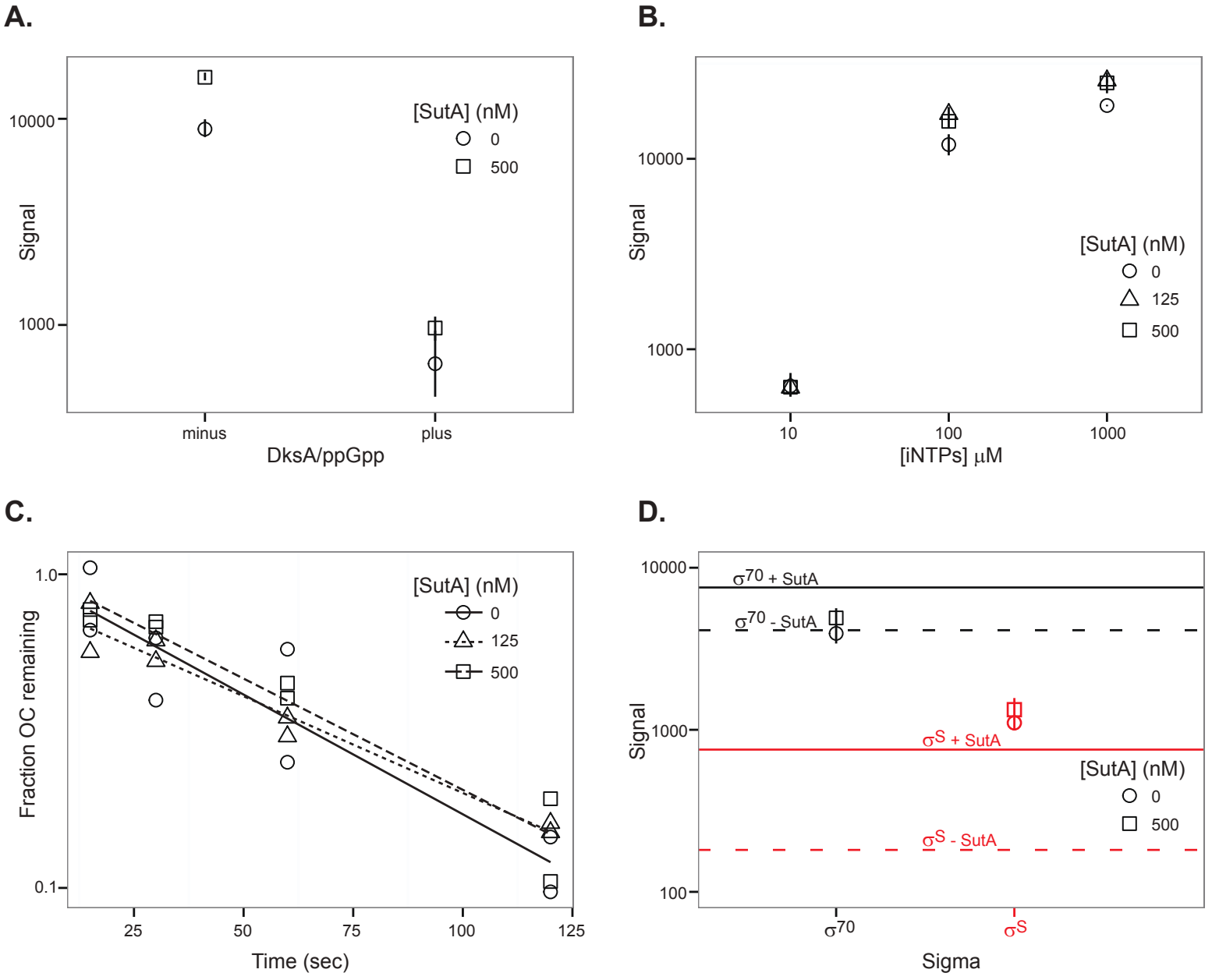

Figure 6. Regulation of the *rrn* OC formed by Eσ^{70} holoenzyme. A. DksA and ppGpp repress initiation from the rrn promoter, and SutA does not overcome these effects. Single turnover initiation reactions were performed using 500 nM SutA and/or 250 nM DksA and 2.5 μM ppGpp as indicated with 20 nM Eσ^{70}, 15 nM promoter DNA, and 20 μg/ml heparin. RNAs were run on a 20% denaturing polyacrylamide gel and visualized by phosphorimaging. Symbols indicate the average value for the three replicates and lines represent the range of values. **B.** SutA effects in the presence of different concentrations of iNTPs, CTP and UTP, the first two nucleotides of the rrn transcript. Symbols reflect the average signal intensity (normalized such that the average signal for the 0 nM SutA condition for a given [iNTP] was the same across different gels) and lines represent the range of values observed in replicate experiments (n=3). **C.** The heparin-resistant *rrn* OC is short-lived and its lifetime is not affected by SutA. The OC was formed with 20 nM Eσ^{70} (black) or Eσ^{S} (red) and 15 nM promoter DNA and challenged with heparin. NTPs were added at the indicated times and transcription was allowed to proceed for 8 minutes before quenching the reaction and running on a 20% gel. Reactions were performed at least in duplicate. **D.** SutA effects are reduced on an artificial transcription bubble. Multiple turnover assays were performed using 15 nM template, 20 nM holoenzyme, and either 500 nM SutA or an equivalent volume of storage buffer. To normalize values across different gels for comparison to single turnover assays on dsDNA template, the median value for the Eσ^{70} reactions with no SutA present on each gel was set to the same level, and other values from that gel adjusted accordingly. Symbols represent the average values for at least 5 replicate bubble transcript reactions, and vertical lines represent the range of values observed. Horizontal lines show values from the experiments on the dsDNA template shown in Figure 2, normalized in the same way as the bubble template data for comparison.

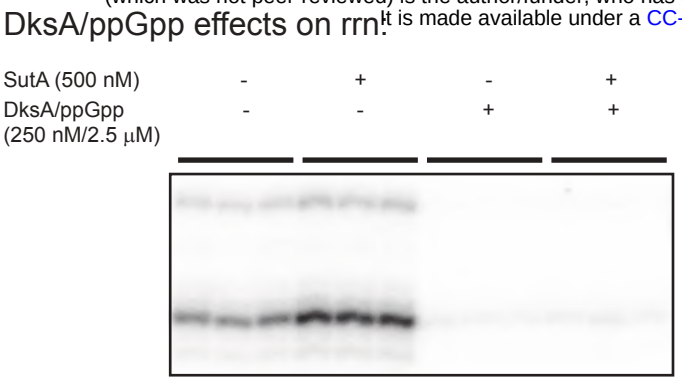

Figure 6 - figure supplement 1. Gel for DksA experiment. Experiment described in main figure legend.

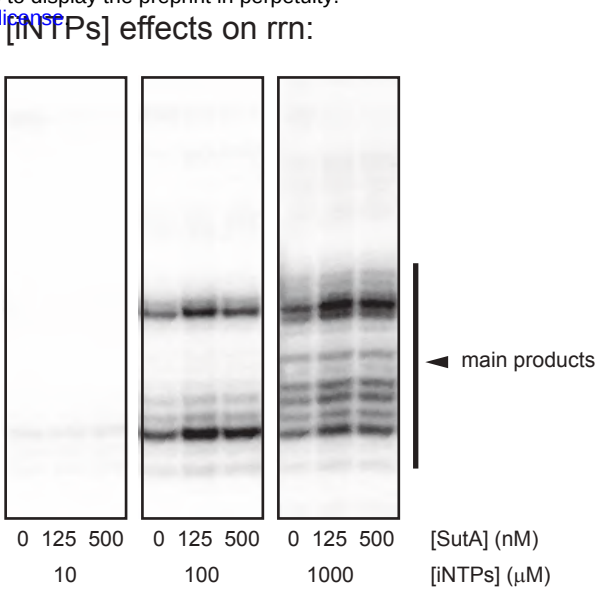

Figure 6 - figure supplement 2. Gel for DksA experiment. Experiment described in main figure legend.

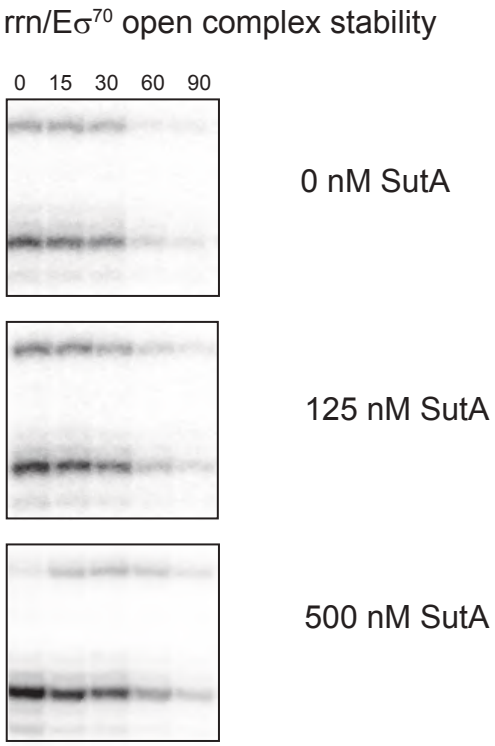

Figure 6 - figure supplement 3. Gel for DksA experiment. Experiment described in main figure legend.

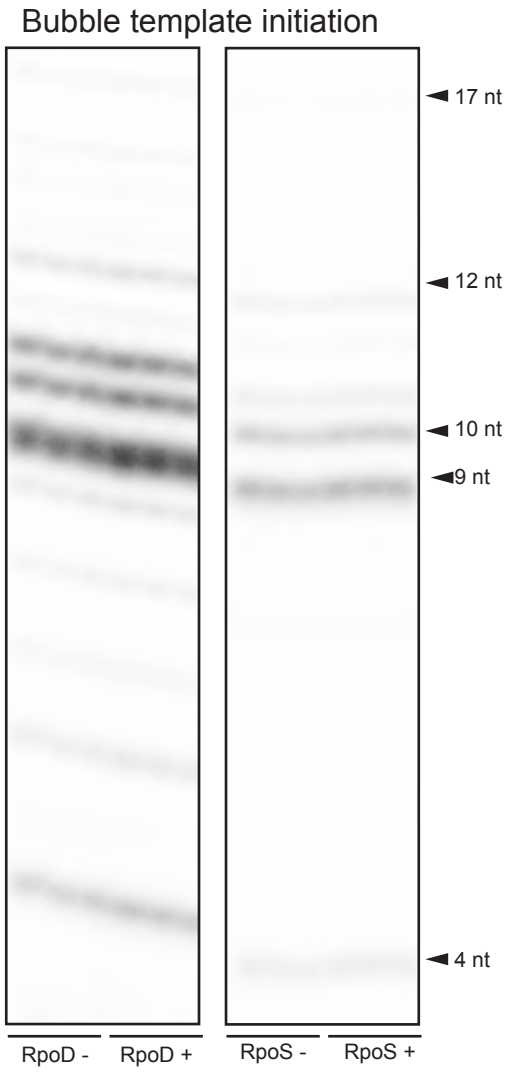

Figure 6 - figure supplement 4. Gel for DksA experiment. Experiment described in main figure legend.

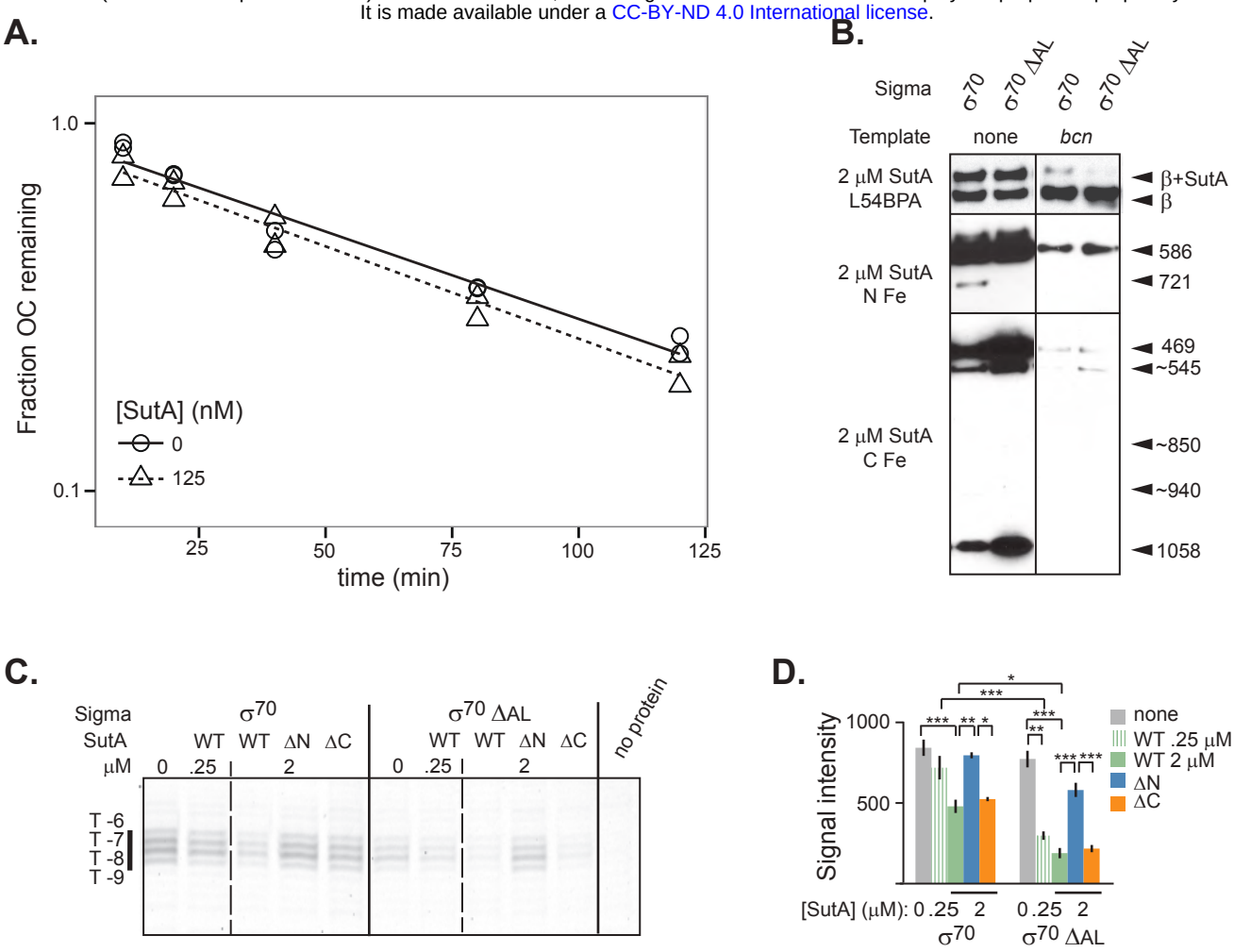

Figure 7. SutA destabilizes RNAP-DNA interactions on the *bcn* promoter. A. The heparin-resistant Eσ^{70}-*bcn* OC is long-lived and its lifetime is not affected by SutA. The OC was formed with 20 nM Eσ^{70} and 15 nM promoter DNA and challenged with heparin. NTPs were added at the indicated times and transcription was allowed to proceed for 8 minutes before quenching the reaction and running on a 20% gel. Reactions were performed at least in duplicate. **B**. SutA interacts only weakly with Eσ^{70}-*bcn* OC, and AL deletion slightly increases the interaction of the C-tail with RNAP. Cross-linking with the L54BPA or cleavage with Fe-conjugated SutA variants were performed as described in Figure 4. **C**. Representative $KMnO_4$ footprinting reactions with either WT or ΔAL σ^{70} holoenzyme. The non-template strand (with a -10 motif sequence of 5' TAATTTT) was probed by primer extension. **D.** Quantification of -6 to -9 footprint signal from experiments performed at least in triplicate. Error bars represent standard error of the mean. P-values for intuitive comparisons that are significantly different, calculated by one-way anova and Tukey's HSD, are indicated by asterisks: *≤ 0.05, **≤0.01, ***≤ 0.001.

Figure 7 - figure supplement 1

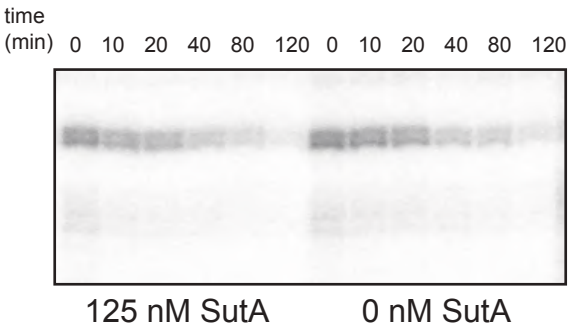

Figure 7 - figure supplement 1. Representative gel for open complex stability assay. Experiment described in main figure legend.

Figure 7 - figure supplement 2. Representative full length gel for one replicate of KMnO4 footprinting assay.

Figure 7 - figure supplement 3. FeBABE DNA cleavage for bcn promoter with Eσ^{70}. Experiment was carried out as described for rrn promoter in Figure 5. No detectable cleavage was observed.

Figure 7 - figure supplement 2

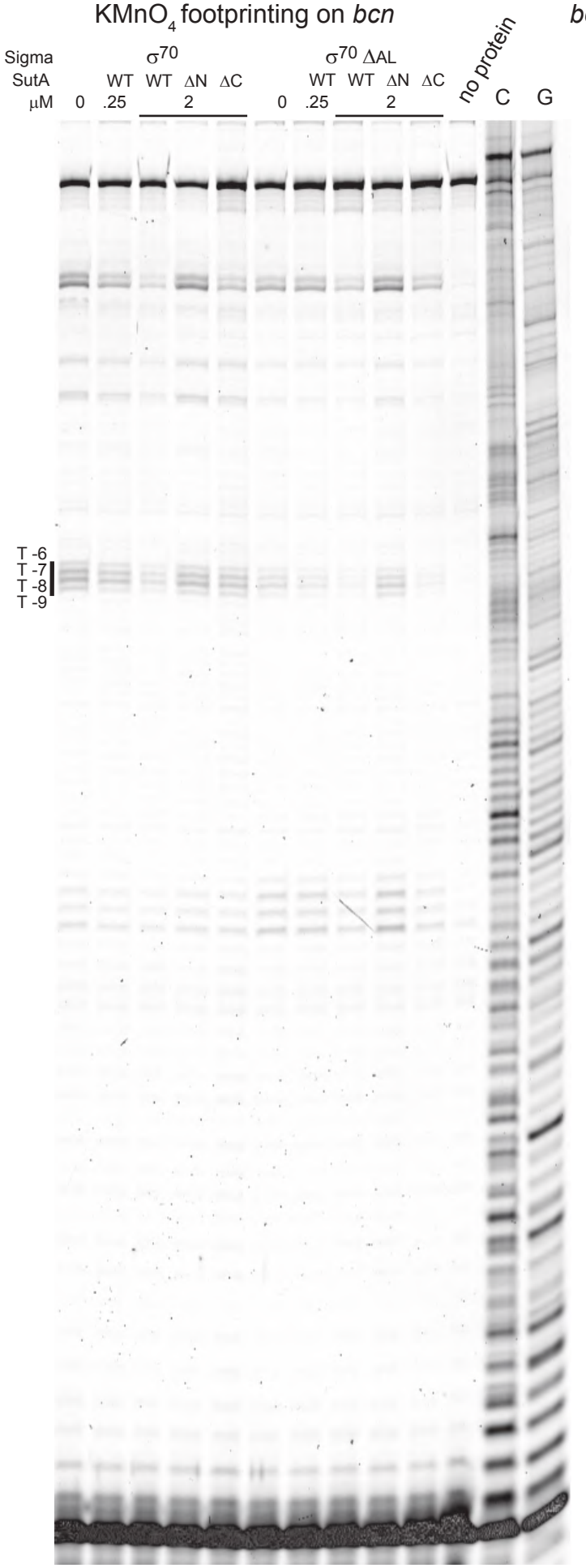

Figure 7 - figure supplement 3

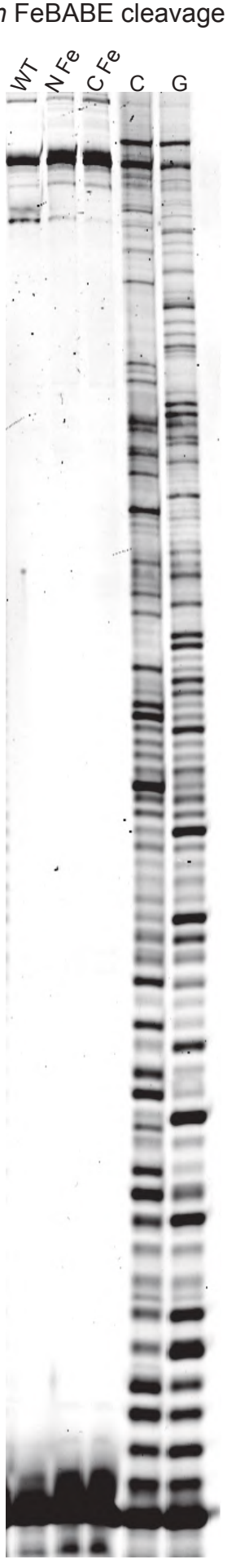

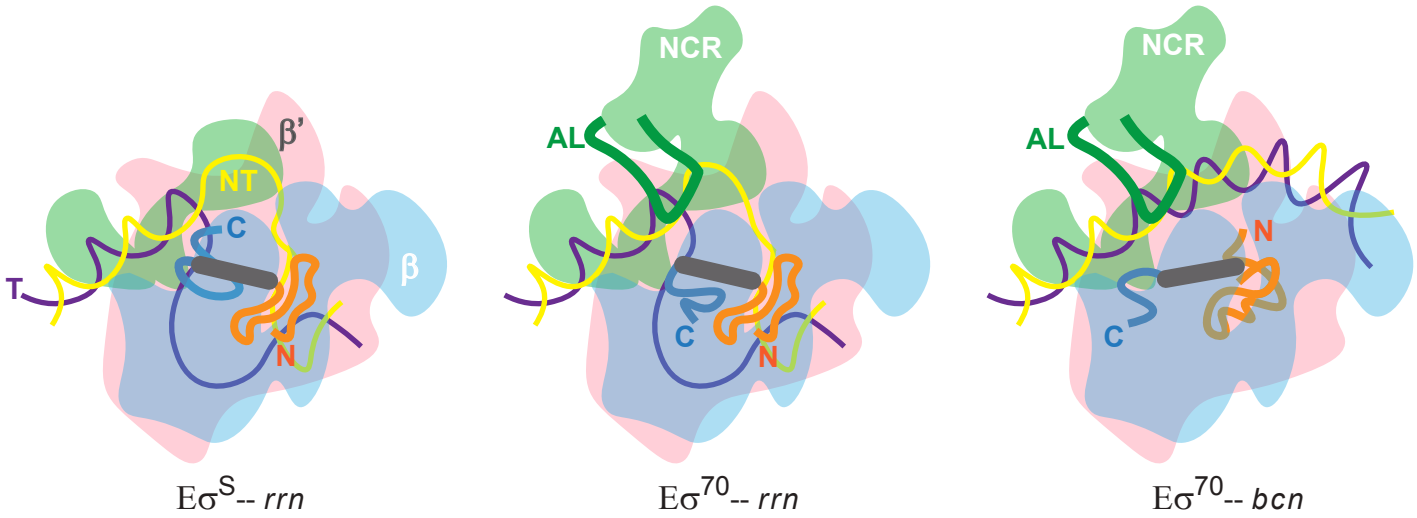

Figure 8. Model of interactions between SutA and RNAP in the context of different promoters and holoenzymes. With $E\sigma^S$ and *rrn* (left), the C-terminus of SutA interacts robustly with β1 and also is in close proximity to the upstream portion of the transcription bubble, and contributes to stabilizing these interactions. The N-terminus of SutA interacts with β near the cleft between the β1 and β2 domains, and also with the non-template strand in the vicinity of the transcription start site. With $E\sigma^{70}$ and *rrn* (center), the interaction between the C-terminus of SutA and β is inhibited by the σ^{70}AL, and the position of the C-terminus relative to the transcription bubble changes, but the N-terminus of SutA can still interact robustly near the β1/β2 cleft and with the non-template strand. With $E\sigma^{70}$ and *bcn*, the presence of SutA blocks open complex formation, and the presence of the *bcn* promoter destabilizes the interaction between SutA and β1 (right).

Table 1: SutA Backbone chemical shift values (ppm)

Residue	number	C	CA	CB	HA	N	HN
Met	1	176.33	55.92	32.94	ND	ND	ND
Ser	2	174.77	58.50	63.86	4.48	117.49	8.60
Glu	3	176.79	57.36	29.98	4.22	122.48	8.63
Glu	4	ND	56.79	30.12	4.25	121.69	8.31
Glu	5	176.49	ND	ND	ND	ND	ND
Leu	6	ND	55.06	42.34	ND	124.68	8.44
Glu	7	176.49	56.41	30.00	ND	121.66	8.43
Gln	8	ND	ND	ND	ND	ND	ND
Asp	9	ND	ND	ND	ND	ND	ND
Glu	10	ND	ND	ND	ND	ND	ND
Leu	11	176.65	56.62	30.05	ND	ND	ND
Asp	12	177.03	55.19	42.18	4.56	123.29	8.40
Gly	13	174.06	45.35	ND	3.86	109.45	8.50
Ala	14	177.61	52.45	19.44	4.80	123.87	8.20
Asp	15	176.36	54.28	41.03	4.56	120.20	8.48
Glu	16	175.75	55.69	29.67	4.24	121.24	8.43
Asp	17	ND	54.63	41.24	4.59	122.29	8.53
Asp	18	ND	ND	ND	ND	122.29	8.53
Gly	19	ND	45.38	ND	ND	109.38	8.49
Glu	20	ND	56.39	30.29	4.24	120.70	8.33
Glu	21	ND	ND	ND	4.24	122.88	8.61
Leu	22	177.18	54.97	42.36	4.18	123.21	8.27
Ala	23	ND	52.25	19.19	4.25	125.88	8.40
Ala	24	ND	ND	ND	ND	ND	ND
Ala	25	ND	52.45	19.28	ND	ND	ND
Asp	26	ND	54.05	41.16	4.59	120.28	8.48
Asp	27	176.85	54.37	41.09	4.56	121.69	8.39
Gly	28	ND	45.39	ND	ND	109.95	8.42
Glu	29	176.53	56.26	30.16	ND	ND	ND
Ala	30	177.54	52.43	19.25	4.25	125.43	8.45
Asp	31	176.47	54.10	41.24	4.56	120.31	8.42
Ser	32	174.86	58.27	63.82	4.43	117.23	8.42
Ser	33	174.51	58.59	63.87	4.48	118.51	8.59
Asp	34	176.76	54.53	40.99	4.25	122.61	8.47
Gly	35	174.40	45.40	ND	3.86	109.45	8.38
Asp	36	ND	54.41	41.17	ND	120.74	8.32
Glu	37	176.00	56.19	30.11	4.32	ND	ND
Ala	38	ND	50.51	17.95	4.55	127.00	8.42
Pro	39	176.39	63.49	31.88	ND	ND	ND
Ala	40	ND	50.46	18.05	ND	125.96	8.51
Pro	41	177.79	ND	ND	ND	ND	ND
Gly	42	ND	ND	ND	3.62	109.42	8.58
Lys	43	176.72	ND	ND	4.24	ND	ND
Lys	44	176.30	56.16	32.95	4.53	123.32	8.45

Ala	45	ND	52.28	19.22	ND	126.21	8.42
Lys	46	176.35	56.07	33.01	4.07	124.22	8.56
Ala	47	177.29	52.36	19.23	ND	126.23	8.46
Ala	48	177.67	52.27	19.11	ND	124.41	8.46
Val	49	177.67	62.24	32.81	ND	120.94	8.28
Val	50	176.04	62.06	32.73	4.08	125.85	8.45
Glu	51	176.17	56.46	30.50	4.08	126.07	8.64
Glu	52	ND	56.39	ND	4.32	122.72	8.55
Glu	53	176.20	56.22	30.48	4.53	123.05	8.56
Leu	54	ND	53.62	41.47	ND	125.63	8.54
Pro	55	177.14	63.23	32.06	ND	ND	ND
Ser	56	175.28	58.39	63.97	ND	116.74	8.44
Val	57	ND	64.43	32.23	ND	122.36	8.38
Glu	58	177.98	58.44	29.51	ND	122.67	8.52
Ala	59	180.86	54.56	18.45	4.25	124.27	8.35
Lys	60	ND	57.55	33.44	ND	121.16	8.14
Gln	61	ND	ND	ND	ND	ND	ND
Lys	62	178.52	57.55	36.17	4.07	120.19	8.26
Glu	63	177.73	ND	ND	ND	120.71	8.03
Arg	64	179.25	59.22	30.12	ND	120.51	8.12
Asp	65	178.26	56.67	40.04	4.32	121.46	8.68
Ala	66	180.75	54.98	17.93	4.18	123.80	8.15
Leu	67	179.26	57.44	41.56	ND	119.14	8.21
Ala	68	ND	54.96	17.89	4.18	122.71	8.06
Lys	69	ND	58.67	32.21	4.14	119.95	8.11
Ala	70	ND	54.66	17.95	4.25	122.00	8.01
Met	71	ND	ND	ND	4.22	119.21	8.30
Glu	72	178.49	58.91	28.29	4.07	120.16	8.28
Glu	73	178.49	58.80	29.30	3.99	120.20	8.23
Phe	74	178.21	60.60	39.18	ND	121.04	8.20
Leu	75	179.73	56.90	41.63	4.02	120.03	8.43
Ser	76	175.43	60.27	63.26	4.32	115.72	8.18
Arg	77	176.94	56.69	30.26	4.32	120.72	7.72
Gly	78	174.73	45.34	ND	3.46	108.39	8.06
Gly	79	173.34	45.18	ND	ND	108.55	8.06
Lys	80	176.52	55.61	33.58	4.40	120.98	8.08
Val	81	175.95	62.58	33.02	ND	122.89	8.43
Gln	82	175.70	55.63	29.56	4.40	124.81	8.60
Glu	83	176.16	56.40	30.33	4.24	123.71	8.60
Ile	84	176.05	60.87	38.75	4.11	122.60	8.34
Glu	85	ND	54.24	29.77	4.59	127.40	8.61
Pro	86	176.54	63.06	32.17	ND	ND	ND
Asn	87	174.99	53.25	38.74	4.66	119.10	8.64
Val	88	176.01	62.31	32.84	4.08	121.53	8.18
Val	89	175.67	62.12	32.55	4.08	125.63	8.37
Ala	90	177.08	52.20	19.44	4.25	128.97	8.48
Asp	91	ND	52.56	40.22	4.25	121.53	8.42

Pro	92	ND	ND	ND	ND	ND	ND
Pro	93	176.82	62.75	31.95	ND	ND	ND
Lys	94	176.57	55.93	33.12	4.40	122.12	8.50
Lys	95	ND	54.29	ND	4.59	124.86	8.56
Pro	96	176.59	63.16	31.97	ND	ND	ND
Asp	97	176.68	54.22	41.11	4.56	121.26	8.56
Ser	98	176.68	58.66	63.74	4.36	117.22	8.42
Lys	99	176.67	56.85	32.54	4.02	123.24	8.49
Tyr	100	176.56	58.22	38.51	4.53	120.61	8.22
Gly	101	174.06	45.21	ND	3.62	110.87	8.30
Ser	102	174.15	58.28	63.87	4.48	115.84	8.24
Arg	103	ND	54.04	30.23	ND	124.12	8.39
Pro	104	176.07	63.34	31.80	ND	ND	ND
Ile	105	181.35	63.20	39.46	ND	125.54	7.87

Table 2: Strains

Strains for *in vivo* experiments:

strain	Strain background genotype	source
DKN263	*P. aeruginosa* UCBPP-PA14	
DKN1625	*P. aeruginosa UCBPP-PA14* ΔsutA	Babin *et al.* 2016
DKN1871	P. aeruginosa UCBPP-PA14 *ΔsutA* attTn7:: P_{BAD} *:sutA* Gm^R	This study
DKN1872	P. aeruginosa UCBPP-PA14 *ΔsutA* attTn7:: P_{BAD} *:sutA ΔN* Gm^R	This study
DKN1873	P. aeruginosa UCBPP-PA14 *ΔsutA* attTn7:: P_{BAD} *:sutA ΔC* Gm^R	This study
DKN1874	P. aeruginosa UCBPP-PA14 *ΔsutAΔrpoS*	This study
DKN1875	P. aeruginosa UCBPP-PA14 *ΔsutAΔrpoS* attTn7:: P_{BAD} *:sutA* Gm^R	A gift from Doug Lies, originally from the laboratory of Carol Gross
DKN81	E. coli MG1655 (F– λ– rph-1)	

E. coli strains for cloning and protein expression:

strain	plasmid description	Strain background genotype	
DKN1298	pTNS1	SM10	Choi and Schweizer 2006
DKN1299	pRK2013	HB101 (F– λ– Δ(gpt-proA)62 leuB6 glnV44(AS) araC14 galK2(Oc) lacY1 Δ(mcrC-mrr) rpsL20(StrR) xylA5 mtl-1 recA13 hsdS20)	Choi and Schweizer 2006
DKN1637	pMQ30_sutA	DH5α (F^- endA1 glnV44 thi-1 recA1 relA1 gyrA96 deoR nupG Φ80d*lacZ* ΔM15 Δ(*lacZYA-argF*)U169, hsdR17(r_K^- m_K^+), λ–)	Babin et al. 2016
DKN548	pMQ72	F– Δ(argF-lac)169 Φ80dlacZ58(ΔM15) glnV44(AS) λ– rfbC1 gyrA96(NalR) recA1 endA1 spoT1 thi-1 hsdR17 deoR	Shanks *et al* . 2006
DKN1640	pMQ72_HASutA	Mach1 (ΔrecA1398 endA1 tonA Φ80ΔlacZM15 ΔlacX74 hsdR(r_K^- m_K^+))	Babin *et al.* 2016
DKN1639	pUC18T-mini-Tn7T-Gm^R P_{BAD} *:sutA*	Mach1 (ΔrecA1398 endA1 tonA Φ80ΔlacZM15 ΔlacX74 hsdR(r_K^- m_K^+))	Babin *et al.* 2016
DKN1876	pUC18T-mini-Tn7T-Gm^R P_{BAD} *:sutAΔN*	DH10β (F^- endA1 recA1 galE15 galK16 nupG rpsL ΔlacX74 Φ80lacZΔM15 araD139 Δ(ara,leu)7697 mcrA Δ(mrr-hsdRMS-mcrBC), λ^-)	
DKN1877	pUC18T-mini-Tn7T-Gm^R P_{BAD} *:sutAΔC*	DH10β (F^- endA1 recA1 galE15 galK16 nupG rpsL ΔlacX74 Φ80lacZΔM15 araD139 Δ(ara,leu)7697 mcrA Δ(mrr-hsdRMS-mcrBC), λ^-)	This study
DKN1697	pQE-80L SutA	BL21 DE3 (F^- ompT gal dcm lon $hsdS_B$(r_B^- m_B^-) λ(DE3 [lacI lacUV5-T7 gene 1 ind1 sam7 nin5]))	
DKN1878	pQE-80L SutA 46-101	BL21 DE3 (F^- ompT gal dcm lon $hsdS_B$(r_B^- m_B^-) λ(DE3 [lacI lacUV5-T7 gene 1 ind1 sam7 nin5]))	This study
DKN1879	pQE-80L SutAΔN	BL21 DE3 (F^- ompT gal dcm lon $hsdS_B$(r_B^- m_B^-) λ(DE3 [lacI lacUV5-T7 gene 1 ind1 sam7 nin5]))	This study
DKN1880	pQE-80L SutAΔC	BL21 DE3 (F^- ompT gal dcm lon $hsdS_B$(r_B^- m_B^-) λ(DE3 [lacI lacUV5-T7 gene 1 ind1 sam7 nin5]))	This study
DKN1881	pQE-80L SutA 6amber	Mach1 (ΔrecA1398 endA1 tonA Φ80ΔlacZM15 ΔlacX74 hsdR(r_K^- m_K^+))	This study
DKN1882	pQE-80L SutA 11amber	Mach1 (ΔrecA1398 endA1 tonA Φ80ΔlacZM15 ΔlacX74 hsdR(r_K^- m_K^+))	This study
DKN1883	pQE-80L SutA 22amber	Mach1 (ΔrecA1398 endA1 tonA Φ80ΔlacZM15 ΔlacX74 hsdR(r_K^- m_K^+))	This study
DKN1884	pQE-80L SutA 54amber	Mach1 (ΔrecA1398 endA1 tonA Φ80ΔlacZM15 ΔlacX74 hsdR(r_K^- m_K^+))	This study
DKN1885	pQE-80L SutA 61amber	Mach1 (ΔrecA1398 endA1 tonA Φ80ΔlacZM15 ΔlacX74 hsdR(r_K^- m_K^+))	This study
DKN1886	pQE-80L SutA 74amber	Mach1 (ΔrecA1398 endA1 tonA Φ80ΔlacZM15 ΔlacX74 hsdR(r_K^- m_K^+))	This study
DKN1887	pQE-80L SutA 84amber	Mach1 (ΔrecA1398 endA1 tonA Φ80ΔlacZM15 ΔlacX74 hsdR(r_K^- m_K^+))	This study
DKN1888	pQE-80L SutA 89amber	Mach1 (ΔrecA1398 endA1 tonA Φ80ΔlacZM15 ΔlacX74 hsdR(r_K^- m_K^+))	This study
DKN1889	pQE-80L SutA 100amber	Mach1 (ΔrecA1398 endA1 tonA Φ80ΔlacZM15 ΔlacX74 hsdR(r_K^- m_K^+))	This study
DKN1890	pQE-80L SutA S2C	DH10β (F^- endA1 recA1 galE15 galK16 nupG rpsL ΔlacX74 Φ80lacZΔM15 araD139 Δ(ara,leu)7697 mcrA Δ(mrr-hsdRMS-mcrBC), λ^-)	This study
DKN1891	pQE-80L SutA S32C	DH10β (F^- endA1 recA1 galE15 galK16 nupG rpsL ΔlacX74 Φ80lacZΔM15 araD139 Δ(ara,leu)7697 mcrA Δ(mrr-hsdRMS-mcrBC), λ^-)	This study
DKN1892	pQE-80L SutA S98C	DH10β (F^- endA1 recA1 galE15 galK16 nupG rpsL ΔlacX74 Φ80lacZΔM15 araD139 Δ(ara,leu)7697 mcrA Δ(mrr-hsdRMS-mcrBC), λ^-)	This study
DKN1893	pQE-80L DksA	BL21 DE3 (F^- ompT gal dcm lon $hsdS_B$(r_B^- m_B^-) λ(DE3 [lacI lacUV5-T7 gene 1 ind1 sam7 nin5]))	This study
DKN1894	pET15b RpoS	BL21 DE3 (F^- ompT gal dcm lon $hsdS_B$(r_B^- m_B^-) λ(DE3 [lacI lacUV5-T7 gene 1 ind1 sam7 nin5]))	This study
DKN1895	pQE-80L RpoB B1	E. coli B F^- ompT hsdS($r_B^-m_B^-$) dcm^+ Tet^r gal λ(DE3) endA Hte [cpn10 cpn60 $Gent^r$] (Arctic Express (DE3) from Agilent)	This study
DKN1896	pQE-80L RpoB355 notag	DH10β (F^- endA1 recA1 galE15 galK16 nupG rpsL ΔlacX74 Φ80lacZΔM15 araD139 Δ(ara,leu)7697 mcrA Δ(mrr-hsdRMS-mcrBC), λ^-)	This study
DKN1897	pQE-80L RpoB450 notag	DH10β (F^- endA1 recA1 galE15 galK16 nupG rpsL ΔlacX74 Φ80lacZΔM15 araD139 Δ(ara,leu)7697 mcrA Δ(mrr-hsdRMS-mcrBC), λ^-)	This study
DKN1898	pQE-80L RpoB520 notag	DH10β (F^- endA1 recA1 galE15 galK16 nupG rpsL ΔlacX74 Φ80lacZΔM15 araD139 Δ(ara,leu)7697 mcrA Δ(mrr-hsdRMS-mcrBC), λ^-)	This study
DKN1899	pQE-80L RpoB626 notag	DH10β (F^- endA1 recA1 galE15 galK16 nupG rpsL ΔlacX74 Φ80lacZΔM15 araD139 Δ(ara,leu)7697 mcrA Δ(mrr-hsdRMS-mcrBC), λ^-)	This study
DKN1900	pQE-80L RpoB1062 notag	DH10β (F^- endA1 recA1 galE15 galK16 nupG rpsL ΔlacX74 Φ80lacZΔM15 araD139 Δ(ara,leu)7697 mcrA Δ(mrr-hsdRMS-mcrBC), λ^-)	This study
DKN1901	pET15b RpoD	BL21 DE3 (F^- ompT gal dcm lon $hsdS_B$(r_B^- m_B^-) λ(DE3 [lacI lacUV5-T7 gene 1 ind1 sam7 nin5]))	This study
DKN1902	pET15b RpoD Δ171-214	BL21 DE3 (F^- ompT gal dcm lon $hsdS_B$(r_B^- m_B^-) λ(DE3 [lacI lacUV5-T7 gene 1 ind1 sam7 nin5]))	This study
DKN1903	pUC18 rrn template	DH10β (F^- endA1 recA1 galE15 galK16 nupG rpsL ΔlacX74 Φ80lacZΔM15 araD139 Δ(ara,leu)7697 mcrA Δ(mrr-hsdRMS-mcrBC), λ^-)	This study
DKN1904	pUC18 bcn template	DH10β (F^- endA1 recA1 galE15 galK16 nupG rpsL ΔlacX74 Φ80lacZΔM15 araD139 Δ(ara,leu)7697 mcrA Δ(mrr-hsdRMS-mcrBC), λ^-)	This study
DKN1905	pUC18 pepB template	DH10β (F^- endA1 recA1 galE15 galK16 nupG rpsL ΔlacX74 Φ80lacZΔM15 araD139 Δ(ara,leu)7697 mcrA Δ(mrr-hsdRMS-mcrBC), λ^-)	

Table 3: Primers

Name	Sequence	Purpose
SutATEV F	gagaacctgtacttccagagcATGAGCGAAGAAGAACTGGA	Plasmid mutagenesis
SutATEV R	GTGATGGTGATGGTGATGCG	Plasmid mutagenesis
SutA46-101 gF	GAACCTGTACTTCCAGAGCATGAAAGCCGCCGTGGTGGAAG	Gibson cloning into plasmid
SutA46-101 gR	AGCTCAGCTAATTAAGCTTTCAGCCGTACTTGCTGTCCGG	Gibson cloning into plasmid
SutA46-101 pF	CCGGACAGCAAGTACGGCTGAAAGCTTAATTAGCTGAGCT	Gibson cloning into plasmid
SutA46-101 pR	CTTCCACCACGGCGGCTTTCATGCTCTGGAAGTACAGGTTC	Gibson cloning into plasmid
SutAdN F	ggcaagaaggcgaaagccg	Plasmid mutagenesis
SutAdN R	CATgctctggaagtacaggt	Plasmid mutagenesis
SutAdC F	TGAAAGCTTAATTAGCTGAGCTTGG	Plasmid mutagenesis
SutAdC R	gttgggttcgatctcctgca	Plasmid mutagenesis
SutAdN MQ72 R	CATGGTCAACCcctcctgag	Plasmid mutagenesis
SutAdC MQ72 F	taaatcagaacgcagaagcgg	Plasmid mutagenesis
SutA S2C F	GCGAAGAAGAACTGGAACAG	Plasmid mutagenesis
SutA S2C R	ACATGCTCTGGAAGTACAGG	Plasmid mutagenesis
SutA S32C F	GCAGTGACGGCGACGAGG	Plasmid mutagenesis
SutA S32C R	AGTCCGCTTCGCCGTCGT	Plasmid mutagenesis
SutA S98C F	GCAAGTACGGCAGCCGCC	Plasmid mutagenesis
SutA S98C R	AGTCCGGCTTCTTCGGCG	Plasmid mutagenesis
SutA 6amber F	gaaTAggaacaggacgagctggacg	Plasmid mutagenesis
SutA 6amber R	ttcttcgctcatGCTCTGGAAGTAC	Plasmid mutagenesis
SutA 11amber F	GtaGGACGGCGCTGACGAG	Plasmid mutagenesis
SutA 11amber R	TCGTCCTGTTCCAGTTCTTCTTCgctc	Plasmid mutagenesis
SutA 22amber F	GCGAAGAGTAGGCCGCGGCCGACGACGGC	Plasmid mutagenesis
SutA 22amber R	CGTCGTCCTCGTCAGCGCCGTCC	Plasmid mutagenesis
SutA 54amber F	GAAGAGGAATAGCCCTCGGTCGAAGCCAAG	Plasmid mutagenesis
SutA 54amber R	CACCACGGCGGCTTTCGCCTTCTTG	Plasmid mutagenesis
SutA 61amber F	gTagaaagagcgtgacgccctcg	Plasmid mutagenesis
SutA 61amber R	ttggcttcgaccgagggcagt	Plasmid mutagenesis
SutA 74amber F	GGAGGAATAGCTTTCCCGCGGTGGAAAGG	Plasmid mutagenesis
SutA 74amber R	ATCGCCTTGGCGAGGGCGTCAC	Plasmid mutagenesis
SutA 84amber F	TAGGAACCCAACGTGGTGGCCGA	Plasmid mutagenesis
SutA 84amber R	CTCCTGCACCTTTCCACCGCG	Plasmid mutagenesis
SutA 89amber F	gTAggccgatccgccgaag	Plasmid mutagenesis
SutA 89amber R	acgttgggttcgatctcctgcacc	Plasmid mutagenesis
SutA 100amber F	TAGGGCAGCCGCCCCATCTGAAAG	Plasmid mutagenesis
SutA 100amber R	CTTGCTGTCCGGCTTCTTCG	Plasmid mutagenesis
RpoS gF	CCATCATCATCATCATCACGAGAACCTGTACTTCCAGGGCATGGCACTCAAAAAAGAAGG	Gibson cloning into plasmid
RpoS gR	GAGGCCCCAAGGGGTTATGCTAGTCACTGGAACAGCGCGTCAC	Gibson cloning into plasmid

RpoS pF	GTGACGCGCTGTTCCAGTGACTAGCATAACCCCTTGGGGCCTC	Gibson cloning into plasmid
RpoS pR	CCTTCTTTTTTGAGTGCCATGCCCTGGAAGTACAGGTTCTCGTGATGATGATGATGATGG	Gibson cloning into plasmid
DksA gF	gagaacctgtacttccagagcATGTCCACCAAAGCAAAACA	Gibson cloning into plasmid
DksA gR	TCCAAGCTCAGCTAATTAAGCTTTCAGGAGCCGAGTTGCTTCT	Gibson cloning into plasmid
DksA pF	AGAAGCAACTCGGCTCCTGAAAGCTTAATTAGCTGAGCTTGGA	Gibson cloning into plasmid
DksA pR	TGTTTTGCTTTGGTGGACATgctctggaagtacaggttctc	Gibson cloning into plasmid
RpoD gF	CCATCATCATCATCATCACGAGAACCTGTACTTCCAGGGCATGTCCGGAAAAGCGCAACA	Gibson cloning into plasmid
RpoD gR	GAGGCCCCAAGGGGTTATGCTAGTCACTCGTCGAGGAAGGAGC	Gibson cloning into plasmid
RpoD pF	GCTCCTTCCTCGACGAGTGACTAGCATAACCCCTTGGGGCCTC	Gibson cloning into plasmid
RpoD pR	TGTTGCGCTTTTCCGGACATGCCCTGGAAGTACAGGTTCTCGTGATGATGATGATGATGG	Gibson cloning into plasmid
RpoD 171-214 F	GGTCCGGATCCGGAAGAA	Plasmid mutagenesis
RpoD 171-214 R	GGGATCGATATAGCCGCTGA	Plasmid mutagenesis
RpoB B1_us F	GAACCTGTACTTCCAGAGCATGTTGCTGGCCATCCAGCTGGATT	Gibson cloning into plasmid
RpoB B1_us R	TCCAGCTGGATGGCCAGCAACATGCTCTGGAAGTACAGGTTCT	Gibson cloning into plasmid
RpoB B1_mid F	TCCCAGCTGCACCGTTCCGGTGGTATCGACCACCTGGGCAAC	Gibson cloning into plasmid
RpoB B1_mid R	GTTGCCCAGGTGGTCGATACCACCGGAACGGTGCAGCTGGGA	Gibson cloning into plasmid
RpoB B1_ds F	TTCGAGCCAGCTGTCGCAGTGAAAGCTTAATTAGCTGAGCT	Gibson cloning into plasmid
RpoB B1_ds R	AGCTCAGCTAATTAAGCTTTCACTGCGACAGCTGGCTCGAA	Gibson cloning into plasmid
RpoBfrag pF	GACATCGAACTGGAAACCGAATGAAAGCTTAATTAGCTGAGCTTGGA	Gibson cloning into plasmid
RpoBfrag pR	CGATCCTCTCATAGTTAATTTCTCCT	Gibson cloning into plasmid
RpoB355 F	GGAGAAATTAACTATGAGAGGATCGCTGAAGATCGACAACACCAGC	Gibson cloning into plasmid
RpoB450 F	GGAGAAATTAACTATGAGAGGATCGATCGACCACCTGGGCAACCG	Gibson cloning into plasmid
RpoB520 F	GGAGAAATTAACTATGAGAGGATCGTTCATGGGCCAGAACAACCCG	Gibson cloning into plasmid
RpoB626 F	GGAGAAATTAACTATGAGAGGATCGACCCTCAACGAGAAGGGTCAAC	Gibson cloning into plasmid
RpoBfrag R	CAGCTAATTAAGCTTTCATTCGGTTTCCAGTTCGATGTCG	Gibson cloning into plasmid
temp_plasmid F	CCGCGCAAGGCACAGTCGAAAGACTGGGCCTTTCGTTTTGCTTAATTAGCTGAGCTTGG	Gibson cloning into plasmid
temp_plasmid R	GCTTCGTGTCGAGCCCTTCGCCACGCCCCTCTTTAATACG	Gibson cloning into plasmid
rrn_temp F	CGAAGGGCTCGACACGAAGCTTGAAGGTCGGGCGCAAGC	Gibson cloning into plasmid
rrn_temp R	TTCGACTGTGCCTTGGCGCGGATTCGACTTGTTAAAGAGCA	Gibson cloning into plasmid
bcn_tempF	CGAAGGGCTCGACACGAAGCGGCGGTCATTTGCCTAACATG	Gibson cloning into plasmid
bcn_temp R	TTCGACTGTGCCTTGCGCGGTGAGCGATAGCCGGCCCTCT	Gibson cloning into plasmid
pepB_temp F	CGAAGGGCTCGACACGAAGCGCCAGCGAGCTATCAGCA	Gibson cloning into plasmid
pepB_temp R	CCAGTCTTTCGACTGTGCCTTGCGCGGCGTTCCTTGTGAGGCGATG	Gibson cloning into plasmid
pepB_cy5 F	GAAAATAACGCTTGACGGAATTCAGGAATTACGCCAGGAC	Template production
pepB_cy3 R	AGAGCAGTTGGTCAAGGCTATTGCCCGAAATGTCGC	Template production
generic_temp F	CGAAGGGCTCGACACGAAGC	Template production
rrn_temp_short R	CTTGTTAAAGAGCAGTTGGTC	Template production
bcn_temp_shortR	GTGACTATCGGTTGCCAGC	Template production
bcn_forPE_R	AGAGCAGTTGGTCAAGGCTATCGGTTGCCAGCCGCT	Template production
bubble_T	AGGCTTTCGTCTCAACCGAGGCGCGCGTAAGAACAGCAACCTCTCTTTCCGTCAAGCGTTATTTTCGAAAATTTTCTTTT	Template production
bubble_NT	AAAAGAAAATTTTCGAAAATAACGCTTGACGGAAAGAGAGGTTGCTGTAGAATGCGCGCGGACGGTTGAGACGAAAGCCT	Template production

Cy5 primer ext.	Cy5_GAAAATAACGCTTGACGGAA	Primer extension
Cy3 primer ext.	Cy3_AGAGCAGTTGGTCAAGGC	Primer extension
rrn RTforRACE	CGAATTCACGAGTGTTAC	5' RACE
rrn RACE_PCR1 F	CGAAGGGCTCGACACGAAGCAAAAAAAAAAAAAAAAAA	5' RACE
rrn RACE_PCR1 R	TTCGACTGTGCCTTGCGCGGTTGCGCTGCTGATAATCTTG	5' RACE
rrn RACE_PCR2 F	CGTATTAAAGAGGGGCGTGGCGAAGGGCTCGACACGAAGC	5' RACE
rrn RACE_PCR2 R	CCAAGCTCAGCTAATTAAGCAAAACGAAAGGCCCAGTCTTTCGACTGTGCCTTGCGCGG	5' RACE
RACE plasmid F	CCGCGCAAGGCACAGTCGAAAGACTGGGCCTTTCGTTTTGCTTAATTAGCTGAGCTTGG	5' RACE
RACE plasmid R	GCTTCGTGTCGAGCCCTTCGCCACGCCCCTCTTTAATACG	5' RACE
oprI qPCR F	AGCAGCCACTCCAAAGAAAC	qPCR
oprI qPCR R	CAGAGCTTCGTCAGCCTTG	qPCR
rrn qPCR F	ACGAAAGCCTTGACCAACTG	qPCR
rrn qPCR R	TTGCGCTGCTGATAATCTTG	qPCR
bcn qPCR F	ACTCGCCACACTTCAGGAAC	qPCR
bcn qPCR R	AGGTCGTTGGACACCTTGAC	qPCR
pepB qPCR F	TGCAGAAGCTGGAAGACATC	qPCR
pepB qPCR R	CTTTCTGCAGGGTCTGCTTC	qPCR
Ec_rrn qPCR F	TGCTCTTTAACAATTTATCAGACAATC	qPCR
Ec_rrn qPCR R	CGTGTTCACTCTTGAGACTTGG	qPCR
Ec_hcaT qPCR F	CTGATGCTGGTGATGATTGG	qPCR
Ec_hcaT qPCR R	AGTCGCACTTTGCCGTAATC	qPCR